Author Response 2

Anonymous Referee #1

Submitted on 15 March, 2018

General remarks:

The authors did a good job in answering the reviewers questions and addressing necessary changes. There is only one issue I'm still struggling with. The new vertical weighting functions considering multiple scattering are a good improvement for the study. However, I still have doubts that this approach does provide the correct solution which is needed to quantify the retrieval biases, which is the main purpose of the manuscript.

Major comments:

1. **Vertical Weighting**

   To find the suitable factors b, the authors did compare the biases using different values of b and finally chose the value which provides the best agreement between retrieval results and the vertical weighted values. In my understanding this is aiming for "moving target". You can not adjust the weighting functions in a way that the correct results are obtained. Doing so, you already rule out any source of uncertainty related to the vertical structure of the cloud.

   Additionally, the authors conclude that the new 2WT weighting function using $b=9$ is similar to the old 2WT weighting function ($b=0$). Can this be explain to be the general case? I don't think this is a general rule. It might only be coincidental due to the profile of $R_{\rm e}$ applied here.
   (By the way, the link to the histograms did not in the PDF.)

   a. The issue of comparing to a "moving target" is of great concern to us, and it was one of the reasons why we focused on a fixed vertical weighting function initially. Our approach to address this issue in this stage of the revision will be to validate our parametric vertical weighting functions more rigorously against the numerically calculated vertical weighting functions from Platnick et al. (2000).

   b. Apologies for the broken links in the previous response. Here are the links to the gifs, despite the fact that they are now out of date compared to the current modeling (see response to #3):

r_e(2.13)-r_e(VW,2.13) Histogram varying b
https://drive.google.com/open?id=1hKfcrhkYj3fiII3RcR-YHmvkPOo6gRXK
r_e(2.13)-r_e(VW,2.13) Histogram varying b (FOR τ>5 ONLY!)
https://drive.google.com/open?id=18Pnc_AgPK3Y_prf7eYzKnk4b15jL-bAI
r_e(3.75)-r_e(VW,3.75) histogram varying b
https://drive.google.com/open?id=1HHQhDvyVww2iqlS7iAnhsiZqhM5DMb7K

r_e(3.75,coupled to v_e(pol))-r_e(VW,3.75) Histogram varying b
https://drive.google.com/open?id=1Sj68TIpGEnziOGS8MWU_FJP4HdAndKnT

2. **Vertical weighting functions**
   The treatment of clouds with $\tau<5$ is arbitrary in my point of view. The weighting function can not simply be changed just because the bias becomes to large. You need to give a reason why the vertical weighting function of clouds smaller than $\tau<5$ is not correct. An I do not see a reason why the concept of the multiple scattering weighting function does not hold for lower tau. Did you normalize the weighting function appropriately?

   a. This restriction is only for determining the optimal value of b in the "tuned/moving target approach" mentioned in the previous author response. Now that the approach has changed this is not so relevant, but the initial reasoning was that the peak of the b=9 vertical weighting function defined previously was located at a depth of tau~5, leading to results that weighted the bottom more than the top of the cloud in instances when the cloud wasn't thicker than that. This is obviously incorrect and something that we no longer deal with for the new parametric vertical weighting defined below.

3. **Vertical weighting functions**
   The authors argue, that their new weighting function considers the inhomogeneous cloud vertical structure compared to the approach by Platnick (2000). Here I disagree. Of course the simulations in the Platnick (2000) approach to calculate the weighting function assumes homogeneous clouds. But the application of the weighting functions can be done for real cloud profiles. The 2WT weighting used by the authors does the same. The 2WT weighting function is also calculated only as a function of τ. Therefore, also here no profile of $R_{\rm e}$ is considered in the calculation. Only when the 2WT weighting is applied to the cloud profile the vertical structure is considered. This is similar to Platnick (2000) and in my point of view no reason to prefer the 2WT weighting functions.

   I see, that it would be a big effort to completely change the weighting functions to Platnick (2000). In order not to need to do this, the authors should convincingly show, that their weighting functions are similar to the Platnick (2000) approach and do not cause any bias, that may affect the study. Such a comparison for only one or some representative cloud profiles could also be used to justify the values of b.

Inhomogeneity Discussion:

Perhaps we can clarify this in the text, but the assertion that we're making is not that we consider inhomogeneous vertical structure in a way that the Platnick approach doesn't. It is instead that our vertical weighting function

doesn't make any assumptions about the form of the microphysical distribution of cloud droplets. The vertical weighting function defined in eq. 4 of Platnick (2000) explicitly weights the vertical profile of $r_e(z)$ (calculated layer by layer). This approach results in a decoupling in the relationship between $r_e(z)$ and $v_e(z)$. Whereas, if one vertically weights the droplet size distribution, $N(r,z)$, they preserve the relationship between size distribution parameters in each layer by calculating r_e(VW) & v_e(VW) for the same effective distribution.

Summary of Differences:

To summarize points made here and previously more succinctly, the main differences between these approaches are:

1. Mathematical formulation: Vertically weighting r_e(z) or N(r,z).
    - **a.** To this end, we will examine in this response how the Platnick vertical weighting function behaves when it is used to vertically weight $N(r,z)$ in the same way as our approach.
    - **b.** This is getting deep into the weeds, but the mathematical difference between these approaches is similar to the spatial averaging discussion in the appendix of the manuscript – with the caveat that vertical inhomogeneity is greater than horizontal inhomogeneity.
2. Derivation: Fixed Parametric vs. Direct Radiative Modeling
    - **a.** The fixed parametric approach does not consider the radiative impact of the r_e(z) profile itself on the definition of the vertical weighting function. The validity of the parametric approach would indeed depend on how important this assumption is.
    - **b.** Direct modeling takes time, and a fixed parametric model might get reasonable results with limited effort.

You do raise some very important points regarding accounting for the impact of dependency on r_e profile, and I think this is one of the core shortcomings of using a fixed empirical function for the entire LES domain. To make sure to emphasize these shortcomings of the fixed parametric vertical weighting function **I've added some additional discussion of this on page 9 of the text.** But it must also be emphasized that the fixed empirical functions are easier to derive, easier to use, and applicable in situations with limited cloud profile information. There are many practical reasons for developing a single parametric function that usefully replicates the behavior of the maximum penetration depth vertical weighting defined in eq. 4 of Platnick et al. (2000). In our case, while it is computationally expensive, it is possible to calculate this weighting function for the entire LES domain, but in other applications a fixed parametric weighting function is the only satisfactory way to describe the impact of vertical penetration on retrieved cloud properties (for example, Zhang et al. (2017)).

Radiatively Derived Vertical Weighting

The radiatively derived vertical weighting functions are calculated following the maximum penetration depth weighting function (eq. 4 of Platnick (2000)). Focusing on a single horizontal transect through the DYCOMS-II LES case, we analyzed the behavior of 128 vertical profiles. The figure below depicts vertical weighting functions for a single column within the transect for different solar geometries. These radiatively derived weighting functions will be used to calculate r_e(VW) from both the $r_e(z)$ and $N(r,z)$ profile weighting approaches.

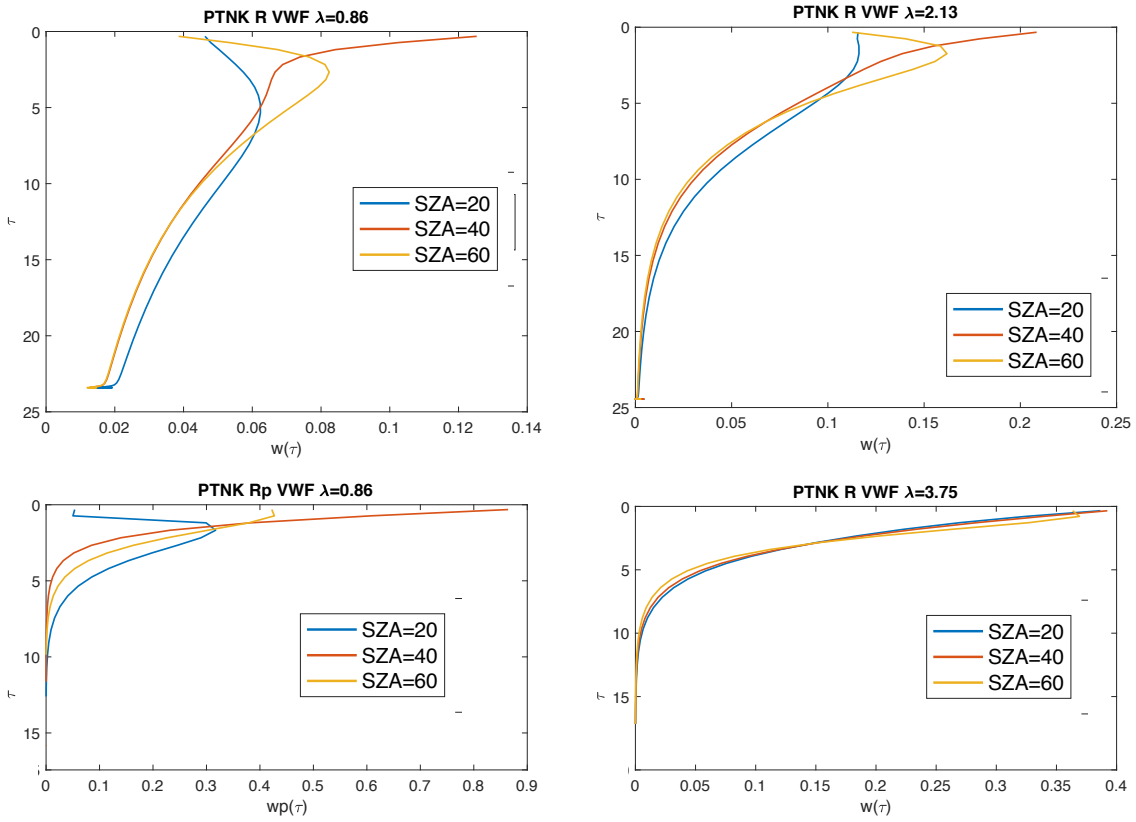

Figure 1: Radiatively derived vertical weighting functions for a nadir view of a single column of the DYCOMS-II LES case. The top left, right, and bottom right panels show total reflectance vertical weighting functions for the 0.865, 2.13, and 3.75 μm bands respectively. The bottom left panel shows a polarized reflectance vertical weighting function (derived using Rp=sqrt(Q^2+U^2)) for the 0.865 μm band. Note that proper accounting for polarimetric vertical weighting should also account for varying viewing geometry. Each figure also includes three curves for different solar zenith angle (in degrees) geometries. Note that for nadir viewing the SZA=40 and RAA=30 case corresponds to a scattering angle of 140, which is close to the cloudbow peak.

A New Parametric Model:

We have again modified the parametric vertical weighting method used in this study. This change was made in part because we found that the single parameter weighting wasn't adequately representing the radiatively derived vertical weighting functions for the 2.13 μm band. The new two-parameter vertical weighting function is,

$$W(\tau) = c\tau^b \exp\left[-a\tau\left(\frac{1}{\mu}+\frac{1}{\mu_0}\right)\right],$$

"where the parameters *a* and *b* are introduced to account for the influence of multiple scattering effects to the vertical weighting function discussed previously in Miller et al. (2016). The parameter *a* scales the optical depth, modelling the enhancement of transmission caused by multiple scattering whereas the parameter *b* produces a peaked vertical weighting function associated with the expected penetration depth of the reflected light and *c* is the normalization factor. Each of these parameters is strictly positive, and for *a*=1 and *b*=0 we obtain the original single-scattering vertical weighting used in Miller et al. (2016). For smaller values of *a* and larger values of *b*, the vertical weighting function extends deeper into the cloud, leading to droplet size distribution properties deeper in the cloud contributing more information to the vertically weighted value. A single value of *a* and *b* are is selected for each retrieval approach based on coefficients that gave best fits to a small number of numerically derived vertical weighting functions based on eq. 4 of Platnick (2000)." - (taken directly from the updated manuscript)

As a brief aside, it should be noted that this new parametric function has a form similar to a gamma distribution with respect to tau.

The radiatively modeled and the parametric weighting functions can now be used to search for the "best fit" parameters, *a* and *b*, suitable for each LES column and in different spectral bands. The results for of these fits are shown in Figure 2. Below are links to animated gifs of the best-fit solutions found throughout the transect for SZA=20 and nadir viewing:

2.13 μm Vertical Weighting Function
https://drive.google.com/open?id=1wZxnmI2xdS3X4JTFxv-oKFFHteyn9hQT
3.75 μm Vertical Weighting Function
https://drive.google.com/open?id=14j2gyv0zZVC1OtBCkPQzktREcnD9Bfyp

The predominance of high quality fits (R^2>0.99) indicates that this functional form is quite reliable. The best-fit *a* and *b* for each of the bands are also well clustered, indicating that a selection of a single value of *a* and *b* for each wavelength (and observation geometry) should sufficiently represent the radiatively modeled vertical weighting functions. Throughout the rest of this work, we make use of the scene aggregated median values of *a* and *b* from

these plots (limited to R^2>0.99). The fitting approach also allows us to verify whether the parametric function has any correlation to cloud property variability like the r_e profile or the total cloud optical thickness. To that end, we observed that there was no clear correlation between the best-fit values of a and b and the retrieval bias, r_e(VW)-r_e(bispectral), or the cloud optical thickness.

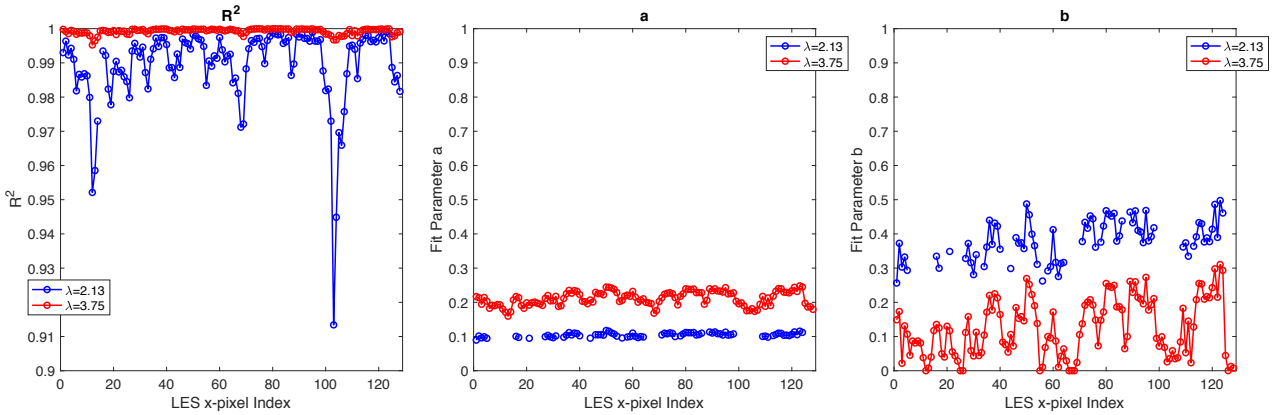

Figure 2: Best-fit parameters from fitting radiatively derived vertical weighting functions. The top panel depicts R^2, the middle a, and the bottom panel b. Parameters are only plotted for higher quality fits with R^2>0.99. The case examined here corresponds to VZA=0, SZA=20, and RAA=30.

With both the parametric and radiatively derived weighting functions we can now derive r_e(VW) and ve using both and compare them. and bispectral (NJK) retrievals. It should also be noted that there is a persistent high bias in the r_e(3.7μm) retrieval that longer exists if the retrieval is coupled to v_e(pol) as previously discussed in the manuscript.

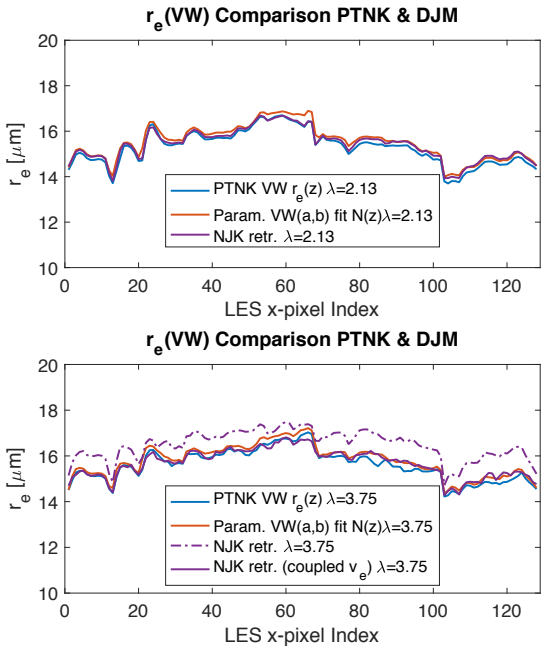

Figure 3: Comparisons of different approaches for obtaining vertically weighted cloud properties using a single horizontal transect of the DYCOMS-II LES case. The top and bottom rows compare vertical weighting results for the 2.13 and 3.75 μm bands respectively. The RT-model-derived Platnick vertical weighting r_e(z) (blue) is compared to the Parametric vertical weighting of N(r,z) (red) and corresponding bispectral (NJK) retrieval is also shown(purple). The case examined here corresponds to VZA=0, SZA=20, and RAA=30.

Additionally we can test the difference between vertical weighting of $r_e(z)$ and N(r,z). A quick comparison of Figure 3 and Figure 4 reveals that the most significant source of difference between the two vertically weighted results is the choice of which vertical profile is being weighted. This choice has a weak impact on r_e(VW), but a more significant impact on the overall shape of the inferred distribution because v_e(VW) changes (for 2.13 μm in particular).

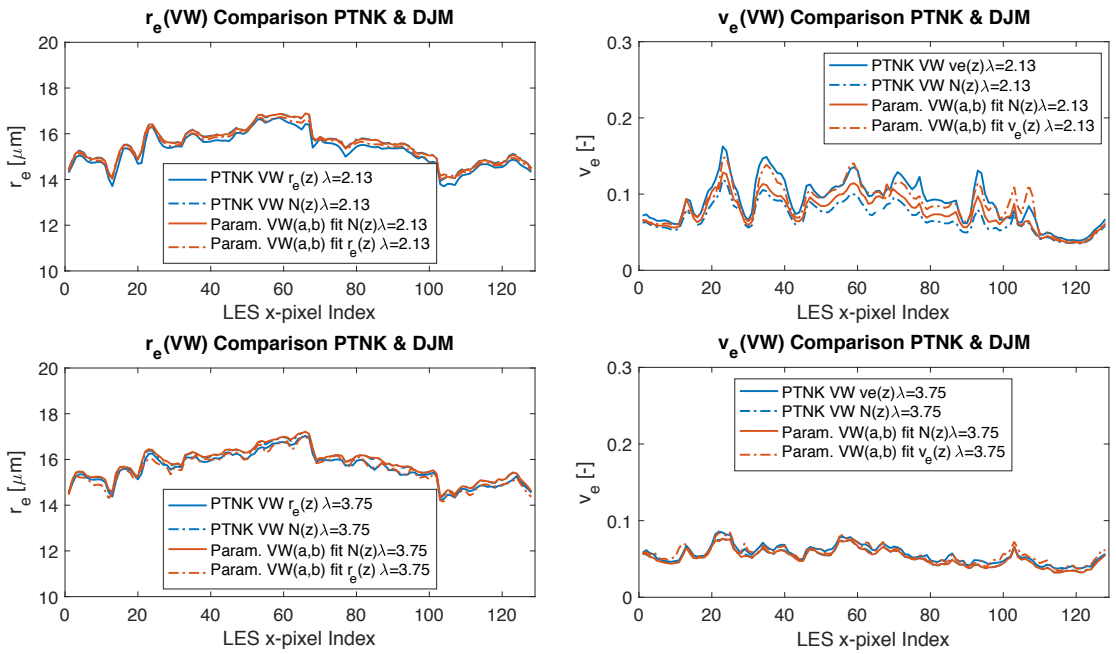

Figure 4: Similar to Figure 4, except the differences between Platnick vertical weighting (red) and the parametric vertical weighting (blue) are shown for both weighting of the profile of $r_e(z)$ (solid) and $N(z)$ (dashed). The left panels are for r_e in the 2.13 and 3.75 μm bands, while the right panels show v_e in the 2.13 and 3.75 μm bands. The case examined here corresponds to VZA=0, SZA=20, and RAA=30.

All results shown here have focused on a single solar and viewing geometry but, as indicated in Figure 1, the vertical weighting function is clearly dependent on observation geometry. The parameters of the parametric function should depend on observation geometry, and indeed they do, as shown in the figure 5.

The scattering angle dependence of these results is prominent. For the purposes of the vertical weighting functions used in our study, we have a table of values for a and b that accounts for spectral band, viewing zenith angle, solar zenith angle, and relative azimuth angle.

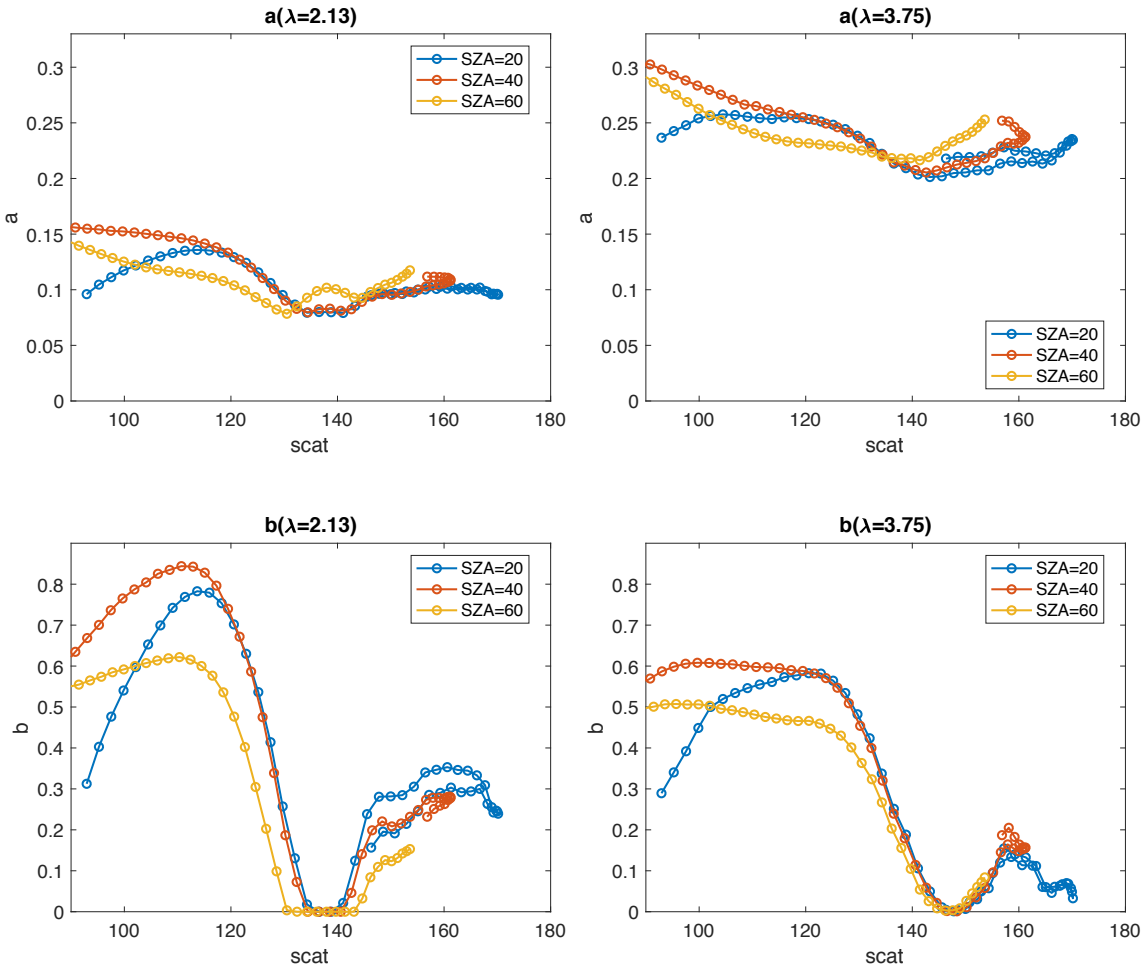

Figure 5: The median (scene aggregated) best-fit solutions for *a* and *b* plotted against scattering angle. The left and right columns examine parameters of the 2.13 and 3.75 µm weighting functions respectively. The top row corresponds to parameter *a*, while the bottom row corresponds to parameter *b*. Additionally, results for three solar zenith angles are shown: SZA=20º (blue), SZA=40º (red), and SZA=60º (yellow).

Updated Comparison of Retrievals and VW:

After all of this has been addressed, we can now again return to the comparison of the full LES vertically weighted dataset to the bispectral retrievals. The results of this comparison are shown in Figure 6. Broadly speaking these results are similar to those discussed in previous iterations of the vertical weighting. This is an indication that the particular vertical weighting definition is not the primary source of differences in these comparisons.

There are two modes in the joint histogram of the r_e(3.75 μm) histogram. The population with high biased r_e(3.75 μm) retrievals relative to VW belongs to the DYCOMS-II LES case and is associated with the impact of v_e on the r_e(3.75 μm) retrieval. The When v_e(pol) information is provided for the 3.75 μm bispectral retrieval – the vertically weighted result compares very well (as we showed previously for the transect in Figure 3). It should be noted that this feature was present, to a lesser extent, in previous vertical weighting iterations.

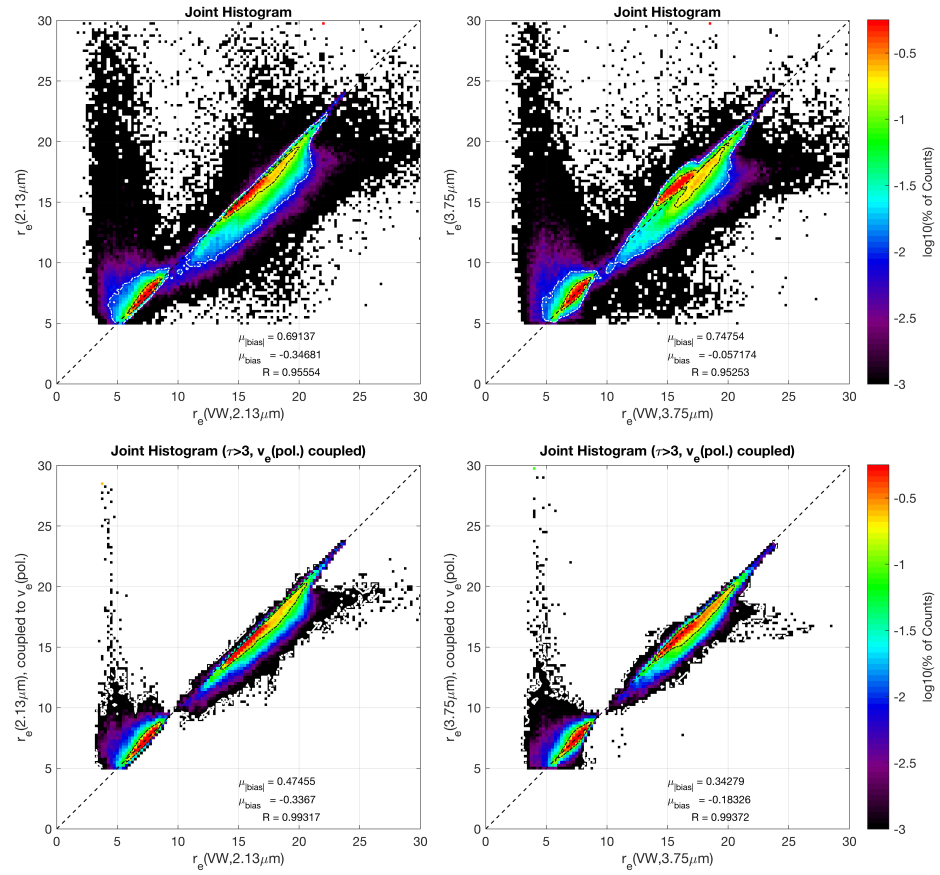

Figure 6: Joint histogram comparisons of bispectral retrievals of r_e (2.13 μm left column and 3.75 μm right column) against new vertically weighted r_e(VW). The top row is the full population, while the bottom row is restricted to the optically thick population and retrievals coupled to the polarimetric v_e retrieval.

Anonymous Referee #2

Submitted on 12 March, 2018

General remarks:

The authors responded sufficiently to most of my comments. However, the first of my minor comments is not addressed. For completeness, I repeat it here, with some updates and some elaboration:

Minor comments:

1. *In figure 4 (and 6), the cases with tau<3 are removed, revealing a better result. However, I am wondering how the 2D histogram for tau<3 looks like. Do the bulk of these retrievals still perform well, or are they all biased? That is not clear from these plots. It is obvious that the outliers are from the cases with tau<3, but the bulk of the results with tau<3 could still lay on the 1:1 line. Also, are the results getting increasingly 'bad' for decreasing tau? I am not asking for an extra figure in the paper, but some brief discussion about this would be good.*
    a. Apologies for missing this during the first response. Each histogram below is normalized with respect to the full population to demonstrate the reduced population of data. The results are shown in Figures 7-10 for different combinations of variables that were sub-selected throughout the study. **The short answer to your question is, no not all of the retrievals are biased, but nearly all of the extreme outliers belong to populations with very small optical thicknesses.** Additionally, less and less data lies near the 1:1 line with decreasing optical thickness, while the population of extreme outliers typically stays similar. Note that the figures here only show results for the 2.13 µm bispectral retrieval, but the results are similar for the 3.75 µm retrieval as well. We will add some discussion of how not all thin cloud retrievals belong to these extreme outlier populations. (Added on line 32 of page 11).

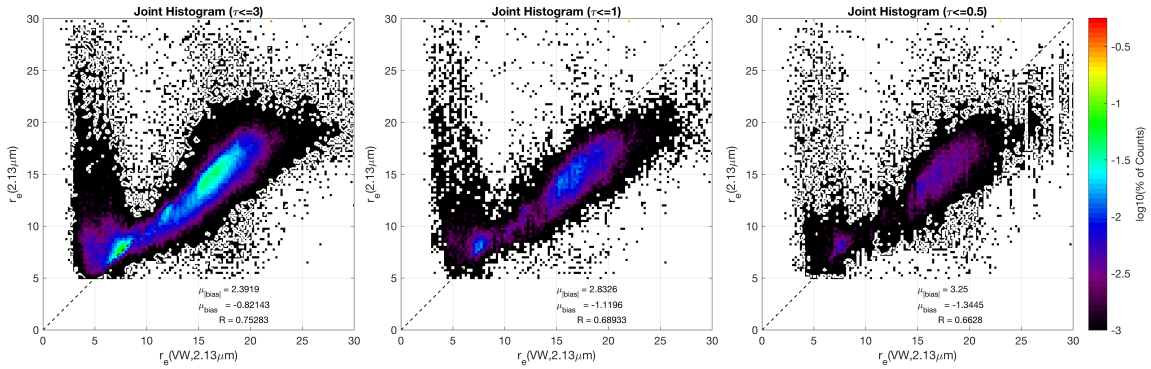

Figure 7: Joint histogram comparison of r_e(2.13 µm) against r_e(VW) for subpopulations of the full dataset. The left panel subselects tau<=3, the middle panel tau <=1, and the right panel tau<=0.5. Each histogram is normalized to the overall population.

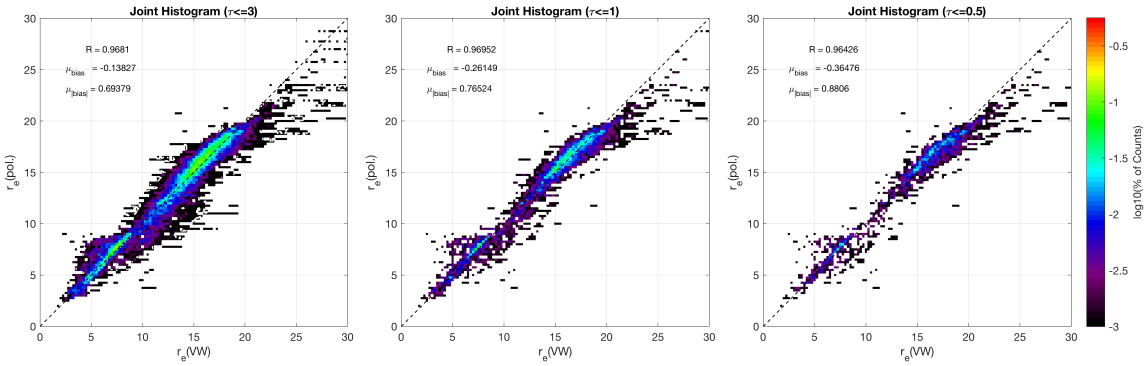

Figure 8: Joint histogram comparison of r_e(pol) against r_e(VW) for subpopulations of the full dataset. The left panel subselects tau<=3, the middle panel tau <=1, and the right panel tau<=0.5. Each histogram is normalized to the overall population.

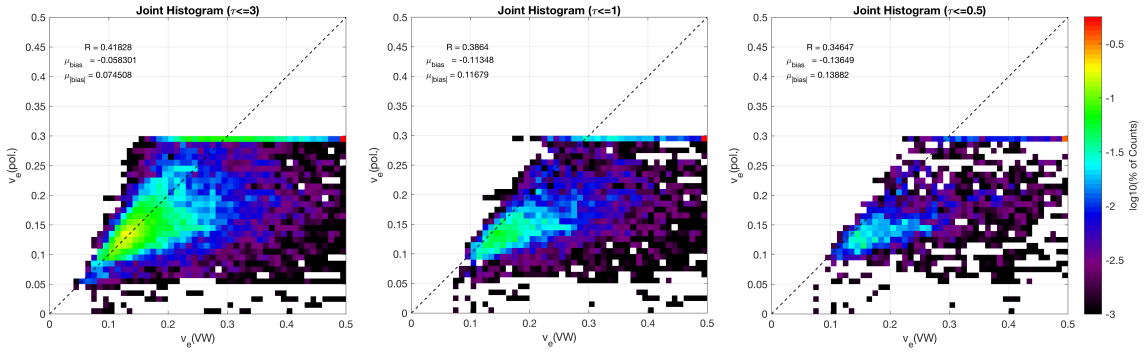

Figure 9: Joint histogram comparison of v_e(pol) against v_e(VW) for subpopulations of the full dataset. The left panel subselects tau<=3, the middle panel tau <=1, and the right panel tau<=0.5. Each histogram is normalized to the overall population.

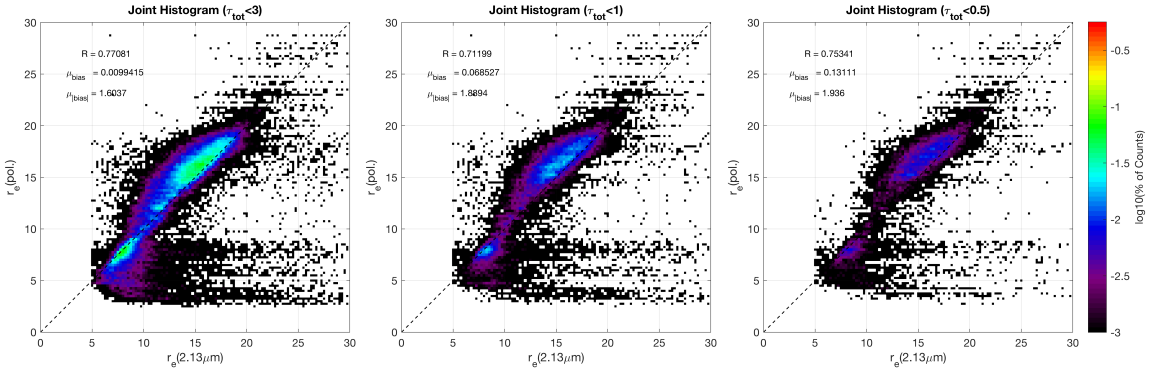

Figure 10:: Joint histogram comparison of r_e(2.13 µm) against r_e(pol) for subpopulations of the full dataset. The left panel subselects tau<=3, the middle panel tau <=1, and the right panel tau<=0.5. Each histogram is normalized to the overall population.

2. *One minor correction: On Page 6, line 27 it says*
   "In this study, we focus on three major sources of retrieval uncertainty for both techniques"
   The number is now five instead of three.
   a. Fixed it. Thanks for catching that.

AMT-2017-325_review_V2_FINAL_RVW_rnd2.docx

Main document changes and comments

Page 1: Inserted	Daniel Miller	1/29/18 10:43 AM

retrievals of marine boundary layer

Page 1: Inserted	Daniel Miller	1/29/18 10:43 AM

s

Page 1: Deleted	Daniel Miller	1/29/18 10:43 AM

al

Page 1: Inserted	Daniel Miller	1/29/18 10:43 AM

: Case studies

Page 1: Deleted	Daniel Miller	1/29/18 10:43 AM

retrievals

Page 1: Inserted	Daniel Miller	1/29/18 10:43 AM

a

Page 1: Inserted	Daniel Miller	1/29/18 10:44 AM

s

Page 1: Deleted	Daniel Miller	1/29/18 10:44 AM

S

Page 1: Inserted	Daniel Miller	3/4/18 5:03 PM

,3

Page 1: Deleted	Daniel Miller	3/4/18 5:04 PM

DJ-Miller@umbc.edu

Page 1: Inserted	Daniel Miller	3/4/18 5:04 PM

Daniel.J.Miller@nasa.gov

Page 1: Inserted	Daniel Miller	3/4/18 5:05 PM

a 1-D

Page 1: Deleted	Daniel Miller	3/4/18 5:05 PM

s

Page 1: Inserted	Daniel Miller	3/4/18 4:34 PM

h

Page 1: Deleted	Daniel Miller	3/4/18 4:34 PM

indeed h

Page 1: Inserted	Daniel Miller	3/4/18 9:19 PM

within expected observational uncertainties

Page 1: Inserted	Daniel Miller	3/4/18 9:20 PM

The relatively small systematic biases

Page 1: Deleted	Daniel Miller	3/4/18 9:20 PM

differences

Page 2: Inserted	Daniel Miller	2/13/18 2:53 PM

which

Page 2: Inserted	Steven Platnick	2/28/18 4:27 PM

typically

Page 2: Inserted	Steven Platnick	2/28/18 10:19 AM

or midwave infared (MWIR)

Page 2: Deleted	Daniel Miller	3/2/18 3:04 PM

2016

Page 2: Inserted	Daniel Miller	3/2/18 3:04 PM

2017

Page 2: Inserted	Daniel Miller	1/23/18 4:16 PM

Suomi

Page 2: Inserted	Daniel Miller	1/23/18 4:16 PM

Suomi

Page 2: Deleted	Steven Platnick	2/28/18 4:26 PM

vastly

Page 2: Inserted	Steven Platnick	2/28/18 4:26 PM

fundamentally

Page 3: Deleted	Daniel Miller	1/23/18 4:17 PM

Because

Page 3: Inserted	Daniel Miller	1/23/18 4:17 PM

The

Page 3: Deleted	Daniel Miller	3/4/18 11:41 AM

,

Page 3: Inserted	Daniel Miller	3/4/18 11:41 AM

. It is therefore essential

Page 3: Deleted	Daniel Miller	1/23/18 4:18 PM

it is important

Page 3: Deleted	Daniel Miller	1/23/18 4:18 PM

the

Page 3: Inserted	Daniel Miller	1/23/18 4:21 PM

between the two techniques

Page 3: Deleted	Daniel Miller	1/23/18 4:18 PM

between them

Page 3: Deleted	Daniel Miller	1/23/18 4:21 PM

the

Page 3: Inserted	Daniel Miller	1/23/18 4:21 PM

their respective

Page 3: Deleted	Daniel Miller	1/23/18 4:21 PM

of each technique

Page 3: Inserted	Daniel Miller	2/26/18 1:23 PM

Bréon and Doutriaux-Boucher (2005)

Page 3: Deleted	Daniel Miller	2/26/18 1:23 PM

Bréon and Doutriaux-Boucher (2005)

Page 3: Inserted	Steven Platnick	2/28/18 4:36 PM

2 µm

Page 3: Inserted	Steven Platnick	2/28/18 4:34 PM

150 km scale

Page 3: Deleted	Steven Platnick	2/28/18 4:36 PM

by about 2 µm

Page 3: Inserted	Daniel Miller	2/26/18 1:23 PM

Bréon and Doutriaux-Boucher (2005)

Page 3: Deleted	Daniel Miller	2/26/18 1:23 PM

Bréon and Doutriaux-Boucher (2005)

Page 3: Inserted	Daniel Miller	2/25/18 10:10 PM

how well

Page 3: Deleted	Daniel Miller	2/25/18 10:10 PM

whether

Page 3: Deleted	Daniel Miller	2/25/18 10:10 PM

well

Page 3: Inserted	Daniel Miller	2/25/18 10:10 PM

and what situations might cause them to differ

Page 3: Deleted	Daniel Miller	2/25/18 10:10 PM

or not

Page 3: Inserted	Daniel Miller	2/25/18 10:11 PM

and

Page 3: Deleted	Daniel Miller	2/25/18 10:11 PM

that

Page 3: Deleted	Daniel Miller	2/25/18 10:11 PM

e

Page 3: Inserted	Daniel Miller	2/25/18 10:11 PM

ing

Page 3: Inserted	Daniel Miller	3/2/18 3:54 PM

Zinner et al., 2010

Page 3: Deleted	Daniel Miller	3/2/18 3:55 PM

Miller et al., 2016

Page 3: Inserted	Daniel Miller	3/2/18 3:55 PM

; Miller et al., 2016

Page 3: Deleted	Daniel Miller	3/2/18 3:55 PM

; Zinner et al., 2010

Page 3: Inserted	Daniel Miller	2/27/18 9:34 AM

The scale of the LES simulations (~10 km) in this study prevents us from examining resolutions as large as the standard POLDER retrieval (~150 km), but we are able to advance understanding how spatial resolutions from 50 m to 1 km. These scales are suitable for airborne instrument comparisons, which certainly fall somewhere in this range.

Page 4: Inserted	Daniel Miller	3/2/18 4:06 PM

; Tampieri and Tomasi, 1976

Page 4: Deleted	Daniel Miller	3/2/18 4:06 PM

; Tampieri and Tomasi, 1976

Page 5: Inserted	Daniel Miller	2/14/18 10:20 AM

-

Page 5: Deleted	Daniel Miller	2/14/18 10:20 AM

Page 5: Inserted	Steven Platnick	2/28/18 10:13 AM

observed

Page 5: Inserted	Steven Platnick	2/28/18 10:13 AM

, typically

Page 5: Deleted	Steven Platnick	2/28/18 10:13 AM

observed in

Page 5: Inserted	Steven Platnick	2/28/18 4:36 PM

using a combination of

Page 5: Inserted	Steven Platnick	2/28/18 10:18 AM

/MWIR

Page 5: Deleted	Steven Platnick	2/28/18 10:13 AM

, respectively

Page 5: Inserted	Daniel Miller	1/29/18 10:45 AM

The VNIR band, dominated by multiple scattering

Page 5: Deleted	Steven Platnick	2/28/18 10:14 AM

dominated by multiple scattering

Page 5: Inserted	Steven Platnick	2/28/18 10:14 AM

with relatively negligible liquid water droplet absorption

Page 5: Inserted	Daniel Miller	1/29/18 10:45 AM

, and the SWIR/MWIR band, where liquid water droplets are moderately absorptive, can be used to remotely infer τ and r_e because of this difference in sensitivity to multiple scattering (thickness) and absorption (droplet size).

Page 5: Deleted	Steven Platnick	2/28/18 10:15 AM

liquid water

Page 5: Deleted	Daniel Miller	1/29/18 10:45 AM

The VNIR band, dominated by multiple scattering, provides sensitivity to τ; the selected SWIR band, where liquid water droplets are moderately absorptive, provides sensitivity to r_e.

Page 5: Inserted	Steven Platnick	2/28/18 10:16 AM

,

Page 5: Deleted	Steven Platnick	2/28/18 10:16 AM

like the one

Page 5: Inserted	Steven Platnick	2/28/18 10:16 AM

graphically

Page 5: Inserted	Daniel Miller	4/27/18 12:01 AM

Figure 1

Page 5: Deleted	Daniel Miller	3/4/18 4:40 PM

SWIR

Page 5: Inserted	Daniel Miller	3/4/18 4:40 PM

MWIR

Page 5: Deleted	Daniel Miller	3/4/18 4:50 PM

a priori

Page 5: Inserted	Steven Platnick	2/28/18 4:41 PM

, though it is kept as an error source in calculating pixel-level uncertainties

Page 5: Deleted	Daniel Miller	3/4/18 4:42 PM

VNIR and SWIR

Page 5: Deleted	Daniel Miller	3/4/18 4:43 PM

and

Page 5: Inserted	Daniel Miller	3/4/18 4:43 PM

with the second band is selected from either a 2.13 µm centered

Page 5: Inserted	Daniel Miller	3/4/18 4:41 PM

band

Page 5: Deleted	Daniel Miller	3/4/18 4:41 PM

reflectances centered on both

Page 5: Inserted	Daniel Miller	3/4/18 4:41 PM

or a

Page 5: Deleted	Daniel Miller	3/4/18 4:41 PM

2.13 and

Page 5: Deleted	Daniel Miller	3/4/18 4:42 PM

.

Page 5: Inserted	Daniel Miller	3/4/18 4:42 PM

centered MWIR band

Page 5: Deleted	Daniel Miller	3/4/18 4:43 PM

SWIR

Page 5: Inserted	Daniel Miller	3/4/18 4:43 PM

set of

Page 5: Inserted	Daniel Miller	3/4/18 4:43 PM

s

Page 5: Inserted	Daniel Miller	3/4/18 4:43 PM

SWIR/MWIR

Page 6: Deleted	Daniel Miller	2/14/18 10:21 AM

Page 6: Inserted	Daniel Miller	2/14/18 10:21 AM

-

Page 6: Inserted	Daniel Miller	4/27/18 12:01 AM

Figure 1

Page 6: Inserted	Daniel Miller	4/27/18 12:01 AM

Figure 1

Page 6: Inserted	Daniel Miller	4/27/18 12:01 AM

Figure 1

Page 6: Inserted	Daniel Miller	2/27/18 9:42 AM

Bréon and Goloub (1998)

Page 6: Inserted	Daniel Miller	2/14/18 10:21 AM

-

Page 6: Deleted	Daniel Miller	2/14/18 10:21 AM

Page 6: Inserted	Daniel Miller	3/4/18 4:51 PM

with a mean penetration depth of $<\tau_{ss}>\leq 0.5$

Page 6: Deleted	Daniel Miller	3/4/18 4:53 PM

within the top

Page 6: Inserted	Daniel Miller	3/4/18 4:53 PM

and sensitivity that saturates for optical depths greater than

Page 6: Deleted	Daniel Miller	3/4/18 4:56 PM

Page 6: Deleted	Daniel Miller	3/4/18 4:57 PM

optical depths

Page 6: Inserted	Daniel Miller	3/4/18 4:53 PM

from

Page 6: Deleted	Daniel Miller	3/4/18 4:53 PM

in

Page 6: Inserted	Daniel Miller	3/4/18 4:53 PM

top

Page 6: Inserted	Daniel Miller	2/26/18 1:23 PM

Alexandrov et al. (2012b)

Page 6: Deleted	Daniel Miller	2/26/18 1:23 PM

Alexandrov et al. (2012b)

Page 6: Inserted	Daniel Miller	2/26/18 1:23 PM

Alexandrov et al. (2012a)

Page 6: Deleted	Daniel Miller	2/26/18 1:23 PM

Alexandrov et al. (2012a)

Page 6: Deleted	Daniel Miller	3/5/18 10:18 AM

multi-modal

Page 6: Inserted	Daniel Miller	3/5/18 10:18 AM

with arbitrary mathematical form

Page 6: Deleted	Daniel Miller	3/30/18 11:11 AM

three

Page 6: Inserted	Daniel Miller	3/30/18 11:11 AM

five

Page 6: Deleted	Daniel Miller	4/26/18 6:57 PM

s

Page 7: Inserted	Daniel Miller	2/26/18 1:23 PM

Alexandrov et al., (2012b)

Page 7: Deleted	Daniel Miller	2/26/18 1:23 PM

Alexandrov et al. (2012b)

Page 7: Inserted	Daniel Miller	3/4/18 4:58 PM

took an approach that focused on the vertical weighting of the droplet size distribution

Page 7: Deleted	Daniel Miller	3/4/18 4:58 PM

modified this method slightly and applied it

Page 7: Deleted	Daniel Miller	4/11/18 11:37 AM

the

Page 7: Inserted	Daniel Miller	4/11/18 11:37 AM

a

Page 7: Inserted	Daniel Miller	4/11/18 11:37 AM

for

Page 7: Deleted	Daniel Miller	4/11/18 11:37 AM

method to

Page 7: Inserted	Daniel Miller	2/13/18 10:40 AM

2) Sensitivity to observational uncertainty: The uncertainties associated with observations of total and polarized reflectances can differ, indicating that uncertainty may also impact bispectral and polarimetric retrievals differently. Additionally, the two retrievals rely on different number of uncertain observations; a pair of uncertain total reflectances (bispectral) as compared to numerous uncertain polarized reflectances (polarimetric). Furthermore the different algorithmic approaches, two-dimensional interpolation vs. nonlinear optimal curve fitting introduce additional layers of complexity in terms of the impact of uncertainty. The impact of uncertainty on retrieval results for each method are highlighted and explored in section 4.2.

Page 7: Deleted	Daniel Miller	2/13/18 10:40 AM

2

Page 7: Inserted	Daniel Miller	2/13/18 10:40 AM

3

Page 7: Deleted	Daniel Miller	2/13/18 10:17 AM

2

Page 7: Inserted	Daniel Miller	2/13/18 10:39 AM

3

Page 7: Inserted	Daniel Miller	2/13/18 10:17 AM

Page 7: Deleted	Daniel Miller	2/13/18 10:40 AM

3

Page 7: Inserted	Daniel Miller	2/13/18 10:18 AM

4

Page 7: Deleted	Daniel Miller	2/13/18 10:17 AM

3

Page 7: Inserted	Daniel Miller	2/13/18 10:17 AM

4

Page 7: Deleted	Daniel Miller	4/26/18 6:10 PM

,

Page 7: Deleted	Daniel Miller	2/13/18 10:18 AM

4

Page 7: Inserted	Daniel Miller	2/13/18 10:18 AM

5

Page 7: Deleted	Daniel Miller	2/13/18 10:31 AM

Page 7: Deleted	Daniel Miller	2/13/18 10:17 AM

4

Page 7: Inserted	Daniel Miller	2/13/18 10:17 AM

5

Page 8: Deleted	Daniel Miller	3/4/18 4:26 PM

; Miller et al., 2016

Page 8: Inserted	Daniel Miller	3/4/18 4:26 PM

; Miller et al., 2016

Page 8: Inserted	Daniel Miller	2/8/18 2:19 PM

a

Page 8: Deleted	Daniel Miller	2/8/18 2:19 PM

the

Page 8: Inserted	Daniel Miller	2/8/18 2:20 PM

Page 8: Deleted	Daniel Miller	2/8/18 2:20 PM

ly fitting

Page 8: Inserted	Daniel Miller	2/8/18 2:20 PM

is then used to identify the

Page 9: Deleted	Daniel Miller	2/8/18 2:20 PM

corresponds

Page 9: Inserted	Daniel Miller	2/8/18 2:20 PM

corresponding

Page 9: Deleted	Daniel Miller	2/8/18 2:20 PM

to the resulting

Page 9: Deleted	Daniel Miller	2/13/18 10:50 AM

2WT

Page 9: Inserted	Daniel Miller	2/13/18 10:50 AM

VW

Page 9: Deleted	Daniel Miller	2/13/18 10:50 AM

2WT

Page 9: Inserted	Daniel Miller	2/13/18 10:50 AM

VW

Page 9: Inserted	Daniel Miller	3/4/18 12:30 PM

weighted (VW)

Page 9: Inserted	Daniel Miller	2/13/18 10:50 AM

vertical

Page 9: Deleted	Daniel Miller	3/4/18 12:30 PM

integration is weighte

Page 9: Inserted	Daniel Miller	3/4/18 12:30 PM

integration is weighted

Page 9: Deleted	Daniel Miller	3/4/18 12:30 PM

d

Page 9: Deleted	Daniel Miller	2/13/18 10:49 AM

two-way transmittance (2WT)

Page 9: Inserted	Daniel Miller	2/13/18 10:51 AM

and multiple scattering

Page 9: Deleted	Daniel Miller	2/13/18 10:49 AM

the

Page 9: Deleted	Daniel Miller	2/13/18 10:49 AM

single-scattered

Page 9: Inserted	Daniel Miller	2/13/18 10:50 AM

in the corresponding wavelength associated with each particular retrieval.

Page 9: Moved from page 9 (Move #1)	Daniel Miller	2/13/18 10:52 AM

Thus, r_e(VW) and v_e(VW) should be directly comparable to the numerically retrieved r_e and v_e from the simulated reflectance (Alexandrov et al., 20152b; Miller et al., 2016; Platnick, 2000; Zhang et al., 2017).

Page 9: Inserted	Daniel Miller	2/13/18 10:53 AM

r_e(VW) and v_e(VW) should be

Page 9: Deleted	Daniel Miller	3/4/18 12:49 PM

directly

Page 9: Deleted	Daniel Miller	2/26/18 6:37 PM

numerically

Page 9: Deleted	Daniel Miller	2/27/18 10:35 AM

5

Page 9: Inserted	Daniel Miller	2/27/18 10:35 AM

2b

Page 9: Deleted	Daniel Miller	3/4/18 12:51 PM

Platnick, 2000;

Page 9: Inserted	Daniel Miller	3/4/18 12:50 PM

7

Page 9: Inserted	Daniel Miller	2/13/18 10:51 AM

The method of vertical weighting in this study is described in detail in

Page 9: Moved from page 9 (Move #2)	Daniel Miller	2/13/18 10:53 AM

section 2 of Miller et al. (2016), however in this study we have modified the vertical weighting function to account for multiple scattering. Motivated by the convenience and flexibility of the parametric approach proposed in eq. 4 of Zhang et al. (2017), we implement a two-variable parametric vertical weighting function:

$$W(\tau) = c\tau^b \exp\left[-a\tau\left(\frac{1}{\mu}+\frac{1}{\mu_0}\right)\right], \quad (4)$$

Page 9: Inserted	Daniel Miller	2/13/18 10:54 AM

Miller et al. (2016), however in this study we have modified the vertical weighting function to account for multiple scattering. Motivated by the convenience and flexibility of the parametric approach proposed in eq. 4 of Zhang et al. (2017), we implement a two-variable parametric vertical weighting function:

Page 9: Inserted	Daniel Miller	2/13/18 11:00 AM

$$W(\tau) = c\tau^b \exp\left[-a\tau\left(\frac{1}{\mu}+\frac{1}{\mu_0}\right)\right]$$

Page 9: Inserted	Daniel Miller	2/13/18 11:00 AM

,

Page 9: Inserted	Daniel Miller	2/13/18 10:49 AM

where the new parameters a and b are introduced to account for the influence of multiple scattering effects not originally considered in the vertical weighting function discussed previously in Miller et al. (2016). The parameter a scales the optical depth, modelling the enhanced transmission caused by multiple scattering whereas the parameter b produces a peaked vertical weighting function associated with the expected penetration depth of the reflected light and c is the normalization factor. Each of these parameters is strictly positive, and for a=1 and b=0 we obtain the original single scattering vertical weighting used in Miller et al. (2016). For smaller values of a and larger values of b, the vertical weighting function extends deeper into the cloud, leading to droplet size distribution properties deeper in the cloud contributing more information to the vertically weighted value. For the polarimetric retrieval, a=1 and b=0 were selected due to the dominance of single scattering in polarized reflectances. In contrast, multiple scattering can significantly impact total reflectances. For total reflectances a single value of a and b was selected for each spectral band and observation geometry based on coefficients that fit best to numerically calculated vertical weighting functions based on the method presented in eq. 4 of Platnick (2000).[1] Generally, we found that a(3.75 μm) was larger than a(2.13 μm), as would be expected because of stronger absorption in 3.75 μm reducing transmission into the cloud. We also found that b was dependent on observation geometry (scattering angle) and b(3.75 μm) was less than b(2.13 μm) because multiply scattered light in the 2.13 μm band can penetrate deeper into the cloud before scattering back out.

Page 9: Deleted	Daniel Miller	2/13/18 11:11 AM

[1] The radiatively derived vertical weighting of Platnick (2000) implicitly depends on the $r_e(z)$ profile whereas a fixed parameter vertical weighting described here does not. However, the importance of this difference should be less than the vertical variability of optical depth or extinction cross section.

(at 0.865 μm). For a complete description on how vertical weighting is accounted for in the calculation of r_e(2WT) and v_e(2WT), see section 2 of (Miller et al., 2016). The r_e(2WT) and v_e(2WT) take into account the first-order sensitivity of the retrieval techniques to the vertical profile of clouds.

Page 9: Moved to page 9 (Move #2) **Daniel Miller** **2/13/18 10:53 AM**

section 2 of (Miller et al., 2016).

Page 9: Moved to page 9 (Move #1) **Daniel Miller** **2/13/18 10:52 AM**

Thus, they are directly comparable to the numerically retrieved r_e and v_e from the simulated reflectance (Alexandrov et al., 2015; Miller et al., 2016; Platnick, 2000; Zhang et al., 2010).

Page 9: Deleted **Daniel Miller** **2/13/18 1:11 PM**

. We note that the 2WT vertical weighting function provides a reasonable approximation when the signal is contributed mainly by single scattering (i.e., 3.7 μm or polarimetric reflectances) but becomes less accurate for spectral bands with more multiple scattering (Platnick, 2000).

Page 9: Deleted **Daniel Miller** **2/13/18 1:11 PM**

2WT

Page 9: Inserted **Daniel Miller** **2/13/18 1:11 PM**

VW

Page 9: Deleted **Daniel Miller** **2/13/18 1:11 PM**

2WT

Page 9: Inserted **Daniel Miller** **2/13/18 1:11 PM**

VW

Page 10: Inserted **Daniel Miller** **2/13/18 2:08 PM**

(for λ=0.865 μm)

Page 10: Deleted **Daniel Miller** **2/13/18 1:11 PM**

2WT

Page 10: Inserted **Daniel Miller** **2/13/18 1:11 PM**

VW

Page 10: Deleted **Daniel Miller** **2/13/18 1:11 PM**

2WT

Page 10: Inserted **Daniel Miller** **2/13/18 1:11 PM**

VW

Page 10: Inserted **Daniel Miller** **2/13/18 2:06 PM**

section 4.1

Page 10: Deleted **Daniel Miller** **2/13/18 1:11 PM**

2WT

Page 10: Inserted **Daniel Miller** **2/13/18 1:11 PM**

VW

Page 10: Deleted Daniel Miller 2/13/18 1:11 PM
2WT

Page 10: Inserted Daniel Miller 2/13/18 1:11 PM
VW

Page 10: Deleted Daniel Miller 2/13/18 1:11 PM
2WT

Page 10: Inserted Daniel Miller 2/13/18 1:11 PM
VW

Page 10: Deleted Daniel Miller 2/13/18 1:11 PM
2WT

Page 10: Inserted Daniel Miller 2/13/18 1:11 PM
VW

Page 10: Deleted Daniel Miller 2/13/18 1:11 PM
2WT

Page 10: Inserted Daniel Miller 2/13/18 1:11 PM
VW

Page 10: Deleted Daniel Miller 2/13/18 1:12 PM
2WT

Page 10: Inserted Daniel Miller 2/13/18 1:12 PM
VW

Page 10: Deleted Daniel Miller 3/4/18 12:58 PM
that have

Page 10: Inserted Daniel Miller 3/4/18 12:58 PM
with

Page 10: Deleted Daniel Miller 2/13/18 1:12 PM
small-scale

Page 10: Deleted Daniel Miller 2/13/18 1:12 PM
tion

Page 10: Inserted Daniel Miller 2/13/18 1:12 PM
bility in the unresolved

Page 10: Deleted Daniel Miller 2/27/18 9:44 AM
of DSD

Page 10: Inserted Daniel Miller 2/27/18 9:44 AM
microphysics,

Page 10: Deleted	Daniel Miller	2/27/18 9:45 AM

(

Page 10: Inserted	Daniel Miller	2/27/18 9:45 AM

Page 10: Deleted	Daniel Miller	2/27/18 9:45 AM

Shang et al. 2015),

Page 10: Deleted	Daniel Miller	2/13/18 1:13 PM

2WT

Page 10: Inserted	Daniel Miller	2/13/18 1:13 PM

VW

Page 10: Deleted	Daniel Miller	2/13/18 1:13 PM

2WT

Page 10: Inserted	Daniel Miller	2/13/18 1:13 PM

VW

Page 10: Inserted	Daniel Miller	3/4/18 12:59 PM

average

Page 10: Deleted	Daniel Miller	3/4/18 12:59 PM

the

Page 10: Inserted	Daniel Miller	2/26/18 1:23 PM

Stevens et al. (2005)

Page 10: Deleted	Daniel Miller	2/26/18 1:23 PM

Stevens et al. (2005)

Page 10: Inserted	Daniel Miller	2/26/18 1:23 PM

Ackerman et al. (2009)

Page 10: Deleted	Daniel Miller	2/26/18 1:23 PM

Ackerman et al. (2009)

Page 10: Inserted	Daniel Miller	2/26/18 1:23 PM

Fridlind and Ackerman (2011)

Page 10: Deleted	Daniel Miller	2/26/18 1:23 PM

Fridlind and Ackerman (2011)

Page 10: Inserted	Daniel Miller	4/27/18 12:01 AM

Figure 2

Page 10: Inserted	Daniel Miller	4/27/18 12:01 AM

Table 1

Page 11: Deleted	Daniel Miller	2/13/18 9:35 AM

at

Page 11: Inserted	Daniel Miller	2/13/18 9:35 AM

for

Page 11: Inserted	Daniel Miller	2/13/18 2:23 PM

pixel

Page 11: Inserted	Daniel Miller	4/27/18 12:01 AM

Table 1

Page 11: Inserted	Daniel Miller	2/13/18 9:35 AM

using the highest-resolution nadir viewing reflectances (50 m). The value of H_σ

Page 11: Deleted	Daniel Miller	2/13/18 9:35 AM

and

Page 11: Inserted	Daniel Miller	2/13/18 9:36 AM

sub-

Page 11: Inserted	Daniel Miller	2/13/18 9:39 AM

, making it a useful measure for unresolved cloud variability

Page 11: Deleted	Daniel Miller	2/13/18 1:15 PM

2WT

Page 11: Inserted	Daniel Miller	2/13/18 1:15 PM

VW

Page 11: Deleted	Daniel Miller	2/13/18 1:15 PM

2WT

Page 11: Inserted	Daniel Miller	2/13/18 1:15 PM

VW

Page 11: Deleted	Daniel Miller	2/13/18 1:15 PM

2WT

Page 11: Inserted	Daniel Miller	2/13/18 1:15 PM

VW

Page 11: Inserted	Daniel Miller	2/13/18 2:22 PM

to one another

Page 11: Deleted	Daniel Miller	2/13/18 2:22 PM

in this section

Page 11: Inserted	Daniel Miller	2/13/18 2:22 PM

must

Page 11: Deleted	Daniel Miller	2/8/18 2:16 PM

significantly

Page 11: Inserted	Daniel Miller	2/8/18 2:16 PM

naturally

Page 11: Inserted	Daniel Miller	2/13/18 9:43 AM

Note that the retrievals compared throughout the following sections are compared for all combinations of viewing and solar geometries indicated in the section 3.

Page 11: Inserted	Daniel Miller	4/27/18 12:01 AM

Figure 3

Page 11: Inserted	Daniel Miller	2/13/18 1:26 PM

s

Page 11: Deleted	Daniel Miller	3/4/18 4:44 PM

SWIR

Page 11: Deleted	Daniel Miller	2/13/18 1:37 PM

2WT

Page 11: Inserted	Daniel Miller	2/13/18 1:37 PM

VW

Page 11: Deleted	Daniel Miller	2/13/18 1:37 PM

2WT

Page 11: Inserted	Daniel Miller	2/13/18 1:37 PM

VW

Page 11: Inserted	Daniel Miller	2/26/18 9:53 AM

It is important to note that these joint histograms are presented as the logarithmic percent of the population, to emphasize deviations from the one-to-one line. Also, the mean regression biases reported throughout this study are stated relative to the plotted axes as, $\mu_{bias}=\langle y-x \rangle$ and $\mu_{|bias|}=\langle |y-x| \rangle$ (i.e., x and y denoting x and y axes).

Page 11: Inserted	Daniel Miller	4/27/18 12:01 AM

Figure 3

Page 11: Deleted	Daniel Miller	3/4/18 9:50 PM

Figure 3

Page 11: Deleted	Daniel Miller	4/26/18 9:18 PM

strong

Page 11: Inserted	Daniel Miller	4/26/18 9:18 PM

good

Page 11: Inserted	Daniel Miller	2/26/18 9:54 AM

Compared to the LES, both

Page 11: Inserted	Daniel Miller	2/26/18 9:55 AM

sub-micron mean biases

Page 11: Deleted	Daniel Miller	2/26/18 9:55 AM

mean biases of less than a micron compared to LES. The

Page 11: Inserted	Daniel Miller	2/26/18 9:55 AM

and the

Page 11: Deleted	Daniel Miller	2/26/18 9:55 AM

less than 1

Page 11: Inserted	Daniel Miller	2/26/18 9:55 AM

sub-micron.

Page 11: Deleted	Daniel Miller	2/26/18 9:55 AM

μm. Note that the mean regression biases reported throughout this study are stated relative to the plotted axes as, $\mu_{bias}=\langle y-x \rangle$ and $\mu_{|bias|}=\langle |y-x| \rangle$ (i.e., x and y denoting x and y axes).

Page 11: Inserted	Daniel Miller	2/26/18 9:57 AM

To examine the

Page 11: Deleted	Daniel Miller	2/26/18 9:56 AM

The

Page 11: Inserted	Daniel Miller	2/26/18 9:56 AM

Page 11: Inserted	Daniel Miller	4/27/18 12:01 AM

Figure 3

Page 11: Deleted	Daniel Miller	3/4/18 9:50 PM

Figure 3

Page 11: Deleted	Daniel Miller	2/26/18 9:56 AM

are

Page 11: Inserted	Daniel Miller	2/26/18 9:56 AM

we

Page 11: Deleted	Daniel Miller	2/26/18 9:57 AM

d

Page 11: Inserted	Daniel Miller	2/26/18 9:57 AM

them

Page 11: Deleted	Daniel Miller	2/26/18 9:57 AM

here

Page 11: Inserted	Daniel Miller	2/26/18 9:57 AM

, because the regression is so highly correlated (R>0.99)

Page 11: Deleted	Daniel Miller	2/26/18 9:58 AM

Each of these τ retrievals also reveal good correlations (R>0.99), despite a

Page 11: Inserted	Daniel Miller	2/26/18 9:58 AM

A

Page 11: Inserted	Daniel Miller	2/26/18 9:48 AM

systematic

Page 11: Inserted	Daniel Miller	2/26/18 9:58 AM

exists.

Page 11: Deleted	Daniel Miller	2/26/18 9:58 AM

.

Page 11: Inserted	Daniel Miller	2/14/18 11:20 AM

The origin of this high bias is likely associated with deviations of the droplet size distribution from the assumed gamma distribution form. The LES size distributions sometimes exhibit longer large-droplet tails than the assumed form.

Page 11: Deleted	Daniel Miller	2/14/18 11:20 AM

Page 11: Inserted	Daniel Miller	3/4/18 1:02 PM

from

Page 11: Inserted	Daniel Miller	2/26/18 10:00 AM

retrieval

Page 12: Inserted	Daniel Miller	2/26/18 10:00 AM

Therefore, if we

Page 12: Deleted	Daniel Miller	2/26/18 10:00 AM

By

Page 12: Deleted	Daniel Miller	2/26/18 10:00 AM

ing

Page 12: Inserted	Daniel Miller	2/26/18 10:00 AM

e

Page 12: Inserted	Daniel Miller	4/27/18 12:01 AM

Figure 3

Page 12: Deleted	Daniel Miller	3/4/18 9:50 PM

Figure 3

Page 12: Inserted	Daniel Miller	4/26/18 11:07 PM

While not all retrievals in the τ<3 population are biased, but the majority of extreme retrieval bias outliers belong to this thin cloud population. Even after this sub-selection of the data

Page 12: Deleted	**Daniel Miller**	**4/26/18 11:08 PM**

However,

Page 12: Inserted	**Daniel Miller**	**4/26/18 11:08 PM**

rs

Page 12: Deleted	**Daniel Miller**	**4/26/18 11:08 PM**

r

Page 12: Deleted	**Daniel Miller**	**4/26/18 11:08 PM**

points

Page 12: Inserted	**Daniel Miller**	**2/26/18 10:02 AM**

a small population of

Page 12: Deleted	**Daniel Miller**	**2/26/18 10:03 AM**

have some cases where

Page 12: Inserted	**Daniel Miller**	**2/26/18 10:03 AM**

retrievals

Page 12: Deleted	**Daniel Miller**	**2/26/18 10:04 AM**

the retrieved

Page 12: Inserted	**Daniel Miller**	**2/26/18 10:03 AM**

have biases

Page 12: Deleted	**Daniel Miller**	**2/26/18 10:03 AM**

values

Page 12: Inserted	**Daniel Miller**	**2/26/18 10:00 AM**

exceeding r_e(VW) by as much as 20

Page 12: Deleted	**Daniel Miller**	**2/26/18 10:01 AM**

(10 ~ 30

Page 12: Deleted	**Daniel Miller**	**2/26/18 10:02 AM**

) are substantially larger than the corresponding r_e(2WT) values (mostly around 5 μm)

Page 12: Deleted	**Daniel Miller**	**2/13/18 10:39 AM**

2

Page 12: Inserted	**Daniel Miller**	**2/13/18 10:39 AM**

3

Page 12: Inserted	**Daniel Miller**	**2/26/18 10:09 AM**

The polarimetric retrieval comparison to LES properties

Page 12: Deleted	Daniel Miller	2/26/18 10:09 AM

The joint histograms

Page 12: Inserted	Daniel Miller	4/27/18 12:01 AM

Figure 4

Page 12: Deleted	Daniel Miller	3/4/18 9:50 PM

Figure 4

Page 12: Inserted	Daniel Miller	2/26/18 10:10 AM

s

Page 12: Deleted	Daniel Miller	4/26/18 9:47 PM

, against corresponding LES properties

Page 12: Deleted	Daniel Miller	2/13/18 1:37 PM

2WT

Page 12: Inserted	Daniel Miller	2/13/18 1:37 PM

VW

Page 12: Inserted	Daniel Miller	4/27/18 12:01 AM

Figure 4

Page 12: Deleted	Daniel Miller	3/4/18 9:50 PM

Figure 4

Page 12: Inserted	Daniel Miller	2/26/18 10:11 AM

,

Page 12: Deleted	Daniel Miller	2/26/18 10:11 AM

and

Page 12: Inserted	Daniel Miller	2/26/18 10:13 AM

further

Page 12: Inserted	Daniel Miller	2/26/18 10:12 AM

single scattering

Page 12: Deleted	Daniel Miller	2/13/18 1:37 PM

2WT

Page 12: Inserted	Daniel Miller	2/13/18 1:37 PM

VW

Page 12: Inserted	Daniel Miller	2/26/18 10:12 AM

for

Page 12: Deleted	Daniel Miller	2/26/18 10:12 AM

, as

Page 12: Deleted	Daniel Miller	2/26/18 10:13 AM

retrieval

Page 12: Inserted	Daniel Miller	2/26/18 10:13 AM

retrieval

Page 12: Deleted	Daniel Miller	2/26/18 10:12 AM

is indeed well represented by the single-scattering “2WT” vertical weighting

Page 12: Deleted	Daniel Miller	2/13/18 1:37 PM

2WT

Page 12: Inserted	Daniel Miller	2/13/18 1:37 PM

VW

Page 12: Inserted	Daniel Miller	4/27/18 12:01 AM

Figure 4

Page 12: Deleted	Daniel Miller	3/4/18 9:50 PM

Figure 4

Page 12: Inserted	Daniel Miller	2/27/18 9:47 AM

R=

Page 12: Deleted	Daniel Miller	4/26/18 9:49 PM

62

Page 12: Inserted	Daniel Miller	4/26/18 9:49 PM

71

Page 12: Inserted	Daniel Miller	4/26/18 9:49 PM

1

Page 12: Deleted	Daniel Miller	4/26/18 9:49 PM

3

Page 12: Deleted	Daniel Miller	2/13/18 1:37 PM

2WT

Page 12: Inserted	Daniel Miller	2/13/18 1:37 PM

VW

Page 12: Inserted	Daniel Miller	2/27/18 2:24 AM

. It should also be noted that the increased concentration of v_e(pol) retrievals at v_e=0.3 is a result of the boundaries of the retrieval space, v_e=[0.01, 0.3]. The upper limit of which is a consequence of the gamma distribution of Hansen and Travis (1974) becoming monotonic for $v_e \geq 0.3$.

Page 12: Deleted	Daniel Miller	2/13/18 9:46 AM

(footnote 1).

Page 12: Deleted	Daniel Miller	2/13/18 1:37 PM

2WT

Page 12: Inserted	Daniel Miller	2/13/18 1:37 PM

VW

Page 12: Inserted	Daniel Miller	2/27/18 9:49 AM

R=

Page 12: Deleted	Daniel Miller	2/27/18 9:49 AM

0.86

Page 12: Inserted	Daniel Miller	2/27/18 9:49 AM

0.81

Page 12: Inserted	Daniel Miller	3/5/18 10:16 AM

The v_e retrieval quality also depends on the assumption that LES droplet size distributions are accurately described using a single-mode gamma distribution. The DSD's in the LES sometimes deviate significantly from this assumption. In the context of the parametric polarimetric retrieval used in this study this is difficult to remedy or address. However, a different polarimetric retrieval, the Rainbow Fourier Transform (RFT) introduced in Alexandrov et al. (2012a) offers the possibility of retrieving an arbitrary droplet size distribution shape.

Page 12: Inserted	Daniel Miller	4/27/18 12:01 AM

Figure 4

Page 12: Deleted	Daniel Miller	3/4/18 9:50 PM

Figure 4

Page 12: Inserted	Daniel Miller	2/25/18 10:10 AM

a

Page 12: Deleted	Daniel Miller	2/25/18 10:10 AM

s

Page 12: Deleted	Daniel Miller	2/25/18 10:10 AM

have

Page 12: Inserted	Daniel Miller	2/25/18 10:10 AM

has

Page 12: Inserted	Daniel Miller	2/14/18 10:29 AM

,

[1] The increased concentration of v_e(pol) retrievals at v_e=0.3. is a result of the boundaries of the retrieval space, v_e=[0.01, 0.3]. This limitation is a consequence of the definition of the modified gamma distribution in Hansen and Travis (1974); for v_e=0.3 the size distribution becomes monotonic.

Page 12: Deleted	Daniel Miller	2/14/18 10:27 AM

,

Page 12: Inserted	Daniel Miller	2/14/18 10:29 AM

, a finding that is consistent with previous work (Alexandrov et al., 2012b)

Page 12: Deleted	Daniel Miller	2/13/18 1:37 PM

2WT

Page 12: Inserted	Daniel Miller	2/13/18 1:37 PM

VW

Page 12: Inserted	Daniel Miller	4/27/18 12:01 AM

Figure 4

Page 12: Deleted	Daniel Miller	3/4/18 9:50 PM

Figure 4

Page 12: Inserted	Daniel Miller	3/5/18 10:14 AM

Page 12: Inserted	Daniel Miller	4/27/18 12:01 AM

Figure 4

Page 12: Deleted	Daniel Miller	3/4/18 9:50 PM

Figure 4

Page 12: Deleted	Daniel Miller	2/13/18 1:37 PM

2WT

Page 12: Inserted	Daniel Miller	2/13/18 1:37 PM

VW

Page 12: Inserted	Daniel Miller	4/27/18 12:01 AM

Figure 4

Page 12: Deleted	Daniel Miller	3/4/18 9:50 PM

Figure 4

Page 12: Inserted	Daniel Miller	2/8/18 2:42 PM

4.2 Sensitivity to Measurement Uncertainty

The measurement uncertainties of total and polarized reflectances differ, leading one to expect that bispectral and polarimetric retrievals may have different sensitivities to uncertainty. Their relationships to uncertainty are further complicated by differences in retrieval approaches; namely interpolating two independent uncertain observations in a LUT (bispectral) or curve fitting through numerous observations that are each independently uncertain (polarimetric). Targeted uncertainties for cloud and aerosol remote

sensing are δDOLP=0.5% in degree of linear polarization and δI=3% in total reflectance (Knobelspiesse et al., 2012). A simple propagation of uncertainty analysis yields a polarized reflectance uncertainty of δQ=2.5% (in the principal plane). Using these uncertainties as a starting point, we can perturb the LES reflectances with uncorrelated random noise and perform retrievals that we can then compare to the original unperturbed retrievals. Note that while the focus here is on uncorrelated randomly distributed noise, other sources of observational uncertainty exist and would need to be accounted for in the context of a specific instruments' uncertainty model. As the properties of particular instruments are not the focus of this study, we will focus on this more general uncertainty analysis.

For the bispectral retrieval, a randomly distributed reflectance perturbation between +/-3% was added to each LES reflectance. A histogram of the percent bias of bispectral retrievals of r_e induced by the addition of the reflectance uncertainty is shown in Figure 5(a). The mean and standard deviation of these bias distributions are stated, allowing us to interpret the results. First, the introduction of uncertainty has very little impact on the mean bias of bispectral r_e retrievals (on the order of 0.1%). Second, the introduction of uncertainty results in a broad distribution of r_e retrieval biases with standard deviations of 5.44% and 4.02% for the 2.13μm and 3.75μm retrievals respectively. Together these two results indicate that biases associated with measurement uncertainty will not be systematic, with absolute variability on the order of 1 μm or less for droplet sizes below 20 μm (the most prevalent population in this LES study). The impact of observational uncertainty on all of the τ retrievals is the focus of Figure 5(b). The two bispectral retrievals, τ(2.13μm) and τ(3.75), each have very minimal mean biases of 0.1%. However, like the biases for the effective radius retrievals, the distribution of retrieval bias is broadened to standard deviations of 8.2% and 5.6% for τ(2.13μm) and τ(3.75) respectively. The polarimetric τ(pol) retrieval on the other hand, being methodically quite similar to the bispectral retrievals, exhibits a small systematic low bias of about -2.43% as shown in Figure 5(b). The origin of this systematic bias is a known characteristic of single-band optical thickness retrievals, and is clearly demonstrated in figure 1 of Marshak et al. (2006). The convexity of a single-band LUT curve produces low-biased retrievals for symmetrically distributed (or averaged) reflectances. The bias distribution also has a smaller variability (3.8%) than the two bispectral retrievals, likely because the uncertainty in the SWIR/MWIR band also (weakly) influences the bispectral τ bias distributions.

The consequences of measurement uncertainty are markedly different for the polarimetric retrieval. This is a result of the polarimetric retrieval being a search for a similar curve in the phase function library, making the deviations in the magnitude of observations in any one angle less important when searching for the optimal curve – and therefore discrete r_e and v_e combination. The discretely binned nature of the polarimetric retrieval makes description of bias distributions like the ones in Figure 5 problematic. One way to describe how uncertainty in polarized reflectances influences polarimetric retrievals is to describe the population of retrievals that are unchanged, and the population of retrievals that changed. After the introduction of random noise 88.1% of the polarimetric r_e(pol) retrievals were unbiased, with 9.1% biased high by one grid point (+0.25 μm) and 2.7% biased low by one grid point (-0.25 μm). All together,

these three populations accounted for the vast majority (99.9%) of retrieval outcomes. The percent bias of the r_e(pol) retrieval had a mean of 0.06% and a standard deviation of 0.78%. These results agree with previous studies, for example the finding of Shang et al. (2015) indicating that the POLDER retrieval performed well as long as reflectance uncertainty was less than 10%. It should be noted however that the sensitivity to uncertainty is also tied to the number of angular measurements available, and the properties of the droplet size distribution. The polarimetric v_e(pol) retrievals behaved similarly, with 85.2% of all retrievals being unaffected, 12.7% were biased high by one grid point (+0.01) and 1.9% were biased low by one grid point (-0.01). Again, these three populations account for the vast majority of (99.9%) of retrieval outcomes. The percent bias of the ve pol retrieval had a mean of 1.14%, consistent with a 0.01 bias and a standard deviation of 22.6%. The greater tendency toward large biases for the effective variance is likely due to smoothing of polarized reflectance curves after the addition of uncertainty. The large majority of biases in the polarimetric retrieval of v_e are coming from the population of v_e near 0.1-0.15 where the supernumerary bow peaks are significantly eroded and small shifts in the magnitude of reflectances at angles near these peaks could easily shift the retrieval to the next grid point.

Overall, the lack of strong systematic biases associated with uncertainty in the case of either retrieval supports an approach of neglecting the measurement uncertainty in further analyses. Of course, this requires acknowledging that biases that are below δr_e=5%, δv_e=10%, or $\delta\tau$=7% in either retrieval are probably not as important because they likely are not detectable due to observational uncertainty.

Page 14: Deleted	**Daniel Miller**	**2/13/18 10:16 AM**

2

Page 14: Inserted	**Daniel Miller**	**2/13/18 10:16 AM**

3

Page 14: Inserted	**Daniel Miller**	**2/13/18 10:16 AM**

In practice, most observational studies do not have access to the underlying cloud properties with which to compare, so instead different instruments and techniques are often compared to one another.

Page 14: Inserted	**Daniel Miller**	**2/13/18 2:40 PM**

a

Page 14: Deleted	**Daniel Miller**	**2/13/18 2:40 PM**

s

Page 14: Inserted	**Daniel Miller**	**2/26/18 9:46 AM**

is possible,

Page 14: Inserted	**Daniel Miller**	**3/4/18 1:54 PM**

providing an opportunity to

Page 14: Deleted	**Daniel Miller**	**3/4/18 1:55 PM**

offer the possibility of diagnosing

Page 14: Inserted	**Daniel Miller**	**3/4/18 1:55 PM**

diagnose

Page 14: Inserted	Daniel Miller	4/27/18 12:01 AM

Figure 6

Page 14: Deleted	Daniel Miller	2/24/18 12:28 PM

Figure 5

Page 14: Inserted	Daniel Miller	4/27/18 12:01 AM

Figure 6

Page 14: Deleted	Daniel Miller	2/24/18 12:28 PM

Figure 5

Page 14: Deleted	Daniel Miller	2/26/18 6:20 PM

4

Page 14: Inserted	Daniel Miller	3/4/18 4:44 PM

/MWIR

Page 15: Inserted	Daniel Miller	4/27/18 12:01 AM

Figure 6

Page 15: Deleted	Daniel Miller	2/24/18 12:28 PM

Figure 5

Page 15: Inserted	Daniel Miller	3/5/18 1:05 AM

This serves as a test of how collocated bispectral and polarimetric retrievals might assist one another.

Page 15: Deleted	Daniel Miller	4/26/18 10:02 PM

coupled the selection of the

Page 15: Inserted	Daniel Miller	4/26/18 10:02 PM

created a

Page 15: Deleted	Daniel Miller	4/26/18 10:39 PM

Page 15: Inserted	Daniel Miller	4/26/18 10:03 PM

for different

Page 15: Deleted	Daniel Miller	4/26/18 10:03 PM

to the

Page 15: Inserted	Daniel Miller	4/26/18 10:02 PM

values of

Page 15: Deleted	Daniel Miller	4/26/18 10:02 PM

pixel-by-pixel value, thus making sure that the respective LUT had a matching

Page 15: Inserted	Daniel Miller	4/26/18 10:03 PM

and then selected a different LUT for each pixel depending on

Page 15: Deleted	Daniel Miller	4/26/18 10:03 PM

to

Page 15: Inserted	Daniel Miller	4/26/18 10:03 PM

coupled

Page 15: Inserted	Daniel Miller	4/27/18 12:01 AM

Figure 6

Page 15: Deleted	Daniel Miller	2/24/18 12:28 PM

Figure 5

Page 15: Inserted	Daniel Miller	4/27/18 12:01 AM

Figure 6

Page 15: Deleted	Daniel Miller	2/24/18 12:28 PM

Figure 5

Page 15: Inserted	Daniel Miller	4/26/18 10:08 PM

.

Page 15: Deleted	Daniel Miller	4/26/18 10:08 PM

, improving

Page 15: Inserted	Daniel Miller	4/26/18 10:41 PM

The coupled 3.75 μm result has an increased

Page 15: Deleted	Daniel Miller	4/26/18 10:06 PM

the

Page 15: Inserted	Daniel Miller	4/26/18 10:06 PM

,

Page 15: Deleted	Daniel Miller	4/26/18 10:05 PM

and reducing the small

Page 15: Inserted	Daniel Miller	4/26/18 10:06 PM

an order of magnitude smaller

Page 15: Deleted	Daniel Miller	4/26/18 10:06 PM

systematic low

Page 15: Deleted	Daniel Miller	4/26/18 10:08 PM

~

Page 15: Deleted	Daniel Miller	4/26/18 10:04 PM

25

Page 15: Inserted	Daniel Miller	4/26/18 10:04 PM

008

Page 15: Inserted **Daniel Miller** **4/26/18 10:07 PM**

, and an absolute bias that is half as large as the original comparison (0.24 μm)

Page 15: Inserted **Daniel Miller** **4/26/18 10:00 PM**

cloud

Page 15: Inserted **Daniel Miller** **4/26/18 10:41 PM**

In the context of measurement uncertainty, as discussed in section 4.2, this effect would be below retrieval uncertainty.

Page 15: Deleted **Daniel Miller** **4/26/18 10:43 PM**

Page 15: Inserted **Daniel Miller** **4/26/18 10:42 PM**

Overall,

Page 15: Deleted **Daniel Miller** **4/26/18 10:47 PM**

The

Page 15: Inserted **Daniel Miller** **4/26/18 10:49 PM**

this demonstrates

Page 15: Deleted **Daniel Miller** **4/26/18 10:49 PM**

slight improvement demonstrates that

Page 15: Inserted **Daniel Miller** **4/26/18 10:49 PM**

that

Page 15: Deleted **Daniel Miller** **4/26/18 10:49 PM**

information

Page 15: Inserted **Daniel Miller** **4/26/18 10:47 PM**

very

Page 15: Inserted **Daniel Miller** **4/26/18 10:47 PM**

, with only slight differences leading to $r_e(2.13\mu m)<r_e(3.75\mu m)<r_e(pol)$ as would be expected based on an increasing droplet size vertical profile and vertical weighting

Page 15: Inserted **Daniel Miller** **4/26/18 10:53 PM**

.

Page 15: Deleted **Daniel Miller** **4/26/18 10:53 PM**

, where such small droplets make up about 5% of the LES scene[1].

Page 15: Deleted **Daniel Miller** **4/26/18 10:53 PM**

Page 15: Inserted **Daniel Miller** **4/26/18 10:53 PM**

3.5%

[1] Additionally, ~12.5% of the cloudy pixels in this scene exhibit values below 4 μm.

Page 15: Deleted	Daniel Miller	4/26/18 10:53 PM

5% of the cloudy pixels (as defined by $\tau_{LES}>0.1$) in

Page 15: Inserted	Daniel Miller	4/26/18 10:54 PM

of

Page 15: Inserted	Daniel Miller	4/26/18 10:54 PM

scene

Page 15: Deleted	Daniel Miller	4/26/18 10:54 PM

scene

Page 15: Deleted	Daniel Miller	2/13/18 1:38 PM

2WT

Page 15: Inserted	Daniel Miller	2/13/18 1:38 PM

VW

Page 15: Inserted	Daniel Miller	4/26/18 10:54 PM

[1]

Page 16: Deleted	Daniel Miller	4/26/18 10:52 PM

covers

Page 16: Inserted	Daniel Miller	4/26/18 10:52 PM

spans

Page 16: Inserted	Daniel Miller	4/26/18 10:52 PM

spans

Page 16: Deleted	Daniel Miller	4/26/18 10:52 PM

covers

Page 16: Inserted	Daniel Miller	4/27/18 12:01 AM

Figure 7

Page 16: Deleted	Daniel Miller	2/24/18 12:28 PM

Figure 6

Page 16: Inserted	Daniel Miller	3/4/18 4:45 PM

bispectral

Page 16: Deleted	Daniel Miller	3/4/18 4:45 PM

r_e(SWIR)–r_e(2WT)

Page 16: Inserted	Daniel Miller	4/27/18 12:01 AM

Figure 7

Page 16: Deleted	Daniel Miller	2/24/18 12:28 PM

[1] Additionally, ~1% of the cloudy pixels in this scene exhibit values below 4 μm.

Figure 6

Page 16: Deleted	Daniel Miller	4/26/18 10:55 PM

Page 16: Inserted	Daniel Miller	4/27/18 12:01 AM

Figure 8

Page 16: Deleted	Daniel Miller	2/24/18 12:28 PM

Figure 7

Page 16: Deleted	Daniel Miller	2/13/18 10:16 AM

3

Page 16: Inserted	Daniel Miller	2/13/18 10:16 AM

4

Page 16: Deleted	Daniel Miller	2/14/18 3:30 PM

affects

Page 16: Inserted	Daniel Miller	2/14/18 3:30 PM

influences

Page 16: Inserted	Daniel Miller	2/14/18 3:31 PM

Even for 100% cloudy pixels

Page 16: Deleted	Daniel Miller	2/14/18 3:31 PM

These

Page 16: Inserted	Daniel Miller	2/14/18 3:31 PM

these

Page 16: Inserted	Daniel Miller	2/14/18 3:31 PM

can

Page 16: Deleted	Daniel Miller	2/14/18 3:31 PM

different

Page 16: Deleted	Daniel Miller	2/14/18 3:32 PM

ies

Page 16: Inserted	Daniel Miller	2/14/18 3:32 PM

y

Page 16: Deleted	Daniel Miller	2/14/18 3:31 PM

even for 100% cloudy pixels

Page 16: Inserted	Daniel Miller	2/14/18 12:53 PM

This section focuses on the ATEX cases because they exhibit a broader distribution of H_{σ}, allowing us to highlight the impact of spatial inhomogeneity on retrievals.

Page 16: Deleted	Daniel Miller	2/14/18 12:54 PM

As coarsened s

Page 16: Inserted	Daniel Miller	2/14/18 12:54 PM

S

Page 16: Deleted	Daniel Miller	2/14/18 12:54 PM

the

Page 16: Deleted	Daniel Miller	2/24/18 8:25 PM

correlated

Page 16: Inserted	Daniel Miller	2/24/18 8:25 PM

intertwined

Page 16: Inserted	Daniel Miller	2/14/18 12:55 PM

r. This is demonstrated in

Page 16: Deleted	Daniel Miller	2/14/18 12:55 PM

r, so our comparisons here address these two properties simultaneously. To that end,

Page 16: Inserted	Daniel Miller	2/14/18 12:55 PM

Figure 9, where the broadening and shifting of the distribution of H_σ for increasingly coarsened spatial resolutions is clearly demonstrated using data from both the ATEX clean and polluted cases. In light of this relationship between resolution and inhomogeneity, the inclusion of data from all spatial resolutions together broadens our sampling of different inhomogeneity regimes. To that end, Figure 10 combines all of the coarse spatial resolution data from the two ATEX cases into a single retrieval bias histogram. For the bispectral retrievals in Figure 10 (a,b) we compare to the polarimetric retrieval, resulting in histograms that clearly show the two retrievals diverging from one another with increasing sub-pixel inhomogeneity, tends to result in larger biases. In contrast, the polarimetric r_e(pol) retrieval in Figure 10 (c) does not appear to have a clear systematic bias. The v_e(pol) retrieval in Figure 10 (d) tells a more complicated story, the median value of the bias is clearly close to zero, but there is a tendency toward low biased retrievals with increasing inhomogeneity. It should be noted that the v_e(VW) itself increases with increasing H_σ, which is presumably a consequence of the anticorrelation between τ and v_e(VW). This might explain why for large values of H_σ, where the v_e(VW)>0.15 population is more common, there are more negative biases.

Page 17: Deleted	Daniel Miller	2/14/18 3:39 PM

panels (a) and (b) of Figure 8 compare r_e(pol) to the r_e(2.13 μm) and r_e(3.75 μm) respectively at increasingly coarsened spatial resolutions (as indicated by the size of the circles). In addition to the spatial resolution, these plots also indicate the magnitude the of sub-pixel inhomogeneity index (H_σ) (as indicated by the color of the circles). It is evident that as the spatial retrieval footprint reaches 800 m the sub-pixel inhomogeneity tends to increase and the r_e(2.13 μm) retrieval suffers from an increasingly high bias relative to the polarimetric retrieval. The presence of this behavior is less pronounced for in the r_e(3.7 μm) comparison is lower, although the trend is still clearly present.

Page 17: Inserted	Daniel Miller	2/14/18 3:21 PM

further emphasize how

Page 17: Deleted	Daniel Miller	2/24/18 8:34 PM

probe how

Page 17: Inserted	Daniel Miller	2/26/18 12:38 PM

can influence

Page 17: Deleted	Daniel Miller	2/26/18 12:38 PM

influences

Page 17: Inserted	Daniel Miller	2/24/18 8:34 PM

highlight

Page 17: Deleted	Daniel Miller	2/24/18 8:34 PM

examine

Page 17: Inserted	Daniel Miller	2/14/18 3:40 PM

the coarsest resolution

Page 17: Deleted	Daniel Miller	2/14/18 3:40 PM

a very coarse resolution

Page 17: Inserted	Daniel Miller	4/27/18 12:01 AM

Figure 11

Page 17: Deleted	Daniel Miller	2/24/18 12:28 PM

Figure 9

Page 17: Inserted	Daniel Miller	2/24/18 12:10 PM

are largely homogeneous in this

Page 17: Deleted	Daniel Miller	2/24/18 12:10 PM

of this

Page 17: Deleted	Daniel Miller	2/24/18 12:10 PM

are largely homogeneous

Page 17: Deleted	Daniel Miller	2/13/18 1:38 PM

2WT

Page 17: Inserted	Daniel Miller	2/13/18 1:38 PM

VW

Page 17: Deleted	Daniel Miller	2/13/18 1:38 PM

2WT

Page 17: Inserted	Daniel Miller	2/13/18 1:38 PM

VW

Page 17: Deleted	Daniel Miller	4/26/18 10:56 PM

23

Page 17: Inserted	Daniel Miller	4/26/18 10:56 PM

71

Page 17: Inserted	Daniel Miller	2/24/18 8:51 PM

(shown in Figure 11Figure (b))

Page 17: Deleted	Daniel Miller	2/25/18 8:47 PM

Figure

Page 17: Inserted	Daniel Miller	4/26/18 10:57 PM

-

Page 17: Deleted	Daniel Miller	4/26/18 10:57 PM

Page 17: Inserted	Daniel Miller	4/26/18 10:57 PM

space

Page 17: Inserted	Daniel Miller	2/16/18 1:04 PM

. This can be demonstrated with

Page 17: Deleted	Daniel Miller	2/16/18 1:04 PM

, as shown in

Page 17: Inserted	Daniel Miller	4/27/18 12:01 AM

Figure 11

Page 17: Deleted	Daniel Miller	2/24/18 12:28 PM

Figure 9

Page 17: Deleted	Daniel Miller	2/26/18 12:58 PM

demonstrate

Page 17: Inserted	Daniel Miller	2/26/18 12:58 PM

create

Page 17: Deleted	Daniel Miller	2/26/18 12:58 PM

the

Page 17: Inserted	Daniel Miller	2/26/18 12:58 PM

a

Page 17: Deleted	Daniel Miller	2/26/18 12:58 PM

50 m sub-pixel

Page 17: Inserted	Daniel Miller	2/26/18 12:58 PM

for the 50 m sub-pixels

Page 17: Deleted	Daniel Miller	2/16/18 1:07 PM

the

Page 17: Inserted	Daniel Miller	2/16/18 1:07 PM

(with appropriate fitting coefficients)

Page 17: Inserted	Daniel Miller	2/25/18 11:23 AM

Note that, while this histogram gives a sense of the variability of the magnitude and scale of the polarized reflectances, what ultimately matters for the coarse resolution polarimetric retrieval is the relative shape of the 800 m averaged polarized reflectance curve.

Page 17: Deleted	Daniel Miller	2/13/18 1:38 PM

2WT

Page 17: Inserted	Daniel Miller	2/13/18 1:38 PM

VW

Page 17: Inserted	Daniel Miller	2/26/18 8:17 PM

This agrees with previous studies on the impact of unresolved inhomogeneity on polarimetric r_e retrievals (Shang et al., 2015).

Page 17: Deleted	Daniel Miller	2/13/18 1:38 PM

2WT

Page 17: Inserted	Daniel Miller	2/13/18 1:38 PM

VW

Page 17: Inserted	Daniel Miller	2/27/18 10:23 AM

(Alexandrov et al., 2012b)

Page 18: Inserted	Daniel Miller	2/26/18 7:22 PM

v_e

Page 18: Deleted	Daniel Miller	2/26/18 7:22 PM

a

Page 18: Deleted	Daniel Miller	2/26/18 7:22 PM

v_e and varying τ

Page 18: Deleted	Daniel Miller	2/13/18 1:38 PM

2WT

Page 18: Inserted	Daniel Miller	2/13/18 1:38 PM

VW

Page 18: Inserted	Daniel Miller	2/26/18 1:56 PM

Each of these effects reduces sensitivity to the cloudbow features; and thus unresolved variability in τ and v_e could influence coarse resolution retrievals. For example, Shang et al. (2015) found that unresolved spatial inhomogeneity of τ and v_e increased retrieval biases in v_e(pol), while they were not able to discern a trend in retrieval biases in their study. However, in our case study featured in Figure 11Figure (b) we do not see a significant difference between coarse ($v_e(\text{pol})_{800\text{ m}}$) and fine scale ($\langle v_e(\text{pol})_{50\text{ m}}\rangle$) retrievals, but both

retrievals are low-biased relative to the mean LES property ($<v_e(\mathrm{VW})_{50\ \mathrm{m}}>$). This result was surprising, because both fine and coarse resolution retrievals were biased similarly. It appears as though coarse resolution retrievals arrive at the same answer as the fine scale retrievals through different processes. The average of fine scale retrievals (that are systematically biased low) and the retrieval based on the average of fine scale reflectances (which are reduced for reasons discussed above) results in a similar retrieval outcome. Unlike the bispectral retrieval, where retrievals differ from one another at different resolutions, the polarimetric retrieval seems to compare well to itself at both resolutions – even when it might be biased relative to the underlying microphysics of the physical scene. To examine this this further we

Page 18: Deleted	**Daniel Miller**	**3/4/18 9:50 PM**

Figure

Page 18: Deleted	**Daniel Miller**	**2/26/18 2:00 PM**

we find that these features do not systematically bias the v_e(pol) retrieval in this case. In fact, rather surprisingly, we

Page 18: Inserted	**Daniel Miller**	**3/4/18 2:44 PM**

performed

Page 18: Deleted	**Daniel Miller**	**3/4/18 2:33 PM**

find that the most important bias for the coarse spatial resolution v_e(pol) retrieval is the lack of sensitivity on $v_e(2\mathrm{WT})>0.15$, a feature that was also present for the high spatial resolution retrievals. This finding is also supported for

Page 18: Inserted	**Daniel Miller**	**3/4/18 2:44 PM**

Page 18: Deleted	**Daniel Miller**	**3/4/18 2:44 PM**

Page 18: Inserted	**Daniel Miller**	**3/4/18 2:44 PM**

on

Page 18: Deleted	**Daniel Miller**	**3/4/18 2:33 PM**

performed on

Page 18: Inserted	**Daniel Miller**	**2/26/18 8:54 PM**

populations

Page 18: Deleted	**Daniel Miller**	**2/26/18 8:54 PM**

samples

Page 18: Inserted	**Daniel Miller**	**3/4/18 2:36 PM**

50 m

Page 18: Inserted	**Daniel Miller**	**2/26/18 8:54 PM**

s within

Page 18: Deleted	Daniel Miller	2/26/18 8:54 PM

of

Page 18: Deleted	Daniel Miller	2/13/18 1:38 PM

2WT

Page 18: Inserted	Daniel Miller	2/13/18 1:38 PM

VW

Page 18: Inserted	Daniel Miller	3/4/18 2:34 PM

. Removing these thin or broad droplet size distributions from the high resolution dataset

Page 18: Deleted	Daniel Miller	3/4/18 2:33 PM

; removing either of them had little

Page 18: Inserted	Daniel Miller	2/27/18 2:36 AM

had little

Page 18: Deleted	Daniel Miller	2/26/18 4:31 PM

.

Page 18: Inserted	Daniel Miller	2/26/18 3:20 PM

From these results and the histogram in Figure 10 (d) it appears that the impact of spatial resolution on v_e(pol) retrievals is largely a consequence of an unresolved anticorrelation between τ and v_e rather than a feature directly related to spatial resolution.

Page 18: Deleted	Daniel Miller	2/26/18 3:47 PM

Possible explanations for this behavior will be discussed in section 5.

Page 18: Deleted	Daniel Miller	2/13/18 10:16 AM

4

Page 18: Inserted	Daniel Miller	2/13/18 10:16 AM

4

Page 18: Inserted	Daniel Miller	4/27/18 12:01 AM

Figure 12

Page 18: Deleted	Daniel Miller	2/24/18 12:28 PM

Figure 10

Page 18: Inserted	Daniel Miller	4/27/18 12:01 AM

Figure 12

Page 18: Deleted	Daniel Miller	2/24/18 12:28 PM

Figure 10

Page 18: Inserted	Daniel Miller	4/27/18 12:01 AM

Figure 13

Page 18: Deleted	Daniel Miller	2/24/18 12:28 PM

Figure 11

Page 19: Inserted	Daniel Miller	3/5/18 10:44 AM

, which could be exacerbated by observational uncertainty

Page 19: Inserted	Daniel Miller	4/27/18 12:01 AM

Figure 13

Page 19: Deleted	Daniel Miller	2/24/18 12:28 PM

Figure 11

Page 19: Deleted	Daniel Miller	3/5/18 10:43 AM

uncertainty

Page 19: Inserted	Daniel Miller	3/5/18 10:43 AM

variability

Page 19: Deleted	Daniel Miller	3/4/18 3:00 PM

vastly

Page 19: Inserted	Daniel Miller	3/4/18 3:00 PM

fundamentally

Page 19: Inserted	Daniel Miller	3/4/18 3:01 PM

(with 1-D radiative transfer assumptions)

Page 19: Inserted	Daniel Miller	3/4/18 4:46 PM

/MWIR

Page 19: Deleted	Daniel Miller	2/13/18 1:38 PM

2WT

Page 19: Inserted	Daniel Miller	2/13/18 1:38 PM

VW

Page 19: Inserted	Daniel Miller	3/4/18 2:56 PM

The uncertainty in observed total and polarized reflectances was found to introduce only weak systematic biases in bispectral or polarimetric r_e retrievals (0.1% or less). Similarly, the bispectral τ retrievals were also not systematically biased. In contrast, total reflectance uncertainty did produce a slight systematic bias of -2.43% in the polarimetric τ(pol) retrieval that can be linked to the convexity of the single-band LUT used to perform the retrieval. This sort of bias, could perhaps be accounted for by introducing a Taylor expansion correction similar to the one discussed in

Page 20: Inserted	Daniel Miller	3/4/18 3:20 PM

Zhang et al. (2016) in the context of unresolved inhomogeneity. Beyond these systematic biases, we found that the induced uncertainties in the bispectral retrievals were δr_e=5% or $\delta\tau$=7%. The influence of polarimetric retrieval is likely sensitive the polarimetric LUT grid spacing, but here we found uncertainties that were less than the bispectral retrieval of r_e, δr_e(pol)=1 to 4%, and δv_e(pol)=10 to 20%. In the context

of the rest of our comparison studies, the lack of systematic biases and relatively small uncertainties allowed us to discuss retrieval behavior in the absence of uncertainty.

Page 20: Deleted	Daniel Miller	3/4/18 3:16 PM

Page 20: Inserted	Daniel Miller	2/26/18 1:28 PM

and τ

Page 20: Inserted	Daniel Miller	2/26/18 1:29 PM

and more deeply penetrating

Page 20: Deleted	Daniel Miller	2/13/18 1:38 PM

2WT

Page 20: Inserted	Daniel Miller	2/13/18 1:38 PM

VW

Page 21: Inserted	Daniel Miller	2/26/18 2:57 PM

still

Page 21: Inserted	Daniel Miller	2/26/18 2:57 PM

is in

Page 21: Deleted	Daniel Miller	2/26/18 2:57 PM

may

Page 21: Inserted	Daniel Miller	2/26/18 1:48 PM

large part

Page 21: Deleted	Daniel Miller	2/26/18 1:48 PM

be

Page 21: Inserted	Daniel Miller	3/4/18 3:46 PM

(

Page 21: Inserted	Daniel Miller	2/26/18 3:49 PM

Page 21: Inserted	Steven Platnick	3/1/18 3:55 PM

Ultimately, the utitlity of any optical property dataset depends on the science questions for which the dataset will be used.

Page 21: Inserted	Daniel Miller	3/5/18 10:58 AM

These questions

Page 21: Inserted	Steven Platnick	3/1/18 3:56 PM

may

Page 21: Inserted	Daniel Miller	3/5/18 10:59 AM

focus on the determination of

Page 21: Inserted	Steven Platnick	3/1/18 3:56 PM

domain-averaged water mass

Page 21: Inserted	Daniel Miller	3/5/18 10:58 AM

,

Page 21: Inserted	Steven Platnick	3/1/18 3:56 PM

radiative flux calculation

Page 21: Inserted	Daniel Miller	3/5/18 10:53 AM

s

Page 21: Inserted	Steven Platnick	3/1/18 3:56 PM

, or

Page 21: Inserted	Daniel Miller	3/4/18 3:48 PM

microp

Page 21: Inserted	Steven Platnick	3/1/18 3:54 PM

hysical process studies on a range of scales.

Page 21: Inserted	Daniel Miller	3/5/18 10:59 AM

The appropriate retrieval may differ for each of these science questions and as a consequence the comparison of the bispectral and polarimetric retrievals discussed here ought to be viewed through the lens of a particular application.

Page 23: Inserted	Daniel Miller	4/27/18 12:01 AM

(2)

Page 23: Inserted	Daniel Miller	4/27/18 12:01 AM

(3)

Page 24: Inserted	Daniel Miller	2/26/18 1:23 PM

Shang et al., (2015)

Page 24: Inserted	Daniel Miller	4/27/18 12:01 AM

Table 2

Page 24: Deleted	Daniel Miller	3/2/18 3:02 PM

v_e’

Page 24: Inserted	Daniel Miller	3/2/18 3:02 PM

v_e'

Page 24: Deleted	Daniel Miller	2/13/18 1:38 PM

2WT

Page 24: Inserted	Daniel Miller	2/13/18 1:38 PM

VW

Page 24: Deleted	Daniel Miller	2/13/18 1:38 PM

2WT

Page 24: Inserted	Daniel Miller	2/13/18 1:38 PM

VW

Page 24: Inserted	Daniel Miller	2/26/18 5:13 PM

. This non-physical variability is something

Page 26: Inserted	Daniel Miller	2/27/18 9:32 AM

Ackerman, A. S., Kirkpatrick, M. P., Stevens, D. E. and Toon, O. B.: The impact of humidity above stratiform clouds on indirect aerosol climate forcing, Nature, 432(7020), 1014–1017, 2004.

Ackerman, A. S., vanZanten, M. C., Stevens, B., Savic-Jovcic, V., Bretherton, C. S., Chlond, A., Golaz, J.-C., Jiang, H., Khairoutdinov, M., Krueger, S. K., Lewellen, D. C., Lock, A., Moeng, C.-H., Nakamura, K., Petters, M. D., Snider, J. R., Weinbrecht, S. and Zulauf, M.: Large-Eddy Simulations of a Drizzling, Stratocumulus-Topped Marine Boundary Layer, Mon. Wea. Rev., 137(3), 1083–1110, doi:10.1175/2008MWR2582.1, 2009.

Alexandrov, M. D., Cairns, B. and Mishchenko, M. I.: Rainbow Fourier transform, Journal of Quantitative Spectroscopy and Radiative Transfer, 113(18), 2521–2535, doi:10.1016/j.jqsrt.2012.03.025, 2012a.

Alexandrov, M. D., Cairns, B., Emde, C., Ackerman, A. S. and van Diedenhoven, B.: Accuracy assessments of cloud droplet size retrievals from polarized reflectance measurements by the research scanning polarimeter, Remote Sensing of Environment, 125, 92–111, doi:10.1016/j.rse.2012.07.012, 2012b.

Alexandrov, M. D., Cairns, B., Wasilewski, A. P., Ackerman, A. S., McGill, M. J., Yorks, J. E., Hlavka, D. L., Platnick, S. E., Thomas Arnold, G., van Diedenhoven, B., Chowdhary, J., Ottaviani, M. and Knobelspiesse, K. D.: Liquid water cloud properties during the Polarimeter Definition Experiment (PODEX), Remote Sensing of Environment, 169, 20–36, doi:10.1016/j.rse.2015.07.029, 2015.

Bréon, F. M. and Doutriaux-Boucher, M.: A comparison of cloud droplet radii measured from space, IEEE Trans. Geosci. Remote Sensing, 43(8), 1796–1805, doi:10.1109/TGRS.2005.852838, 2005.

Bréon, F. M. and Goloub, P.: Cloud droplet effective radius from spaceborne polarization measurements, Geophys. Res. Lett., 25(11), 1879–1882, 1998.

Cairns, B., Russell, E. E. and Travis, L. D.: Research Scanning Polarimeter: calibration and ground-based measurements, SPIE's Conference on Polarization: Measurement, Analysis, and Remote Sensing II, 186–196, doi:10.1117/12.366329, 1999.

Cho, H. M., Zhang, Z., Meyer, K., Lebsock, M., Platnick, S., Ackerman, A. S., Di Girolamo, L., C Labonnote, L., Cornet, C., Riedi, J. and Holz, R. E.: Frequency and causes of failed MODIS cloud property retrievals for liquid phase clouds over global oceans, J. Geophys. Res., 120(9), 4132–4154, doi:10.1002/2015JD023161, 2015.

De Haan, J. F., Bosma, P. B. and Hovenier, J. W.: The adding method for multiple scattering calculations of polarized light, Astronomy and Astrophysics, 183, 371–391, 1987.

Deirmendjian, D.: Scattering and polarization properties of water clouds and hazes in the visible and infrared, Appl. Opt., 3(2), 187–196, 1964.

Deschamps, P. Y., Breon, F. M., Leroy, M., Podaire, A., Bricaud, A., Buriez, J. C. and Seze, G.: The

POLDER mission: instrument characteristics and scientific objectives, IEEE Trans. Geosci. Remote Sensing, 32(3), 598–615, doi:10.1109/36.297978, 1994.

Diner, D. J., Xu, F., Garay, M. J., Martonchik, J. V., Rheingans, B. E., Geier, S., Davis, A., Hancock, B. R., Jovanovic, V. M., Bull, M. A., Capraro, K., Chipman, R. A. and McClain, S. C.: The Airborne Multiangle SpectroPolarimetric Imager (AirMSPI): a new tool for aerosol and cloud remote sensing, Atmos. Meas. Tech., 6(8), 2007–2025, doi:10.5194/amt-6-2007-2013, 2013.

Fridlind, A. M. and Ackerman, A. S.: Estimating the Sensitivity of Radiative Impacts of Shallow, Broken Marine Clouds to Boundary Layer Aerosol Size Distribution Parameter Uncertainties for Evaluation of Satellite Retrieval Requirements, J. Atmos. Oceanic Technol., 28(4), 530–538, doi:10.1175/2010JTECHA1520.1, 2011.

Hansen, J. E.: Circular Polarization of Sunlight Reflected by Clouds, http://dx.doi.org/10.1175/1520-0469(1971)028<1515:CPOSRB>2.0.CO;2, doi:10.1175/1520-0469(1971)028<1515:CPOSRB>2.0.CO;2, 2010.

Hansen, J. E. and Travis, L. D.: Light scattering in planetary atmospheres, Space Sci Rev, 16(4), 527–610, 1974.

King, M. D., Menzel, W. P., Kaufman, Y. J., Tanré, D., Bo-Cai Gao, Platnick, S., Ackerman, S. A., Remer, L. A., Pincus, R. and Hubanks, P. A.: Cloud and aerosol properties, precipitable water, and profiles of temperature and water vapor from MODIS, IEEE Trans. Geosci. Remote Sensing, 41(2), 442–458, doi:10.1109/TGRS.2002.808226, 2003.

Knobelspiesse, K., Cairns, B., Mishchenko, M., Chowdhary, J., Tsigaridis, K., van Diedenhoven, B., Martin, W., Ottaviani, M. and Alexandrov, M.: Analysis of fine-mode aerosol retrieval capabilities by different passive remote sensing instrument designs, Opt. Express, 20(19), 21457–21484, doi:10.1364/OE.20.021457, 2012.

Knobelspiesse, K., Segal-Rosenhaimer, M., Redemann, J., Cairns, B. and Alexandrov, M. D.: Multi-angle, polarimetric cloud observations using a radiative transfer model trained neural network, College Park, MD. 2017.

Liu, Y. and Diner, D. J.: Multi-Angle Imager for Aerosols, Public Health Reports, 132(1), 14–17, doi:10.1177/0033354916679983, 2017.

Lohmann, U., Stier, P., Hoose, C., Ferrachat, S., Kloster, S., Roeckner, E. and Zhang, J.: Cloud microphysics and aerosol indirect effects in the global climate model ECHAM5-HAM, Atmos. Chem. Phys., 7(13), 3425–3446, doi:10.5194/acp-7-3425-2007, 2007.

Marbach, T., Phillips, P., Lacan, A. and Schlussel, P.: The 3MI Mission: Multi-Viewing -Channel - Polarisation Imager of the EUMETSAT Polar System - Second Generation (EPS-SG) dedicated to aerosol and cloud monitoring, in Sensors, Systems, and Next-Generation Satellites XVII, vol. 8889, p. 88890I, International Society for Optics and Photonics. 2013.

Marshak, A., Platnick, S., Várnai, T., Wen, G. and Cahalan, R. F.: Impact of three-dimensional radiative effects on satellite retrievals of cloud droplet sizes, J. Geophys. Res., 111(D9), D09207, doi:10.1029/2005JD006686, 2006.

Martin, G. M., Johnson, D. W. and Spice, A.: The measurement and parameterization of effective radius of droplets in warm stratocumulus clouds, J. Atmos. Sci., 51(13), 1823–1842, 1994.

Martins, J. V., Fernandez-Borda, R., McBride, B., Espinosa, R. and Remer, L.: Combination between in-situ and remote sensing of tropospheric aerosols, College Park, MD. 2017.

Miles, N. L., Verlinde, J. and Clothiaux, E. E.: Cloud Droplet Size Distributions in Low-Level Stratiform Clouds, J. Atmos. Sci., 57(2), 295–311, doi:10.1175/1520-0469(2000)057<0295:CDSDIL>2.0.CO;2, 2000.

Miller, D. J., Zhang, Z., Ackerman, A. S., Platnick, S. and Baum, B. A.: The impact of cloud vertical profile on liquid water path retrieval based on the bispectral method: A theoretical study based on large-eddy simulations of shallow marine boundary layer clouds, J. Geophys. Res., 121(8), 4122–4141, doi:10.1002/2015JD024322, 2016.

Mishchenko, M. I., Cairns, B., Travis, L. D., Kopp, G., Schueler, C. F., Fafaul, B. A., Hooker, R. J., Maring, H. B., Itchkawich, T., Hansen, J. E., Kopp, G., Schueler, C. F., Fafaul, B. A., Hooker, R. J., Maring, H. B. and Itchkawich, T.: Accurate Monitoring of Terrestrial Aerosols and Total Solar Irradiance: Introducing the Glory Mission, http://dx.doi.org/10.1175/BAMS-88-5-677, 88(5), 677–691, doi:10.1175/BAMS-88-5-677, 2007.

Nakajima, T. and King, M. D.: Determination of the Optical Thickness and Effective Particle Radius of Clouds from Reflected Solar Radiation Measurements. Part I: Theory, J. Atmos. Sci., 47(15), 1878–1893, doi:10.1175/1520-0469(1990)047<1878:dotota>2.0.co;2, 1990a.

Nakajima, T. and King, M. D.: Determination of the optical thickness and effective particle radius of clouds from reflected solar radiation measurements. Part I: Theory, J. Atmos. Sci., 47(15), 1878–1893, 1990b.

Planck, M.: The theory of heat radiation, 2nd ed., P. Blakiston's Son & Co., Philadelphia, PA. [online] Available from: http://gutenberg.org/ebooks/40030, 1914.

Platnick, S.: Vertical photon transport in cloud remote sensing problems, J. Geophys. Res., 105(D18), 22919–22935, 2000.

Platnick, S., King, M. D., Ackerman, S. A., Menzel, W. P., Baum, B. A., Riedi, J. C. and Frey, R. A.: The MODIS cloud products: algorithms and examples from terra, IEEE Trans. Geosci. Remote Sensing, 41(2), 459–473, doi:10.1109/TGRS.2002.808301, 2003.

Platnick, S., Meyer, K. G., King, M. D., Wind, G., Amarasinghe, N., Marchant, B., Arnold, G. T., Zhang, Z., Hubanks, P. A., Holz, R. E., Yang, P., Ridgway, W. L. and Riedi, J.: The MODIS Cloud Optical and Microphysical Products: Collection 6 Updates and Examples From Terra and Aqua, IEEE Trans. Geosci. Remote Sensing, 55(1), 502–525, doi:10.1109/TGRS.2016.2610522, 2017.

Pruppacher, H. R. and Klett, J. D.: Diffusion Growth and Evaporation of Water Drops and Ice Crystals, in Microphysics of Clouds and Precipitation, pp. 412–463, Springer Netherlands, Dordrecht. 1978.

Roebeling, R. A., Feijt, A. J. and Stammes, P.: Cloud property retrievals for climate monitoring: Implications of differences between Spinning Enhanced Visible and Infrared Imager (SEVIRI) on METEOSAT-8 and Advanced Very High Resolution Radiometer (AVHRR) on NOAA-17, J. Geophys. Res., 111(D20), D20210, doi:10.1029/2005JD006990, 2006.

Rosenfeld, D., Liu, G., Yu, X., Zhu, Y., Dai, J., Xu, X. and Yue, Z.: High-resolution (375 m) cloud microstructure as seen from the NPP/VIIRS satellite imager, Atmos. Chem. Phys., 14(5), 2479–2496, doi:10.5194/acp-14-2479-2014, 2014.

Shang, H., Chen, L., Breon, F. M., Letu, H., Li, S., Wang, Z. and Su, L.: A better understanding of POLDER's cloud droplet size retrieval: impact of cloud horizontal inhomogeneity and directional sampling, Atmos. Meas. Tech. Discuss., 8(7), 6559–6597, doi:10.5194/amtd-8-6559-2015, 2015.

Stevens, B., Ackerman, A. S. and Albrecht, B. A.: Simulations of trade wind cumuli under a strong inversion, J. Atmos. Sci., 58(14), 1870–1891, doi:10.1175/1520-0469(2001)058<1870:sotwcu>2.0.co;2, 2001.

Stevens, B., Lenschow, D. H., Vali, G., Gerber, H., Bandy, A., Blomquist, B., Brenguier, J. L., Bretherton, C. S., Burnet, F., Campos, T., Chai, S., Faloona, I., Friesen, D., Haimov, S., Laursen, K., Lilly, D. K., Loehrer, S. M., Malinowski, S. P., Morley, B., Petters, M. D., Rogers, D. C., Russell, L., Savic-Jovcic, V., Snider, J. R., Straub, D., Szumowski, M. J., Takagi, H., Thornton, D. C., Tschudi, M., Twohy, C., Wetzel, M. and van Zanten, M. C.: Dynamics and chemistry of marine stratocumulus–DYCOMS-II, Bull. Amer. Meteor. Soc., 84(5), 579–593, doi:10.1175/BAMS-84-5-579, 2003.

Stevens, B., Moeng, C.-H., Ackerman, A. S., Bretherton, C. S., Chlond, A., de Roode, S., Edwards, J., Golaz, J.-C., Jiang, H., Khairoutdinov, M., Kirkpatrick, M. P., Lewellen, D. C., Lock, A., Müller, F., Stevens, D. E., Whelan, E. and Zhu, P.: Evaluation of Large-Eddy Simulations via Observations of Nocturnal Marine Stratocumulus, Mon. Wea. Rev., 133(6), 1443–, doi:10.1175/MWR2930.1, 2005.

Tampieri, F. and Tomasi, C.: Size distribution models of fog and cloud droplets in terms of the modified gamma function, Tellus, 28(4), 333–347, doi:10.1111/j.2153-3490.1976.tb00682.x, 1976.

Twomey, S.: The Influence of Pollution on the Shortwave Albedo of Clouds, J. Atmos. Sci., 34(7), 1149–1152, doi:10.1175/1520-0469(1977)034<1149:TIOPOT>2.0.CO;2, 1977.

Werner, F., Siebert, H., Pilewskie, P., Schmeissner, T., Shaw, R. A. and Wendisch, M.: New airborne retrieval approach for trade wind cumulus properties under overlying cirrus, J. Geophys. Res., 118(9), 3634–3649, doi:10.1002/jgrd.50334, 2013.

Wiscombe, W. J.: Mie scattering calculations: Advances in technique and fast, vector-speed computer codes, NCAR Tech, National Center for Atmospheric Research, Boulder, Colorado. 1979.

Zhang, Z. and Platnick, S.: An assessment of differences between cloud effective particle radius retrievals for marine water clouds from three MODIS spectral bands, J. Geophys. Res., 116(D20), D20215, doi:10.1029/2011JD016216, 2011.

Zhang, Z., Ackerman, A. S., Feingold, G., Platnick, S., Pincus, R. and Xue, H.: Effects of cloud horizontal inhomogeneity and drizzle on remote sensing of cloud droplet effective radius: Case studies based on large-eddy simulations, J. Geophys. Res., 117(D19), n/a–n/a, doi:10.1029/2012JD017655, 2012.

Zhang, Z., Dong, X., Xi, B., Song, H., Ma, P. L., Ghan, S. J., Platnick, S. and Minnis, P.: Intercomparisons of marine boundary layer cloud properties from the ARM CAP-MBL campaign and two MODIS cloud products, J. Geophys. Res., 122(4), 2351–2365, doi:10.1002/2016JD025763, 2017.

Zhang, Z., Platnick, S., Yang, P., Heidinger, A. K. and Comstock, J. M.: Effects of ice particle size vertical inhomogeneity on the passive remote sensing of ice clouds, J. Geophys. Res., 115(D17), doi:10.1029/2010JD013835, 2010.

Zhang, Z., Werner, F., Cho, H. M. and Wind, G.: A framework based on 2-D Taylor expansion for quantifying the impacts of subpixel reflectance variance and covariance on cloud optical thickness and effective …, Journal of …, doi:10.1063/1.4975502, 2016.

Zinner, T., Wind, G., Platnick, S. and Ackerman, A. S.: Testing remote sensing on artificial observations: impact of drizzle and 3-D cloud structure on effective radius retrievals, Atmos. Chem. Phys., 10(19), 9535–9549, doi:10.5194/acp-10-9535-2010, 2010.

Page 29: Deleted **Daniel Miller** **2/26/18 1:23 PM**

Ackerman, A. S., Kirkpatrick, M. P., Stevens, D. E. and Toon, O. B.: The impact of humidity above stratiform clouds on indirect aerosol climate forcing, Nature, 432(7020), 1014–1017, 2004.

Ackerman, A. S., vanZanten, M. C., Stevens, B., Savic-Jovcic, V., Bretherton, C. S., Chlond, A., Golaz, J.-

C., Jiang, H., Khairoutdinov, M., Krueger, S. K., Lewellen, D. C., Lock, A., Moeng, C.-H., Nakamura, K., Petters, M. D., Snider, J. R., Weinbrecht, S. and Zulauf, M.: Large-Eddy Simulations of a Drizzling, Stratocumulus-Topped Marine Boundary Layer, Mon. Wea. Rev., 137(3), 1083–1110, doi:10.1175/2008MWR2582.1, 2009.

Alexandrov, M. D., Cairns, B. and Mishchenko, M. I.: Rainbow Fourier transform, Journal of Quantitative Spectroscopy and Radiative Transfer, 113(18), 2521–2535, doi:10.1016/j.jqsrt.2012.03.025, 2012a.

Alexandrov, M. D., Cairns, B., Emde, C., Ackerman, A. S. and van Diedenhoven, B.: Accuracy assessments of cloud droplet size retrievals from polarized reflectance measurements by the research scanning polarimeter

, Remote Sensing of Environment, 125, 92–111, doi:10.1016/j.rse.2012.07.012, 2012b.

Alexandrov, M. D., Cairns, B., Wasilewski, A. P., Ackerman, A. S., McGill, M. J., Yorks, J. E., Hlavka, D. L., Platnick, S. E., Thomas Arnold, G., van Diedenhoven, B., Chowdhary, J., Ottaviani, M. and Knobelspiesse, K. D.: Liquid water cloud properties during the Polarimeter Definition Experiment (PODEX), Remote Sensing of Environment, 169, 20–36, doi:10.1016/j.rse.2015.07.029, 2015.

Bréon, F. M. and Doutriaux-Boucher, M.: A comparison of cloud droplet radii measured from space, IEEE Trans. Geosci. Remote Sensing, 43(8), 1796–1805, doi:10.1109/TGRS.2005.852838, 2005.

Bréon, F. M. and Goloub, P.: Cloud droplet effective radius from spaceborne polarization measurements, Geophys. Res. Lett., 25(11), 1879–1882, 1998.

Cairns, B., Russell, E. E. and Travis, L. D.: Research Scanning Polarimeter: calibration and ground-based measurements, SPIE's Conference on Polarization: Measurement, Analysis, and Remote Sensing II, 186–196, doi:10.1117/12.366329, 1999.

Cho, H. M., Zhang, Z., Meyer, K., Lebsock, M., Platnick, S., Ackerman, A. S., Di Girolamo, L., C Labonnote, L., Cornet, C., Riedi, J. and Holz, R. E.: Frequency and causes of failed MODIS cloud property retrievals for liquid phase clouds over global oceans, J. Geophys. Res., 120(9), 4132–4154, doi:10.1002/2015JD023161, 2015.

De Haan, J. F., Bosma, P. B. and Hovenier, J. W.: The adding method for multiple scattering calculations of polarized light, Astronomy and Astrophysics, 183, 371–391, 1987.

Deirmendjian, D.: Scattering and polarization properties of water clouds and hazes in the visible and infrared, Appl. Opt., 3(2), 187–196, 1964.

Deschamps, P. Y., Breon, F. M., Leroy, M., Podaire, A., Bricaud, A., Buriez, J. C. and Seze, G.: The POLDER mission: instrument characteristics and scientific objectives, IEEE Trans. Geosci. Remote Sensing, 32(3), 598–615, doi:10.1109/36.297978, 1994.

Diner, D. J., Xu, F., Garay, M. J., Martonchik, J. V., Rheingans, B. E., Geier, S., Davis, A., Hancock, B. R., Jovanovic, V. M., Bull, M. A., Capraro, K., Chipman, R. A. and McClain, S. C.: The Airborne Multiangle SpectroPolarimetric Imager (AirMSPI): a new tool for aerosol and cloud remote sensing, Atmos. Meas. Tech., 6(8), 2007–2025, doi:10.5194/amt-6-2007-2013, 2013.

Fridlind, A. M. and Ackerman, A. S.: Estimating the Sensitivity of Radiative Impacts of Shallow, Broken Marine Clouds to Boundary Layer Aerosol Size Distribution Parameter Uncertainties for Evaluation of Satellite Retrieval Requirements, J. Atmos. Oceanic Technol., 28(4), 530–538, doi:10.1175/2010JTECHA1520.1, 2011.

Hansen, J. E.: Circular Polarization of Sunlight Reflected by Clouds, http://dx.doi.org/10.1175/1520-

0469(1971)028<1515:CPOSRB>2.0.CO;2, doi:10.1175/1520-0469(1971)028<1515:CPOSRB>2.0.CO;2, 2010.

Hansen, J. E. and Travis, L. D.: Light scattering in planetary atmospheres, Space Sci Rev, 16(4), 527–610, 1974.

King, M. D., Menzel, W. P., Kaufman, Y. J., Tanré, D., Bo-Cai Gao, Platnick, S., Ackerman, S. A., Remer, L. A., Pincus, R. and Hubanks, P. A.: Cloud and aerosol properties, precipitable water, and profiles of temperature and water vapor from MODIS, IEEE Trans. Geosci. Remote Sensing, 41(2), 442–458, doi:10.1109/TGRS.2002.808226, 2003.

Knobelspiesse, K., Segal-Rosenhaimer, M., Redemann, J., Cairns, B. and Alexandrov, M. D.: Multi-angle, polarimetric cloud observations using a radiative transfer model trained neural network, College Park, MD. 2017.

Liu, Y. and Diner, D. J.: Multi-Angle Imager for Aerosols, Public Health Reports, 132(1), 14–17, doi:10.1177/0033354916679983, 2017.

Lohmann, U., Stier, P., Hoose, C., Ferrachat, S., Kloster, S., Roeckner, E. and Zhang, J.: Cloud microphysics and aerosol indirect effects in the global climate model ECHAM5-HAM, Atmos. Chem. Phys., 7(13), 3425–3446, doi:10.5194/acp-7-3425-2007, 2007.

Marbach, T., Phillips, P., Lacan, A. and Schlussel, P.: The 3MI Mission: Multi-Viewing -Channel - Polarisation Imager of the EUMETSAT Polar System - Second Generation (EPS-SG) dedicated to aerosol and cloud monitoring, in Sensors, Systems, and Next-Generation Satellites XVII, vol. 8889, p. 88890I, International Society for Optics and Photonics. 2013.

Martin, G. M., Johnson, D. W. and Spice, A.: The measurement and parameterization of effective radius of droplets in warm stratocumulus clouds, J. Atmos. Sci., 51(13), 1823–1842, 1994.

Martins, J. V., Fernandez-Borda, R., McBride, B., Espinosa, R. and Remer, L.: Combination between in-situ and remote sensing of tropospheric aerosols, College Park, MD. 2017.

Miles, N. L., Verlinde, J. and Clothiaux, E. E.: Cloud Droplet Size Distributions in Low-Level Stratiform Clouds, J. Atmos. Sci., 57(2), 295–311, doi:10.1175/1520-0469(2000)057<0295:CDSDIL>2.0.CO;2, 2000.

Miller, D. J., Zhang, Z., Ackerman, A. S., Platnick, S. and Baum, B. A.: The impact of cloud vertical profile on liquid water path retrieval based on the bispectral method: A theoretical study based on large-eddy simulations of shallow marine boundary layer clouds, J. Geophys. Res., 121(8), 4122–4141, doi:10.1002/2015JD024322, 2016.

Mishchenko, M. I., Cairns, B., Travis, L. D., Kopp, G., Schueler, C. F., Fafaul, B. A., Hooker, R. J., Maring, H. B., Itchkawich, T., Hansen, J. E., Kopp, G., Schueler, C. F., Fafaul, B. A., Hooker, R. J., Maring, H. B. and Itchkawich, T.: Accurate Monitoring of Terrestrial Aerosols and Total Solar Irradiance: Introducing the Glory Mission, http://dx.doi.org/10.1175/BAMS-88-5-677, 88(5), 677–691, doi:10.1175/BAMS-88-5-677, 2007.

Nakajima, T. and King, M. D.: Determination of the Optical Thickness and Effective Particle Radius of Clouds from Reflected Solar Radiation Measurements. Part I: Theory, J. Atmos. Sci., 47(15), 1878–1893, doi:10.1175/1520-0469(1990)047<1878:dotota>2.0.co;2, 1990a.

Nakajima, T. and King, M. D.: Determination of the optical thickness and effective particle radius of clouds from reflected solar radiation measurements. Part I: Theory, J. Atmos. Sci., 47(15), 1878–1893, 1990b.

Planck, M.: The theory of heat radiation, 2nd ed., P. Blakiston's Son & Co., Philadelphia, PA. [online]

Available from: http://gutenberg.org/ebooks/40030, 1914.

Platnick, S.: Vertical photon transport in cloud remote sensing problems, J. Geophys. Res., 105(D18), 22919–22935, 2000.

Platnick, S., King, M. D., Ackerman, S. A., Menzel, W. P., Baum, B. A., Riedi, J. C. and Frey, R. A.: The MODIS cloud products: algorithms and examples from terra, IEEE Trans. Geosci. Remote Sensing, 41(2), 459–473, doi:10.1109/TGRS.2002.808301, 2003.

Platnick, S., Meyer, K. G., King, M. D., Wind, G., Amarasinghe, N., Marchant, B., Arnold, G. T., Zhang, Z., Hubanks, P. A., Holz, R. E., Yang, P., Ridgway, W. L. and Riedi, J.: The MODIS Cloud Optical and Microphysical Products: Collection 6 Updates and Examples From Terra and Aqua, IEEE Trans. Geosci. Remote Sensing, 55(1), 502–525, doi:10.1109/TGRS.2016.2610522, 2016.

Pruppacher, H. R. and Klett, J. D.: Diffusion Growth and Evaporation of Water Drops and Ice Crystals, in Microphysics of Clouds and Precipitation, pp. 412–463, Springer Netherlands, Dordrecht. 1978.

Roebeling, R. A., Feijt, A. J. and Stammes, P.: Cloud property retrievals for climate monitoring: Implications of differences between Spinning Enhanced Visible and Infrared Imager (SEVIRI) on METEOSAT-8 and Advanced Very High Resolution Radiometer (AVHRR) on NOAA-17, J. Geophys. Res., 111(D20), D20210, doi:10.1029/2005JD006990, 2006.

Rosenfeld, D., Liu, G., Yu, X., Zhu, Y., Dai, J., Xu, X. and Yue, Z.: High-resolution (375 m) cloud microstructure as seen from the NPP/VIIRS satellite imager, Atmos. Chem. Phys., 14(5), 2479–2496, doi:10.5194/acp-14-2479-2014, 2014.

Shang, H., Chen, L., Breon, F. M., Letu, H., Li, S., Wang, Z. and Su, L.: A better understanding of POLDER's cloud droplet size retrieval: impact of cloud horizontal inhomogeneity and directional sampling, Atmos. Meas. Tech. Discuss., 8(7), 6559–6597, doi:10.5194/amtd-8-6559-2015, 2015.

Stevens, B., Ackerman, A. S. and Albrecht, B. A.: Simulations of trade wind cumuli under a strong inversion, J. Atmos. Sci., 58(14), 1870–1891, doi:10.1175/1520-0469(2001)058<1870:sotwcu>2.0.co;2, 2001.

Stevens, B., Lenschow, D. H., Vali, G., Gerber, H., Bandy, A., Blomquist, B., Brenguier, J. L., Bretherton, C. S., Burnet, F., Campos, T., Chai, S., Faloona, I., Friesen, D., Haimov, S., Laursen, K., Lilly, D. K., Loehrer, S. M., Malinowski, S. P., Morley, B., Petters, M. D., Rogers, D. C., Russell, L., Savic-Jovcic, V., Snider, J. R., Straub, D., Szumowski, M. J., Takagi, H., Thornton, D. C., Tschudi, M., Twohy, C., Wetzel, M. and van Zanten, M. C.: Dynamics and chemistry of marine stratocumulus–DYCOMS-II, Bull. Amer. Meteor. Soc., 84(5), 579–593, doi:10.1175/BAMS-84-5-579, 2003.

Stevens, B., Moeng, C.-H., Ackerman, A. S., Bretherton, C. S., Chlond, A., de Roode, S., Edwards, J., Golaz, J.-C., Jiang, H., Khairoutdinov, M., Kirkpatrick, M. P., Lewellen, D. C., Lock, A., Müller, F., Stevens, D. E., Whelan, E. and Zhu, P.: Evaluation of Large-Eddy Simulations via Observations of Nocturnal Marine Stratocumulus, Mon. Wea. Rev., 133(6), 1443–, doi:10.1175/MWR2930.1, 2005.

Tampieri, F. and Tomasi, C.: Size distribution models of fog and cloud droplets in terms of the modified gamma function, Tellus, 28(4), 333–347, doi:10.1111/j.2153-3490.1976.tb00682.x, 1976.

Twomey, S.: The Influence of Pollution on the Shortwave Albedo of Clouds, J. Atmos. Sci., 34(7), 1149–1152, doi:10.1175/1520-0469(1977)034<1149:TIOPOT>2.0.CO;2, 1977.

Werner, F., Siebert, H., Pilewskie, P., Schmeissner, T., Shaw, R. A. and Wendisch, M.: New airborne retrieval approach for trade wind cumulus properties under overlying cirrus, J. Geophys. Res., 118(9), 3634–3649, doi:10.1002/jgrd.50334, 2013.

Wiscombe, W. J.: Mie scattering calculations: Advances in technique and fast, vector-speed computer codes, NCAR Tech, National Center for Atmospheric Research, Boulder, Colorado. 1979.

Zhang, Z. and Platnick, S.: An assessment of differences between cloud effective particle radius retrievals for marine water clouds from three MODIS spectral bands, J. Geophys. Res., 116(D20), D20215, doi:10.1029/2011JD016216, 2011.

Zhang, Z., Ackerman, A. S., Feingold, G., Platnick, S., Pincus, R. and Xue, H.: Effects of cloud horizontal inhomogeneity and drizzle on remote sensing of cloud droplet effective radius: Case studies based on large-eddy simulations, J. Geophys. Res., 117(D19), n/a–n/a, doi:10.1029/2012JD017655, 2012.

Zhang, Z., Platnick, S., Yang, P., Heidinger, A. K. and Comstock, J. M.: Effects of ice particle size vertical inhomogeneity on the passive remote sensing of ice clouds, J. Geophys. Res., 115(D17), doi:10.1029/2010JD013835, 2010.

Zhang, Z., Werner, F., Cho, H. M. and Wind, G.: A framework based on 2-D Taylor expansion for quantifying the impacts of subpixel reflectance variance and covariance on cloud optical thickness and effective …, Journal of …, doi:10.1063/1.4975502, 2016.

Zinner, T., Wind, G., Platnick, S. and Ackerman, A. S.: Testing remote sensing on artificial observations: impact of drizzle and 3-D cloud structure on effective radius retrievals, Atmos. Chem. Phys., 10(19), 9535–9549, doi:10.5194/acp-10-9535-2010, 2010.

Page 30: Deleted	**Daniel Miller**	**2/13/18 1:38 PM**

2WT

Page 30: Inserted	**Daniel Miller**	**2/13/18 1:38 PM**

VW

Page 30: Deleted	**Daniel Miller**	**2/13/18 1:38 PM**

2WT

Page 30: Inserted	**Daniel Miller**	**2/13/18 1:38 PM**

VW

Page 30: Deleted	**Daniel Miller**	**2/27/18 2:24 AM**

.

Page 30: Inserted	**Daniel Miller**	**2/27/18 2:24 AM**

. Note that vertically weighted properties are listed for the polarimetric vertical weighting function and H_o for nadir viewing 0.865 µm reflectance.

Page 30: Deleted	**Daniel Miller**	**2/13/18 1:38 PM**

2WT

Page 30: Inserted	**Daniel Miller**	**2/13/18 1:38 PM**

VW

Page 30: Deleted	**Daniel Miller**	**2/13/18 1:38 PM**

2WT

Page 30: Inserted	**Daniel Miller**	**2/13/18 1:38 PM**

VW

Page 31: Inserted	**Daniel Miller**	**4/27/18 12:01 AM**

(7)

Page 31: Inserted	**Daniel Miller**	**4/27/18 12:01 AM**

(8)

Page 32: Comment [1]	Daniel Miller	2/12/18 11:29 AM

Figure updated to correct error in original axes label of panel (a).

Page 32: Inserted	Daniel Miller	3/4/18 4:47 PM

/

Page 33: Inserted	Daniel Miller	2/14/18 10:19 AM

Note that the vertically weighting functions used for the displayed re(VW) and ve(VW) correspond to single-scattering assumptions.

Page 33: Inserted	Daniel Miller	2/13/18 4:23 PM

Axes labels have been removed to enlarge each map, but the spatial dimensions of each scene are roughly 7 x 7 km (refer to section 3 for the specific resolutions of each LES case.)

Page 34: Comment [3]	Daniel Miller	2/25/18 4:25 PM

Figure updated to include data from the new vertical weighting defintions.

Page 34: Comment [2]	Daniel Miller	4/26/18 3:00 PM

Figure updated again to newest vertical weighted properties

Page 34: Deleted	Daniel Miller	2/13/18 2:35 PM

or

Page 34: Inserted	Daniel Miller	2/13/18 2:35 PM

of

Page 34: Deleted	Daniel Miller	2/13/18 1:38 PM

2WT

Page 34: Inserted	Daniel Miller	2/13/18 1:38 PM

VW

Page 35: Comment [5]	Daniel Miller	3/2/18 11:31 AM

Figure updated to include data from the new vertical weighting defintions.

Page 35: Comment [4]	Daniel Miller	4/26/18 9:45 PM

Updated for new VW properties…

Page 35: Deleted	Daniel Miller	2/13/18 1:38 PM

2WT

Page 35: Inserted	Daniel Miller	2/13/18 1:38 PM

VW

Page 35: Deleted	Daniel Miller	2/13/18 1:38 PM

2WT

Page 35: Inserted	Daniel Miller	2/13/18 1:38 PM

VW

Page 35: Inserted	Daniel Miller	2/23/18 4:04 PM

Figure 5: Histograms of the percent retrieval bias of retrievals based on perturbed reflectances stated relative to unperturbed retrievals. Panel (a) displays retrieval biases for the bispectral r_e retrieval. Panel (b) displays retrieval biases for the bispectral and polarimetric τ retrievals. Refer to the text for more information about the polarimetric r_e and v_e retrieval biases.

Page 37: Comment [7]	Daniel Miller	3/2/18 12:13 PM

Figure updated to include data from the new vertical weighting defintions.

Page 37: Comment [6]	**Daniel Miller**	**4/26/18 3:02 PM**

Figure updated for newest vertical weighting definition.

Page 37: Inserted	**Daniel Miller**	**4/27/18 12:01 AM**

6

Page 37: Deleted	**Daniel Miller**	**2/23/18 4:08 PM**

5

Page 38: Comment [8]	**Daniel Miller**	**2/25/18 6:07 PM**

Figure updated with new vertically weighted properties.

Page 38: Inserted	**Daniel Miller**	**4/27/18 12:01 AM**

7

Page 38: Inserted	**Daniel Miller**	**3/4/18 4:47 PM**

(bispectral

Page 38: Deleted	**Daniel Miller**	**3/4/18 4:47 PM**

(SWIR

Page 38: Deleted	**Daniel Miller**	**2/13/18 1:38 PM**

2WT

Page 38: Inserted	**Daniel Miller**	**2/13/18 1:38 PM**

VW

Page 38: Deleted	**Daniel Miller**	**2/13/18 2:36 PM**

reflectance

Page 38: Deleted	**Daniel Miller**	**2/13/18 2:37 PM**

standard

Page 39: Inserted	**Daniel Miller**	**4/27/18 12:01 AM**

8

Page 39: Deleted	**Daniel Miller**	**2/23/18 4:08 PM**

7

Page 40: Comment [9]	**Daniel Miller**	**4/26/18 6:00 PM**

Figure updated for line thickness and readability.

Page 40: Inserted	**Daniel Miller**	**4/27/18 12:01 AM**

9

Page 40: Deleted	**Daniel Miller**	**2/25/18 9:45 AM**

10

Page 40: Inserted	**Daniel Miller**	**2/25/18 9:45 AM**

Probability distributions of H_σ for the combined ATEX polluted and clean datasets at all coarsened spatial resolution (100, 200, 300, 400, 800 m).

Page 41: Inserted	**Daniel Miller**	**2/25/18 7:44 PM**

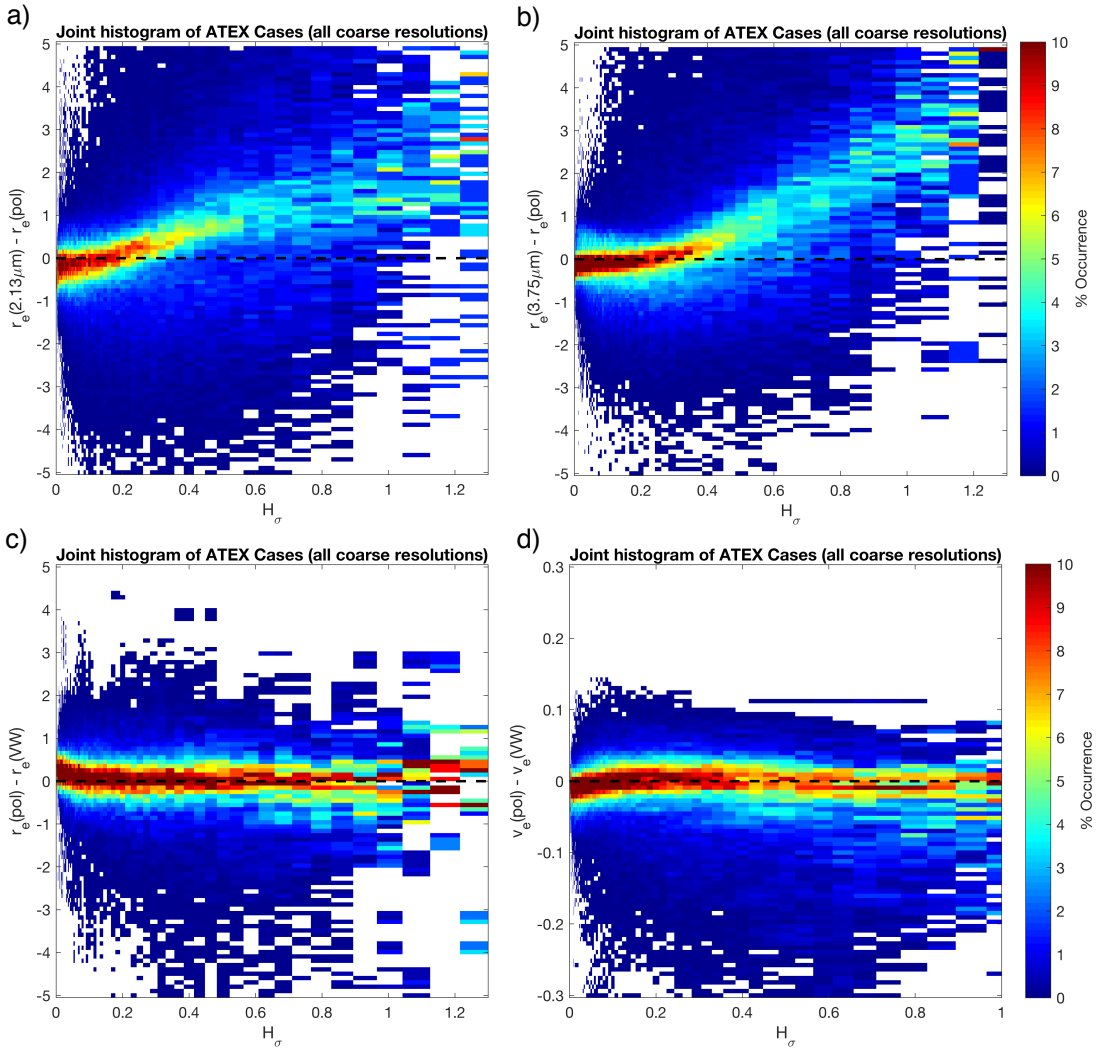

Figure 10: Joint histograms of retrieval biases (relative to each relevant vertically weighted LES property) with respect to H_σ for the combined ATEX clean and polluted datasets at all observation geometries and including all coarsened spatial resolutions (100, 200, 300, 400, 800 m). The color bar indicates percent occurrence. Panels (a) and (b) depict the difference between the two bispectral r_e retrievals and the polarimetric retrieval, while panels (c) and (d) depict biases for the polarimetric r_e and v_e retrieval against r_e(VW).

Page 41: Comment [10]	Daniel Miller	4/26/18 5:57 PM

Figure changed and updated.

Page 42: Comment [11]	Daniel Miller	4/26/18 6:53 PM

Figure updated with new vertically weighted retrieval information, font sizes increased, and background adjusted.

Page 42: Inserted	Daniel Miller	4/27/18 12:01 AM

11

Page 42: Deleted	Daniel Miller	2/14/18 11:45 AM

9

Page 42: Inserted	Daniel Miller	3/4/18 4:47 PM

bispectral

Page 42: Deleted	Daniel Miller	3/4/18 4:47 PM

SWIR

Page 42: Deleted	Daniel Miller	2/13/18 1:38 PM

2WT

Page 42: Inserted	Daniel Miller	2/13/18 1:38 PM

VW

Page 43: Inserted	Daniel Miller	4/27/18 12:01 AM

12

Page 43: Deleted	Daniel Miller	2/14/18 11:45 AM

10

Page 44: Inserted	Daniel Miller	4/27/18 12:01 AM

13

Page 44: Deleted	Daniel Miller	2/14/18 11:45 AM

11

Header and footer changes

Text box changes

Header and footer text box changes

Footnote changes

Page 9: Inserted	Daniel Miller	4/26/18 11:13 PM

[1] The radiatively derived vertical weighting of Platnick (2000) implicitly depends on the $r_e(z)$ profile whereas a fixed parameter vertical weighting described here does not. However, the importance of this difference should be less than the vertical variability of optical depth or extinction cross section.

Page 12: Deleted	Daniel Miller	2/13/18 9:46 AM

[1] The increased concentration of v_e(pol) retrievals at v_e=0.3. is a result of the boundaries of the retrieval space, v_e=[0.01, 0.3]. This limitation is a consequence of the definition of the modified gamma distribution in Hansen and Travis (1974); for v_e=0.3 the size distribution becomes monotonic.

Page 14: Deleted	Daniel Miller	2/27/18 2:24 AM

.

Page 14: Inserted	Daniel Miller	2/27/18 2:24 AM

.

Page 15: Deleted	Daniel Miller	4/26/18 10:53 PM

[1] Additionally, ~12.5% of the cloudy pixels in this scene exhibit values below 4 μm.

Page 15: Inserted	Daniel Miller	2/25/18 5:30 PM

1

Page 15: Inserted	Daniel Miller	4/26/18 10:54 PM

[1] Additionally, ~1% of the cloudy pixels in this scene exhibit values below 4 μm.

Endnote changes

Comparisons of bispectral and polarimetric retrievals of marine boundary layer cloud microphysics: Case studies using a LES-satellite retrieval simulator

Daniel J. Miller[1,3], Zhibo Zhang[1,2], Steven Platnick[3], Andrew S. Ackerman[4], Frank Werner[2], Celine Cornet[5], Kirk Knobelspiesse[3]

[1]Physics, UMBC, Baltimore, 21250, USA
[2]Joint Center for Earth Systems Technology, UMBC, Baltimore, MD, USA
[3]NASA Goddard Space Flight Center, Greenbelt, MD, USA
[4]NASA Goddard Institute for Space Studies, New York, NY, USA
[5]Laboratoire d'Optique Atmosphérique, Université des Sciences et Technologies de Lille, Villeneuve d'Ascq, France

Correspondence to: Daniel J. Miller (Daniel.J.Miller@nasa.gov)

Abstract. Many passive remote sensing techniques have been developed to retrieve cloud microphysical properties from satellite-based sensors, with the most common approaches being the bispectral and polarimetric techniques. These two vastly different retrieval techniques have been implemented for a variety of polar-orbiting and geostationary satellite platforms, providing global climatological datasets. Prior instrument comparison studies have shown that there are systematic differences between the droplet size retrieval products (effective radius) of bispectral (e.g. MODIS, Moderate Resolution Imaging Spectroradiometer) and polarimetric (e.g. POLDER, Polarization and Directionality of Earth's Reflectances) instruments. However, intercomparisons of airborne bispectral and polarimetric instruments have yielded results that do not appear to be systematically biased relative to one another. Diagnosing this discrepancy is complicated, because it is often difficult for instrument intercomparison studies to isolate differences between retrieval technique sensitivities and specific instrumental differences such as calibration, atmospheric correction, etc. In addition to these technical differences the polarimetric retrieval is also sensitive to the dispersion of the droplet size distribution (effective variance), which could influence the interpretation of the droplet size retrieval. To avoid these instrument-dependent complications, this study makes use of a cloud remote sensing retrieval simulator. Created by coupling a large eddy simulation (LES) cloud model with a 1-D radiative transfer model, the simulator serves as a test bed for understanding differences between bispectral and polarimetric retrievals. With the help of this simulator we can not only compare the two techniques to one another (retrieval intercomparison), but also validate retrievals directly against the LES cloud properties. Using the satellite retrieval simulator we are able to verify that at high spatial resolution (50 m) the bispectral and polarimetric retrievals are highly correlated with one another within expected observational uncertainties. The relatively small systematic biases at high spatial resolution can be attributed to different sensitivity limitations of the two retrievals. In contrast, a systematic difference between the two retrievals emerges at coarser resolution. This bias largely stems from differences related to sensitivity of the two retrievals to

Daniel Miller 1/29/2018 10:43 AM
Deleted: al

Daniel Miller 1/29/2018 10:43 AM
Deleted: retrievals

Daniel Miller 1/29/2018 10:44 AM
Deleted: S

Daniel Miller 3/4/2018 5:04 PM
Deleted: DJ-Miller@umbc.edu

Daniel Miller 3/4/2018 5:05 PM
Deleted: s

Daniel Miller 3/4/2018 4:34 PM
Deleted: indeed h

Daniel Miller 3/4/2018 9:20 PM
Deleted: differences

unresolved inhomogeneities in effective variance and optical thickness. The influence of coarse angular resolution is found to increase uncertainty in the polarimetric retrieval, but generally maintains a constant mean value.

1 Introduction

The cloud droplet size distribution (DSD) is an important microphysical property of liquid-phase clouds. Given the cloud water content, it largely determines the shortwave radiative effects of clouds (Twomey, 1977). It also plays a critical role in cloud-precipitation processes (Pruppacher and Klett, 1978). As a result, anthropogenic perturbation to the DSD could lead to a variety of cloud property changes with significant climate implications (Lohmann et al., 2007).

Many satellite-based techniques have been developed to retrieve cloud DSD properties from regional to global scales. These techniques typically infer DSD properties based on an assumed size distribution shape, characterized by an effective radius (r_e), and an effective variance (v_e). One such retrieval method is called the bispectral total reflectance technique, hereafter referred to as the "bispectral technique," which simultaneously retrieves cloud optical thickness (τ) and r_e from a pair of cloud reflectances, typically one in the visible to near infrared (VNIR) and the other in the shortwave infrared (SWIR) or midwave infared (MWIR) spectral range (Nakajima and King, 1990b). This retrieval technique has been implemented for numerous satellite and airborne instruments, such as the Moderate Resolution Imaging Spectro-radiometer (MODIS, (King et al., 2003; Platnick et al., 2003; 2017)), the Spinning Enhanced Visible and Infrared Imager (SEVIRI, (Roebeling et al., 2006)), and the Suomi National Polar-orbiting Partnership Visible Infrared Imaging Radiometer Suite (Suomi NPP VIIRS, (Rosenfeld et al., 2014)).

A second, fundamentally different, retrieval technique is the multi-angular polarimetric reflectance technique, hereafter referred to as the "polarimetric technique". This retrieval requires multi-angular observations of the polarized reflectance in the cloudbow scattering region. In addition to r_e, the polarimetric technique can also retrieve v_e (Bréon and Goloub, 1998). Global retrievals using the polarimetric technique were first demonstrated by the Polarization and Directionality of Earth Reflectance (POLDER, (Deschamps et al., 1994)) instruments operating from 1996 to 2013 on three different satellite platforms. The Aerosol Polarimetry Sensor (APS, (Mishchenko et al., 2007)) would have been the first space-borne multi-angular polarimeter from U.S. to provide global aerosol and cloud property retrievals. Unfortunately, it was lost as a result of the satellite launch failure in 2011, which suddenly interrupted development of polarimetric-based remote sensing in the U.S. Recognizing the great potential of polarimetric techniques for aerosol and cloud remote sensing, NASA has invested heavily in recent years on the development of airborne polarimeters, such as the Research Scanning Polarimeter (RSP, (Cairns et al., 1999)), the Airborne Multi-angle Spectro-Polarimetric Imager (AirMSPI, (Diner et al., 2013)) and the Airborne Hyper-Angular Rainbow Polarimeter (Air-HARP, (Martins et al., 2017)). Moreover, several space-borne missions are in development, such as the Multi-Angle Imager for Aerosols (MAIA, (Liu and Diner, 2017)), HARP, the Plankton, Aerosols, Cloud, ocean Ecosystem mission (PACE) and the Multi-viewing, Multi-channel, Multi-polarization imaging mission (3MI, (Marbach et al., 2013)). Each of these missions will have a multi-angular polarimeter on-board. In

Daniel Miller 3/2/2018 3:04 PM
Deleted: 2016

Steven Platnick 2/28/2018 4:26 PM
Deleted: vastly

the foreseeable future, we may expect to have operational global retrievals of cloud droplet size distributions from both bispectral and polarimetric methods.

The bispectral and polarimetric remote sensing techniques are the primary tools we have to obtain DSD observations on a global scale. It is therefore essential to identify and explain differences between the two techniques so we can better understand their respective advantages and limitations. A satellite retrieval intercomparison of POLDER and MODIS r_e retrievals by Bréon and Doutriaux-Boucher (2005) represented one of the first attempts to identify and understand the differences between the two techniques. The main finding from this study is that the bispectral-based MODIS retrieval of r_e(2.13µm) (using the 2.13 µm SWIR band) is persistently 2 µm larger than the 150 km scale polarimetric-based POLDER retrieval over ocean, despite a close correlation between the two. A variety of factors, from differences in sensitivity to cloud vertical profile to influence of cloud horizontal inhomogeneity, have been suggested to explain this difference. However, as pointed out by the authors, all these factors might contribute to the difference. It is difficult, if not impossible, to untangle them in observations and determine their relative importance. In addition, POLDER observations in this study were aggregated from the nominal 6 km spatial resolution to a much coarser 150 km resolution to achieve the angular resolution needed to resolve the cloud bow. The vast difference in spatial resolution (i.e., 150 km for POLDER and 1 km for MODIS) makes the interpretation of the 2 µm r_e difference between the two retrievals even more difficult.

A more recent study by Alexandrov et al. (2015) is based on observations from the recent sub-orbital Polarimeter Definition Experiment (PODEX) in 2013. In that study, the polarimetric r_e retrievals for marine stratocumulus decks off the California coast from the airborne RSP instrument are compared to collocated bispectral retrievals from the Autonomous Modular Sensor (AMS). Interestingly, the two retrievals are found to be in close agreement, with a correlation of 0.928 and negligible bias of less than a micron. Beyond the clear instrument differences of the Alexandrov et al. (2015) and Bréon and Doutriaux-Boucher (2005) studies, it is still unclear how well the bispectral and polarimetric retrievals should compare to one another and what situations might cause them to differ, raising numerous questions and motivating this study.

A great challenge facing these observational studies is the intertwining of various instrument and scene dependent factors that lead to retrieval differences. For example, the polarimetric and bispectral methods have different sensitivity to the cloud vertical profile, and at the same time they are also both affected by cloud horizontal inhomogeneity (Zinner et al., 2010; Zhang et al., 2012; 2016; Miller et al., 2016). It is difficult, if not impossible, to disentangle these factors based on observations alone. This study approaches the intercomparison of bispectral and polarimetric retrievals through a different route: rather than use observational remote sensing data, synthetic retrievals are generated from large-eddy simulations (LES) of clouds. Modeling radiative transfer in an LES scene to obtain total and polarized reflectances opens up the possibility of using the LES to perform synthetic bispectral and polarimetric retrievals. This retrieval simulator framework has proven to be a useful tool in other cloud remote sensing studies (Miller et al., 2016; Zhang et al., 2012). Using this idealized simulation at high spatial resolution, we can attempt to parse the effects of unresolved sub-pixel inhomogeneity, spatial resolution, and angular resolution on the intercomparison of polarimetric and bispectral retrievals. The scale of the LES simulations (~10 km) in this study prevents us from examining resolutions as large as the standard POLDER retrieval

Daniel Miller 1/23/2018 4:17 PM
Deleted: Because

Daniel Miller 3/4/2018 11:41 AM
Deleted: ,

Daniel Miller 1/23/2018 4:18 PM
Deleted: it is important

Daniel Miller 1/23/2018 4:18 PM
Deleted: the

Daniel Miller 1/23/2018 4:18 PM
Deleted: between them

Daniel Miller 1/23/2018 4:21 PM
Deleted: the

Daniel Miller 1/23/2018 4:21 PM
Deleted: of each technique

Daniel Miller 2/26/2018 1:23 PM
Deleted: Bréon and Doutriaux-Boucher (2005)

Steven Platnick 2/28/2018 4:36 PM
Deleted: by about 2 µm

Daniel Miller 2/26/2018 1:23 PM
Deleted: Bréon and Doutriaux-Boucher (2005)

Daniel Miller 2/25/2018 10:10 PM
Deleted: whether

Daniel Miller 2/25/2018 10:10 PM
Deleted: well

Daniel Miller 2/25/2018 10:10 PM
Deleted: or not

Daniel Miller 2/25/2018 10:11 PM
Deleted: that

Daniel Miller 2/25/2018 10:11 PM
Deleted: e

Daniel Miller 3/2/2018 3:55 PM
Deleted: Miller et al., 2016

Daniel Miller 3/2/2018 3:55 PM
Deleted: ; Zinner et al., 2010

(~150 km), but we are able to advance understanding how spatial resolutions from 50 m to 1 km. These scales are suitable for airborne instrument comparisons, which certainly fall somewhere in this range. The use of a satellite retrieval simulator opens up two unique opportunities for developing and studying cloud microphysical retrievals: First, it provides the means to compare retrievals directly to LES cloud microphysics. Second, it allows us to perform a retrieval technique intercomparison that is independent of instrument characteristics and other differences that complicate observational studies. This study focuses on three particular questions:

- How well do the bispectral and polarimetric retrievals perform relative to the LES fields used as input to the retrievals?
- How do the bispectral and polarimetric retrieval techniques compare to one another at high spatial resolution?
- How are the bispectral and polarimetric retrieval techniques sensitive to specific observational conditions (i.e., the influence of spatial and angular resolution)?

The rest of the paper is organized as follows: Section 2 provides a brief introduction to the theoretical basis of the two retrieval techniques; Section 3 describes the LES-based satellite retrieval simulations used in this study; the comparisons between the two techniques based on the LES cases are presented in Section 4; followed by summary and discussion in Section 5.

2 Background

2. Cloud microphysical and optical properties

In satellite remote sensing DSDs are often described using theoretical distributions that fit well with in situ observations, in addition to being mathematically convenient (Deirmendjian, 1964; Tampieri and Tomasi, 1976; Martin et al., 1994; Miles et al., 2000). A popular theoretical DSD is the gamma distribution proposed by Hansen and Travis (1974):

Daniel Miller 3/2/2018 4:06 PM
Deleted: ; Tampieri and Tomasi, 1976

$$N\left(r;r_e,v_e\right)\equiv N_0 C r^{\left(1-3v_e\right)/v_e}\exp\left[-r/\left(r_e v_e\right)\right], \quad (1)$$

where the independent variable r is the cloud droplet radius, $N(r)$ is the droplet size distribution, N_0 is the droplet number concentration, and C is a normalization constant. The two distribution parameters are the effective radius (r_e) and the effective variance (v_e) of the DSD:

$$r_e \equiv \frac{\int_0^\infty Q_e(r) r^3 N(r) dr}{\int_0^\infty Q_e(r) r^2 N(r) dr} \approx \frac{\int_0^\infty r^3 N\left(r;r_e,v_e\right) dr}{\int_0^\infty r^2 N\left(r;r_e,v_e\right) dr} = \frac{\left\langle r^3\right\rangle}{\left\langle r^2\right\rangle}, \quad (2)$$

$$v_e \equiv \frac{1}{r_e^2}\frac{\int_0^\infty Q_e(r)(r-r_e)^2 r^2 N(r) dr}{\int_0^\infty Q_e(r) r^2 N(r) dr} \approx \frac{1}{r_e^2}\frac{\int_0^\infty (r-r_e)^2 r^2 N\left(r;r_e,v_e\right) dr}{\int_0^\infty r^2 N\left(r;r_e,v_e\right) dr} = \frac{\left\langle r^4\right\rangle\left\langle r^2\right\rangle}{\left\langle r^3\right\rangle^2} - 1. \quad (3)$$

where $\langle r^n \rangle = \int_0^\infty r^n N(r) dr$ is the n^{th} moment of the DSD. For the spectral bands relevant to this study, the extinction efficiency (Q_e) is approximately constant (i.e., Q_e(r)~const.=2). Thus, the relationships between r_e and v_e can be conveniently reduced to relations between arithmetic moments of the DSD. The DSD plays an important role in defining the bulk optical properties of a cloud. The optical property libraries used in this study are based on single-scattering Mie calculations of monodisperse droplet optical properties that are averaged with respect to size, according to the gamma DSD (Wiscombe, 1979). In addition, these single-scattering optical properties are averaged with respect to wavelength over an instrument-specific spectral response function (based on MODIS bands in this study) and solar source functions (Planck blackbody function (Planck, 1914)). The single-scattering bulk cloud optical properties are subsequently used to run radiative transfer calculations for the creation of the so-called bispectral reflectance look-up-table (LUT). This LUT is made up of pre-calculated reflectances of plane-parallel and homogeneous (PPH) clouds over a high-resolution grid of combinations of τ, r_e, and v_e. Here, τ is defined in terms of the DSD:

$$\tau_{tot,\lambda} \equiv \int_{TOA}^{0} \left[\int_0^\infty Q_{e,\lambda}(r) \pi r^2 N_0 n(r) dr \right] dz \quad (4)$$

2.2 Bispectral and Polarimetric Retrieval Methods

The bispectral method retrieves τ and r_e simultaneously from a pair of observed cloud reflectances, typically using a combination of VNIR and SWIR/MWIR bands. The VNIR band, with relatively negligible liquid water droplet absorption, and the SWIR/MWIR band, where droplets are moderately absorptive, can be used to remotely infer τ and r_e because of this difference in sensitivity to multiple scattering (thickness) and absorption (droplet size). This method is usually implemented using a LUT, shown graphically in Figure 1(a), which has a fixed v_e. Cloud reflectance in the VNIR band (centered around 0.865 µm) increases with τ (gray) for a fixed r_e, while the reflectance in the MWIR band (centered around 3.75 µm) decreases with r_e (colored) when τ is fixed. The retrieved properties are obtained by performing a two-dimensional inverse interpolation between observed reflectance and the τ-r_e grid. A notable characteristic of the bispectral LUT is that when the optical thickness is low (τ<3), the isolines of the LUT are more densely packed and less orthogonal, which results in reduced sensitivity and increased retrieval uncertainty (Werner et al., 2013). The bispectral technique is not particularly sensitive to v_e, so typically a fixed value is assumed (e.g., v_e=0.1 in the operational MODIS retrieval, though it is kept as an error source in calculating pixel-level uncertainties). While different combinations of bands are used to perform the bispectral retrieval, in this study we focus on VNIR reflectances centered on 0.865 µm with the second band is selected from either a 2.13 µm centered SWIR band or a 3.75 µm centered MWIR band There are consequences for the r_e retrieval depending on the particular set of bands selected. For example, a strongly absorbing SWIR/MWIR band limits penetration into the cloud and

Daniel Miller 2/14/2018 10:20 AM
Deleted:

Steven Platnick 2/28/2018 10:13 AM
Deleted: observed in

Steven Platnick 2/28/2018 10:13 AM
Deleted: , respectively

Steven Platnick 2/28/2018 10:14 AM
Deleted: dominated by multiple scattering

Steven Platnick 2/28/2018 10:15 AM
Deleted: liquid water

Daniel Miller 1/29/2018 10:45 AM
Deleted: The VNIR band, dominated by multiple scattering, provides sensitivity to τ; the selected SWIR band, where liquid water droplets are moderately absorptive, provides sensitivity to r_e.

Steven Platnick 2/28/2018 10:16 AM
Deleted: like the one

Daniel Miller 3/4/2018 4:40 PM
Deleted: SWIR

Daniel Miller 3/4/2018 4:50 PM
Deleted: a priori

Daniel Miller 3/4/2018 4:42 PM
Deleted: VNIR and SWIR

Daniel Miller 3/4/2018 4:43 PM
Deleted: and

Daniel Miller 3/4/2018 4:41 PM
Deleted: reflectances centered on both

Daniel Miller 3/4/2018 4:41 PM
Deleted: 2.13 and

Daniel Miller 3/4/2018 4:42 PM
Deleted: .

Daniel Miller 3/4/2018 4:43 PM
Deleted: SWIR

as a result the retrieved r_e is vertically weighted toward the microphysics prevalent in the uppermost part of the cloud (Platnick, 2000).

For the polarimetric retrieval, the angular pattern of the linearly polarized reflectance[1] is the source of sensitivity to cloud microphysical properties. Polarized reflectances are dominated by single scattering because multiple scattering induces depolarization. As a result, the single-scattering polarized phase functions ($-P_{12}$) shown in Figure 1 (b) and (c) are good approximations to the observed angular pattern of polarized cloud reflectances (Bréon and Goloub, 1998). These phase functions demonstrate the sensitivity of the polarimetric retrieval to both r_e and v_e. As r_e increases in Figure 1(b) the supernumerary bow peaks (around a scattering angle of 142°) become narrower and shift toward smaller scattering angles. In contrast, as v_e increases in Figure 1(c) the supernumerary bow peaks erode in magnitude, eventually smoothing out for broad DSDs (v_e>0.15). A consequence of this erosion of the supernumerary peaks is that the polarimetric retrieval has less sensitivity to both r_e and v_e for very broad DSDs. The polarimetric retrieval does not significantly rely on multispectral information, although observations in several bands may help provide stronger observational constraints due to the shift in the supernumerary bows with changing wavelength (refer to figure 3 of Bréon and Goloub (1998). The dominance of the single scattering contributions to the polarized reflectance leads to cloud retrievals that represent microphysical properties with a mean penetration depth of $<\tau_{SS}>\leq 0.5$ and sensitivity that saturates for optical depths greater than ~3 from the cloud top. The polarimetric retrieval is often based on a parametric curve fitting retrieval algorithm like the one presented in Alexandrov et al. (2012b), although there are other techniques (e.g., the Rainbow Fourier Transform technique of Alexandrov et al. (2012a), which can retrieve DSD's with arbitrary mathematical form.) The parametric technique relies on a library of $-P_{12}$ curves with varying r_e and v_e that are parametrically scaled and adjusted to fit the observed reflectance via a nonlinear least squares optimization procedure. This process yields the phase function that best matches the angular pattern of the observation, thus determining the r_e(pol) and v_e(pol) retrieval. The polarimetric method described above does not result in a retrieval of τ; however, it can still be obtained by implementing a simplified variant of the bispectral τ retrieval. With simultaneous measurements of the total reflectance in a VNIR band and the r_e(pol) retrieval, a VNIR-only LUT curve can be used to perform a 1-D interpolation of the corresponding bispectral LUT curve for $R_{VNIR}(r_e(\text{pol}), \tau)$.

Both bispectral and polarimetric techniques are susceptible to a variety of retrieval uncertainties. The main objective of this study is to understand how the retrieval uncertainties influence each technique and whether they can lead to deviation between the two techniques in terms of retrieval results. In this study, we focus on five major sources of retrieval uncertainty for both techniques:

1) Cloud vertical profile: In the operational retrievals, both bispectral and polarimetric techniques assume vertically homogenous clouds. However, clouds in reality often have significant vertical variability resulting from various processes (e.g., condensational growth, coalescence, sedimentation, entrainment). Deviation from the assumed profile gives rise to many questions. For example, how do we interpret the r_e and v_e retrievals based on the homogenous cloud assumption? To

1 Note that throughout this paper, we will refer to "linearly polarized reflectances" simply as "polarized reflectances" in recognition of the negligible contribution of circularly polarized light in the atmosphere (Hansen, 2010).

Daniel Miller 2/14/2018 10:21 AM
Deleted:

Daniel Miller 2/14/2018 10:21 AM
Deleted:

Daniel Miller 3/4/2018 4:53 PM
Deleted: within the top

Daniel Miller 3/4/2018 4:56 PM
Deleted:

Daniel Miller 3/4/2018 4:57 PM
Deleted: optical depths

Daniel Miller 3/4/2018 4:53 PM
Deleted: in

Daniel Miller 2/26/2018 1:23 PM
Deleted: Alexandrov et al. (2012b)

Daniel Miller 2/26/2018 1:23 PM
Deleted: Alexandrov et al. (2012a)

Daniel Miller 3/5/2018 10:18 AM
Deleted: multi-modal

Daniel Miller 3/30/2018 11:11 AM
Deleted: three

Daniel Miller 4/26/2018 6:57 PM
Deleted: s

what extent does cloud vertical profile influence the bispectral and polarimetric techniques? Note that Platnick (2000) developed a method utilizing the so-called "vertical weighting function" to interpret the r_e retrieval from the bispectral method for clouds with vertically varying r_e profile. Recently, Alexandrov et al., (2012b) took an approach that focused on the vertical weighting of the droplet size distribution to interpret the r_e and v_e retrievals from the polarimetric technique. Miller et al. (2016) demonstrated the usefulness of this vertical weighting approach for understanding both bispectral and polarimetric r_e retrievals. In Section 4.1, we will apply a vertical weighting function for both techniques on the basis of the LES cloud fields, to help understand if cloud vertical structure could lead to significant differences between the two techniques.

2) Sensitivity to observational uncertainty: The uncertainties associated with observations of total and polarized reflectances can differ, indicating that uncertainty may also impact bispectral and polarimetric retrievals differently. Additionally, the two retrievals rely on different number of uncertain observations; a pair of uncertain total reflectances (bispectral) as compared to numerous uncertain polarized reflectances (polarimetric). Furthermore the different algorithmic approaches, two-dimensional interpolation vs. nonlinear optimal curve fitting introduce additional layers of complexity in terms of the impact of uncertainty. The impact of uncertainty on retrieval results for each method are highlighted and explored in section 4.2.

3) Reduced sensitivity: It can be clearly seen from Figure 1 (a) that when clouds are optically thin (τ<3), the LUT for the bispectral retrieval becomes less orthogonal and the isolines of r_e become more densely packed. This reduction in sensitivity can lead to significant retrieval uncertainties in bispectral techniques for optically thin clouds (τ<3). Similarly, the sensitivity of the polarimetric technique to r_e and v_e is reduced when DSD becomes very broad (i.e., v_e>0.15), in which case the supernumerary bow features are barely distinguishable (Figure 1 (c)). In Section 4.3 we will investigate the impacts of the reduction of sensitivity on retrieval consistency between the two techniques.

4) Sub-pixel inhomogeneity: The impact of spatial resolution and unresolved sub-pixel cloud inhomogeneity on bispectral retrievals has been well studied (Zhang and Platnick, 2011; Zhang et al., 2012; 2016). An important conclusion from these studies is that the so-called plane-parallel homogenous bias (PPHB) can cause the bispectral technique to significantly overestimate r_e. In contrast, the sensitivity of the polarimetric retrieval to unresolved sub-pixel inhomogeneity and resolution has not been thoroughly studied. In Section 4.4 we will compare the impacts of sub-pixel inhomogeneity on bispectral and polarimetric techniques, and investigate whether it can cause deviation between the two techniques.

5) Angular resolution and sampling for polarimetric technique: In addition to spatial resolution, angular resolution and sampling is also important for the polarimetric technique. A coarse angular resolution may not be able to resolve the feature of the supernumerary bows. Similarly, if the scattering angles corresponding to the supernumerary bows are not or only partly sampled, then the polarimetric technique may not have enough information content for retrieval. This issue will be discussed in Section 4.5.

Daniel Miller 2/26/2018 1:23 PM
Deleted: Alexandrov et al. (2012b)

Daniel Miller 3/4/2018 4:58 PM
Deleted: modified this method slightly and applied it

Daniel Miller 4/11/2018 11:37 AM
Deleted: the

Daniel Miller 4/11/2018 11:37 AM
Deleted: method to

Daniel Miller 2/13/2018 10:40 AM
Deleted: 2

Daniel Miller 2/13/2018 10:17 AM
Deleted: 2

Daniel Miller 2/13/2018 10:40 AM
Deleted: 4

Daniel Miller 2/13/2018 10:17 AM
Deleted: 3

Daniel Miller 4/26/2018 6:10 PM
Deleted: ,

Daniel Miller 2/13/2018 10:18 AM
Deleted: 4

Daniel Miller 2/13/2018 10:31 AM
Deleted:

Daniel Miller 2/13/2018 10:17 AM
Deleted: 4

3 Model and Methodology

The satellite retrieval simulator implemented in this study is built around an LES model (DHARMA) with bin microphysics (Ackerman et al., 2004; Zhang et al., 2012; Miller et al., 2016). The LES provides freely evolving 3-D cloud microphysical properties, which are used as reference when comparing to numerically simulated retrievals. The LES in this study adopts 25 droplet size bins to represent droplet size distributions (Ackerman et al., 1995). The optical properties of each size bin are computed by bulk averaging Mie scattering properties over a highly resolved flat sub-bin droplet size distribution. The optical properties of each bin are provided as input to radiative transfer simulations based on the size distributions of the LES cloud fields. Vector radiative transfer calculations are performed using a polarized doubling-adding technique (PDA) to produce 1-D total and polarized reflectances at the horizontal resolution of the LES grid (described below) (De Haan et al., 1987). The sole consideration of 1-D retrievals avoids 3-D radiative effects and focuses this study on retrieval technique differences rather than on radiative processes. A future study will focus on the comparison of 3-D retrievals to these 1-D bispectral and polarimetric retrievals. The radiative transfer modeling in this work is performed for numerous solar zenith angles (SZA=[20, 40, 60]°), viewing zenith angles (VZA=[−70 : +70]°), and a constant relative azimuthal angle ($\Delta\Phi$ = 30°). The VZA resolution results in a scattering angle (Θ) resolution on the order of 0.5°. Reflectances in spectral bands (based on MODIS spectral response functions) are centered on 0.865, 2.13, and 3.75 µm wavelengths. Total reflectances in all bands are used to produce bispectral retrievals, whereas linearly polarized reflectances in the 0.865 µm band are used to produce polarimetric retrievals. Subsequently, bispectral and polarimetric retrievals are performed on the simulated reflectances to obtain r_e, v_e, and τ retrievals. Bispectral and polarimetric retrievals are performed over a subset of observation geometries, with bispectral retrievals performed for VZA=[50, 40, 30, 20, 10, 0, −10]° and all SZA. Meanwhile, the polarimetric retrievals are performed for a SZA=20° and a range of VZA=[0:27]° that result in reflectances spanning scattering angles required to observe the primary and supernumerary bow features (i.e., Θ=[135:160]°). Reflectances are also aggregated from the 50 m native LES resolution up to coarser 100, 200, 400, and 800 m horizontal resolutions to reflect the influence of different remote sensing footprints. The retrievals in this study are also performed at all of the footprint resolutions. The bispectral LUT implemented in this study spans microphysical properties r_e=[2:30] µm in steps of 0.5 µm and v_e=[0.01:0.11] in steps of 0.01. The τ retrieval in this study is anchored to the 0.865 band optical properties and spans τ=[0.1:100] with 101 logarithmically spaced grid points. Including v_e variability in the bispectral LUT allows for the comparison of standard MODIS-like retrievals (the v_e=0.1 LUT) to retrievals with other v_e assumptions. The bispectral retrieval is then accomplished by performing a 2-D linear interpolation of the observed reflectances and inverting between the reflectance and retrieval space. For the polarimetric retrieval, the polarimetric phase function library spans r_e=[2:40] µm in steps of 0.25 µm and v_e=[0.01:0.3] in steps of 0.01. The polarimetric retrieval implemented in this study is based on the approach of Alexandrov et al. (2012a), fitting the polarized phase functions in their eq. (3) to the modeled polarized reflectances of the LES scene. The optimal parametric fit in the $-P_{12}$ library is determined by using a Levenberg-Marquardt nonlinear least squares algorithm. This optimal phase function is then used to identify the

Daniel Miller 3/4/2018 4:26 PM
Deleted: ; Miller et al., 2016

Daniel Miller 2/8/2018 2:19 PM
Deleted: the

Daniel Miller 2/8/2018 2:20 PM
Deleted: ly fitting

corresponding r_e(pol) and v_e(pol) retrieval. As previously stated in section 2.2 the polarimetric retrieval of τ is accomplished by using a constrained 1-D version of the bispectral LUT.

The LES cloud fields are used not only to drive the radiative transfer simulations, but also to help interpret and understand the retrieval results. As mentioned in Section 2.2, it is not trivial to interpret the r_e and v_e retrievals based on the homogenous cloud assumption when the cloud has significant vertical structure. To address this issue, for each LES column with detailed vertical profiles of DSD, we derive two reference variables r_e(VW) and v_e(VW) from the vertical weighted (VW) integration of the DSD profile. The vertical integration is weighted by a function to account for the penetration depth and multiple scattering of radiation in the corresponding wavelength associated with each particular retrieval. Thus, r_e(VW) and v_e(VW) should be comparable to the retrieved r_e and v_e from the simulated reflectance (Alexandrov et al., 2012b; Miller et al., 2016; Zhang et al., 2017). The method of vertical weighting in this study is described in detail in section 2 of Miller et al. (2016), however in this study we have modified the vertical weighting function to account for multiple scattering. Motivated by the convenience and flexibility of the parametric approach proposed in eq. 4 of Zhang et al. (2017), we implement a two-variable parametric vertical weighting function:

$$W(\tau) = c\tau^b \exp\left[-a\tau\left(\frac{1}{\mu}+\frac{1}{\mu_0}\right)\right], \quad (4)$$

where the new parameters a and b are introduced to account for the influence of multiple scattering effects not originally considered in the vertical weighting function discussed previously in Miller et al. (2016). The parameter a scales the optical depth, modelling the enhanced transmission caused by multiple scattering whereas the parameter b produces a peaked vertical weighting function associated with the expected penetration depth of the reflected light and c is the normalization factor. Each of these parameters is strictly positive, and for a=1 and b=0 we obtain the original single scattering vertical weighting used in Miller et al. (2016). For smaller values of a and larger values of b, the vertical weighting function extends deeper into the cloud, leading to droplet size distribution properties deeper in the cloud contributing more information to the vertically weighted value. For the polarimetric retrieval, a=1 and b=0 were selected due to the dominance of single scattering in polarized reflectances. In contrast, multiple scattering can significantly impact total reflectances. For total reflectances a single value of a and b was selected for each spectral band and observation geometry based on coefficients that fit best to numerically calculated vertical weighting functions based on the method presented in eq. 4 of Platnick (2000).[2] Generally, we found that a(3.75 μm) was larger than a(2.13 μm), as would be expected because of stronger absorption in 3.75 μm reducing transmission into the cloud. We also found that b was dependent on observation geometry (scattering angle) and b(3.75 μm) was less than b(2.13 μm) because multiply scattered light in the 2.13 μm band can penetrate deeper into the cloud before scattering back out. In addition to r_e(VW) and v_e(VW), we also derive τ_{LES} for each LES column simply by

[2] The radiatively derived vertical weighting of Platnick (2000) implicitly depends on the $r_e(z)$ profile whereas a fixed parameter vertical weighting described here does not. However, the importance of this difference should be less than the vertical variability of optical depth or extinction cross section.

Daniel Miller 2/8/2018 2:20 PM
Deleted: corresponds

Daniel Miller 2/8/2018 2:20 PM
Deleted: to the resulting

Daniel Miller 2/13/2018 10:50 AM
Deleted: 2WT

Daniel Miller 2/13/2018 10:50 AM
Deleted: 2WT

Daniel Miller 3/4/2018 12:30 PM
Deleted: integration is weighte

Daniel Miller 3/4/2018 12:30 PM
Deleted: d

Daniel Miller 2/13/2018 10:49 AM
Deleted: two-way transmittance (2WT)

Daniel Miller 2/13/2018 10:49 AM
Deleted: the

Daniel Miller 2/13/2018 10:49 AM
Deleted: single-scattered

Daniel Miller 2/13/2018 10:52 AM
Moved (insertion) [1]

Daniel Miller 3/4/2018 12:49 PM
Deleted: directly

Daniel Miller 2/26/2018 6:37 PM
Deleted: numerically

Daniel Miller 2/27/2018 10:35 AM
Deleted: 5

Daniel Miller 3/4/2018 12:51 PM
Deleted: Platnick, 2000;

Daniel Miller 2/13/2018 10:53 AM
Moved (insertion) [2]

Daniel Miller 2/13/2018 11:11 AM
Deleted: (at 0.865 μm). For a complete description on how vertical weighting is accounted for in the calculation of r_e(2WT) and v_e(2WT), see section 2 of (Miller et al., 2016). The r_e(2WT) and v_e(2WT) take into account the first-order sensitivity of the retrieval techniques to the vertical profile of clouds.

Daniel Miller 2/13/2018 10:53 AM
Moved up [2]: section 2 of (Miller et al., 2016).

Daniel Miller 2/13/2018 10:52 AM
Moved up [1]: Thus, they are directly con ... [1]

Daniel Miller 2/13/2018 1:11 PM
Deleted: . We note that the 2WT vertical ... [2]

Daniel Miller 2/13/2018 1:11 PM
Deleted: 2WT

Daniel Miller 2/13/2018 1:11 PM
Deleted: 2WT

integrating the extinction coefficient (for λ=0.865 μm) from cloud bottom to cloud top. The r_e(VW), v_e(VW) and τ_{LES} are used as references in the retrieval and LES property comparison in section 4.1 to understand the differences between the retrievals and the original LES fields. After obtaining the r_e(VW), v_e(VW) and τ_{LES} at the 50 m native LES resolution, they are aggregated to 100, 200, 400, and 800 m to help interpret the retrievals at these coarser resolutions. It is important to note that there is a subtle difference between directly aggregating r_e(VW) or v_e(VW), and aggregating the DSD (i.e., $N(r)$) first and then deriving the corresponding r_e(VW) and v_e(VW). The differences between the two methods are discussed in the Appendix. The main conclusion is that, although the two aggregation methods could be different in some hypothetical cases with unrealistically large variability in the unresolved microphysics, they are essentially equivalent for practical purposes. In this study, we simply aggregate r_e(VW) and v_e(VW) from the native LES resolution of 50 m to obtain average values at desired resolution (e.g., 800 m).

Three LES cases are the focus of this study. The first (referred to as "ATEX clean" hereafter) and second ("ATEX polluted") cases are based on an idealized case study from the Atlantic Trade Wind Experiment (ATEX), with different aerosol loadings (Stevens et al., 2001). The ATEX cases are representative of a trade wind cumulus regime in which scattered cumuli rise into a thin, broken stratocumulus layer. The third case (referred to as "DYCOMS-II" hereafter), originally presented in Stevens et al. (2005), is an idealized setup based on clouds observed during the second research flight (RF02) of the Second Dynamics and Chemistry of Marine Stratocumulus project (DYCOMS-II) (Stevens et al., 2003). This case is representative of nocturnal marine stratocumulus under a dry inversion. The DYCOMS-II case has a domain size of 6.4×6.4×1.5 km (128x128x96 grid points), while each of the ATEX simulations has a domain size of 7.2×7.2×3 km (144×144×200 grid points). The horizontal grid spacing of these LES cases is fixed at 50 m, while the vertical grid is stretched, with a minimum spacing of 5 m near the surface and the capping temperature inversion to better resolve small-scale turbulence there. Further details of the model setup for the DYCOMS-II case are provided in Ackerman et al. (2009). The ATEX cases are updated model runs with increased spatial resolution that are similar to the cases discussed in Fridlind and Ackerman (2011). For each LES scene a snapshot of cloud microphysical and optical properties is saved every half hour after the first hour of each simulation, resulting in numerous cloud fields. A single time step of each of the cases was selected to be the focus of this retrieval study, each occurring ~3 hours into the simulation.

The variability of cloud optical and microphysical properties in each of the LES cases is highlighted in Figure 2 and Table 1. Spatial inhomogeneity of both optical and microphysical properties of these scenes is evident, with the ATEX polluted and DYCOMS-II cases exhibiting lower spatial inhomogeneity and the ATEX clean case being more broken and inhomogeneous. One method for quantifying the optical inhomogeneity of a cloud scene is to use the sub-pixel inhomogeneity index,

$$H_\sigma(\text{resolution}) = \frac{\text{std}\left[R_i(0.865\ \mu\text{m}, 50\ \text{m})\right]}{\text{mean}\left[R_i(0.865\ \mu\text{m}, 50\ \text{m})\right]}, \quad (4)$$

Daniel Miller 2/13/2018 1:11 PM
Deleted: 2WT

Daniel Miller 2/13/2018 1:11 PM
Deleted: 2WT

Daniel Miller 2/13/2018 1:11 PM
Deleted: 2WT

Daniel Miller 2/13/2018 1:11 PM
Deleted: 2WT

Daniel Miller 2/13/2018 1:11 PM
Deleted: 2WT

Daniel Miller 2/13/2018 1:11 PM
Deleted: 2WT

Daniel Miller 2/13/2018 1:11 PM
Deleted: 2WT

Daniel Miller 2/13/2018 1:12 PM
Deleted: 2WT

Daniel Miller 3/4/2018 12:58 PM
Deleted: that have

Daniel Miller 2/13/2018 1:12 PM
Deleted: small-scale

Daniel Miller 2/13/2018 1:12 PM
Deleted: tion

Daniel Miller 2/27/2018 9:44 AM
Deleted: of DSD

Daniel Miller 2/27/2018 9:45 AM
Deleted: (

Daniel Miller 2/27/2018 9:45 AM
Deleted: Shang et al. 2015),

Daniel Miller 2/13/2018 1:13 PM
Deleted: 2WT

Daniel Miller 2/13/2018 1:13 PM
Deleted: 2WT

Daniel Miller 3/4/2018 12:59 PM
Deleted: the

Daniel Miller 2/26/2018 1:23 PM
Deleted: Stevens et al. (2005)

Daniel Miller 2/26/2018 1:23 PM
Deleted: Ackerman et al. (2009)

Daniel Miller 2/26/2018 1:23 PM
Deleted: Fridlind and Ackerman (2011)

where the numerator and denominator are the standard deviation and mean of the native LES resolution (50 m) reflectances within a coarser resolution pixel. Thus, the value of H_σ is computed for a coarser spatial resolution pixel (800 m in Table 1) using the highest-resolution nadir viewing reflectances (50 m). The value of H_σ increases with increasing sub-pixel inhomogeneity, making it a useful measure for unresolved cloud variability. In addition to optical inhomogeneity, each of the LES scenes also has characteristically different microphysical properties. The average value of r_e(VW) of each scene varies, in part because of the initial background CCN in each particular case but also cloud top height variability. In these LES cases v_e is spatially anti-correlated with τ and organized in a cellular structure — regions with higher τ tend to have smaller v_e(VW) and regions with lower τ tend to have large v_e(VW).

Daniel Miller 2/13/2018 9:35 AM
Deleted: at …or a coarser spatial resolution … [3]

4 Results and Analysis

4.1 Retrieval and LES Property Comparison

Before comparing the retrieval results from the two techniques to one another, we must first carry out a comparison of LES and retrieval properties to assess and understand the differences between the retrieval results and the original LES cloud fields at the native 50 m spatial resolution. This is a necessary sanity check that will help understand the accuracy and uncertainty of our retrieval routines. More importantly, this study will help to interpret the retrievals based on homogeneous cloud assumption when the LES cloud fields have naturally inhomogeneous vertical profiles. Note that the retrievals compared throughout the following sections are compared for all combinations of viewing and solar geometries indicated in the section 3.

Daniel Miller 2/13/2018 2:22 PM
Deleted: in this section …e must first carry … [4]

The bispectral retrieval comparison to LES properties in Figure 3 depicts joint histograms of r_e and τ retrievals using both the 2.13 and 3.75 µm bands against the reference values derived from the LES fields, r_e(VW), v_e(VW), and τ_{LES}. It is important to note that these joint histograms are presented as the logarithmic percent of the population, to emphasize deviations from the one-to-one line. Also, the mean regression biases reported throughout this study are stated relative to the plotted axes as, μ_{bias}=<y−x> and $\mu_{|bias|}$=<|y−x|> (i.e., x and y denoting x and y axes). The two bispectral r_e retrievals, r_e(2.13 µm) and r_e(3.75 µm), are in agreement with the LES ground-truth (Figure 3(a) and (b)) with good correlations, both exceeding 0.95. The biases between these two retrievals and the LES properties differ slightly. Compared to the LES, both r_e retrievals have relatively small sub-micron mean biases and the mean absolute biases are also sub-micron. Additionally, it is important to note a limitation of this population: none of the LES scenes in this study have a mean cloud top r_e near 10 µm. To examine the two bispectral τ retrievals, τ(2.13 µm) and τ(3.75 µm) in Figure 3(c) and (d), we compare them in terms of percent differences, because the regression is so highly correlated (R>0.99). A slight systematic high bias on the order of 2-5% exists. The origin of this high bias is likely associated with deviations of the droplet size distribution from the assumed gamma distribution form. The LES size distributions sometimes exhibit longer large-droplet tails than the assumed form. As explained earlier in Section 2.2, the bispectral method suffers from a reduction of retrieval sensitivity when clouds are

Daniel Miller 3/4/2018 4:44 PM
Deleted: SWIR …ands against the referenc … [5]

optically thin. Therefore, if we sample only LES columns that are optically thick (τ>3) a substantial improvement in the regression correlations of the two r_e retrievals (Figure 3(e) and (f)) is achieved. While not all retrievals in the τ<3 population are biased, but the majority of extreme retrieval bias outliers belong to this thin cloud population. Even after this sub-selection of the data some outliers still remain. In particular, a small population of both r_e(2.13 μm) and r_e(3.75 μm) retrievals have biases exceeding r_e(VW) by as much as 20 μm. The cause of these outliers and some other differences between the retrievals and LES fields will be discussed in detail in section 4.3.

The polarimetric retrieval comparison to LES properties in Figure 4 depicts comparisons of the polarimetric retrievals, r_e(pol) v_e(pol), and τ(pol). The r_e(pol) retrieval compares very well to r_e(VW) (Figure 4(a)), with a regression correlation exceeding 0.98, a mean bias of less than 0.1 μm. The quality of this retrieval comparison to LES properties also further supports the single scattering definition of r_e(VW) for the polarimetric retrieval. In contrast, the polarimetric retrieval of v_e(pol) reveals a regression against v_e(VW) (Figure 4(c)) that does not perform quite as well. In this case the regression correlation is much weaker (R=0.71) with a mean bias of −0.011. While the mean bias is on the order of the v_e LUT grid spacing, it is clear that the regression correlation is poor because of a systematic low bias for v_e(VW) larger than about 0.15. It should also be noted that the increased concentration of v_e(pol) retrievals at v_e=0.3 is a result of the boundaries of the retrieval space, v_e=[0.01, 0.3]. The upper limit of which is a consequence of the gamma distribution of Hansen and Travis (1974) becoming monotonic for v_e≥0.3. Comparing only the population with v_e(VW)≤0.15 (not shown here) results in an improved correlation of R=0.81 with negligible mean bias. The v_e retrieval quality also depends on the assumption that LES droplet size distributions are accurately described using a single-mode gamma distribution. The DSD's in the LES sometimes deviate significantly from this assumption. In the context of the parametric polarimetric retrieval used in this study this is difficult to remedy or address. However, a different polarimetric retrieval, the Rainbow Fourier Transform (RFT) introduced in Alexandrov et al. (2012a) offers the possibility of retrieving an arbitrary droplet size distribution shape. The final retrieval product, τ(pol) (Figure 4(e)), indicates that a more accurate a priori r_e and v_e estimate has little impact on the retrieval of τ. As explained earlier in Section 2.2, the polarimetric method suffers a reduction of sensitivity when the DSD is broad, a finding that is consistent with previous work (Alexandrov et al., 2012b). This explains, for the r_e(pol) retrieval, why limiting the regression population to LES columns with v_e(VW)≤0.15 in Figure 4(b) increases the correlation and decreases the absolute bias. This appears to be an indication of sensitivity to degradation of the supernumerary bow features for large v_e, features that are necessary for reliable r_e(pol) and v_e(pol) retrievals.

For v_e(pol) we find that by sampling LES columns that are optically thick (τ>3), there is moderate improvement in the correlation and reduced biases (Figure 4(d)). This improvement stems from the correlation between the population of optically thin clouds and high v_e(VW) (Figure 4(f)) that are found near cloud edges in the LES scenes. It should be noted that an increased τ does not implicitly lead to better polarimetric retrievals, but here it is observed to be a consequence of aforementioned correlated relationship between DSD and optical properties.

Daniel Miller 2/26/2018 10:00 AM
Deleted: By …ampling… only LES colum ... [6]

Daniel Miller 2/26/2018 10:09 AM
Deleted: The joint histograms …n Figure 4 ... [7]

Daniel Miller 3/4/2018 9:50 PM
Deleted: Figure 4…(d)). This improvement ... [8]

4.2 Sensitivity to Measurement Uncertainty

The measurement uncertainties of total and polarized reflectances differ, leading one to expect that bispectral and polarimetric retrievals may have different sensitivities to uncertainty. Their relationships to uncertainty are further complicated by differences in retrieval approaches; namely interpolating two independent uncertain observations in a LUT (bispectral) or curve fitting through numerous observations that are each independently uncertain (polarimetric). Targeted uncertainties for cloud and aerosol remote sensing are δDOLP=0.5% in degree of linear polarization and δI=3% in total reflectance (Knobelspiesse et al., 2012). A simple propagation of uncertainty analysis yields a polarized reflectance uncertainty of δQ=2.5% (in the principal plane). Using these uncertainties as a starting point, we can perturb the LES reflectances with uncorrelated random noise and perform retrievals that we can then compare to the original unperturbed retrievals. Note that while the focus here is on uncorrelated randomly distributed noise, other sources of observational uncertainty exist and would need to be accounted for in the context of a specific instruments' uncertainty model. As the properties of particular instruments are not the focus of this study, we will focus on this more general uncertainty analysis.

For the bispectral retrieval, a randomly distributed reflectance perturbation between +/-3% was added to each LES reflectance. A histogram of the percent bias of bispectral retrievals of r_e induced by the addition of the reflectance uncertainty is shown in Figure 5(a). The mean and standard deviation of these bias distributions are stated, allowing us to interpret the results. First, the introduction of uncertainty has very little impact on the mean bias of bispectral r_e retrievals (on the order of 0.1%). Second, the introduction of uncertainty results in a broad distribution of r_e retrieval biases with standard deviations of 5.44% and 4.02% for the 2.13μm and 3.75μm retrievals respectively. Together these two results indicate that biases associated with measurement uncertainty will not be systematic, with absolute variability on the order of 1 μm or less for droplet sizes below 20 μm (the most prevalent population in this LES study). The impact of observational uncertainty on all of the τ retrievals is the focus of Figure 5(b). The two bispectral retrievals, τ(2.13μm) and τ(3.75), each have very minimal mean biases of 0.1%. However, like the biases for the effective radius retrievals, the distribution of retrieval bias is broadened to standard deviations of 8.2% and 5.6% for τ(2.13μm) and τ(3.75) respectively. The polarimetric τ(pol) retrieval on the other hand, being methodically quite similar to the bispectral retrievals, exhibits a small systematic low bias of about -2.43% as shown in Figure 5(b). The origin of this systematic bias is a known characteristic of single-band optical thickness retrievals, and is clearly demonstrated in figure 1 of Marshak et al. (2006). The convexity of a single-band LUT curve produces low-biased retrievals for symmetrically distributed (or averaged) reflectances. The bias distribution also has a smaller variability (3.8%) than the two bispectral retrievals, likely because the uncertainty in the SWIR/MWIR band also (weakly) influences the bispectral τ bias distributions.

The consequences of measurement uncertainty are markedly different for the polarimetric retrieval. This is a result of the polarimetric retrieval being a search for a similar curve in the phase function library, making the deviations in the magnitude of observations in any one angle less important when searching for the optimal curve – and therefore discrete r_e and v_e combination. The discretely binned nature of the polarimetric retrieval makes description of bias distributions like the

ones in Figure 5 problematic. One way to describe how uncertainty in polarized reflectances influences polarimetric retrievals is to describe the population of retrievals that are unchanged, and the population of retrievals that changed. After the introduction of random noise 88.1% of the polarimetric r_e(pol) retrievals were unbiased, with 9.1% biased high by one grid point (+0.25 µm) and 2.7% biased low by one grid point (-0.25 µm). All together, these three populations accounted for the vast majority (99.9%) of retrieval outcomes. The percent bias of the r_e(pol) retrieval had a mean of 0.06% and a standard deviation of 0.78%. These results agree with previous studies, for example the finding of Shang et al. (2015) indicating that the POLDER retrieval performed well as long as reflectance uncertainty was less than 10%. It should be noted however that the sensitivity to uncertainty is also tied to the number of angular measurements available, and the properties of the droplet size distribution. The polarimetric v_e(pol) retrievals behaved similarly, with 85.2% of all retrievals being unaffected, 12.7% were biased high by one grid point (+0.01) and 1.9% were biased low by one grid point (-0.01). Again, these three populations account for the vast majority of (99.9%) of retrieval outcomes. The percent bias of the ve pol retrieval had a mean of 1.14%, consistent with a 0.01 bias and a standard deviation of 22.6%. The greater tendency toward large biases for the effective variance is likely due to smoothing of polarized reflectance curves after the addition of uncertainty. The large majority of biases in the polarimetric retrieval of v_e are coming from the population of v_e near 0.1-0.15 where the supernumerary bow peaks are significantly eroded and small shifts in the magnitude of reflectances at angles near these peaks could easily shift the retrieval to the next grid point.

Overall, the lack of strong systematic biases associated with uncertainty in the case of either retrieval supports an approach of neglecting the measurement uncertainty in further analyses. Of course, this requires acknowledging that biases that are below δr_e=5%, δv_e=10%, or $\delta\tau$=7% in either retrieval are probably not as important because they likely are not detectable due to observational uncertainty.

4.3 Retrieval Comparison at High Resolution

In practice, most observational studies do not have access to the underlying cloud properties with which to compare, so instead different instruments and techniques are often compared to one another. At the native spatial resolution of the LES (50 m) a direct intercomparison of polarimetric and bispectral retrieval techniques is possible, providing an opportunity to diagnose different sources of bias. The joint histograms of r_e retrievals in Figure 6 compare the two bispectral retrievals, r_e(2.13 µm) and r_e(3.75 µm), to the polarimetric retrieval, r_e(pol), for all LES cases and observation geometries[4]. The regressions for the comparison of both r_e(2.13 µm) (Figure 6(a)) and r_e(3.75 µm) (panel b) indicate high correlation (R≈0.95) and have relatively small mean biases of less than a micron. A couple of notable features are evident in these regressions. **(1)** The sign of the mean bias appears to be sensitive to the SWIR/MWIR band selection due to vertical weighting differences,

[4] Note that ~1% of pixels in the LES retrieval data correspond to a "failed" bispectral retrieval due to falling outside of the LUT space. These pixels are omitted from the intercomparison. Different reasons for bispectral retrieval failure are discussed in (Cho et al., 2015).

Daniel Miller 2/13/2018 10:16 AM
Deleted: 2

Daniel Miller 2/13/2018 2:40 PM
Deleted: s

Daniel Miller 3/4/2018 1:55 PM
Deleted: offer the possibility of diagnosing

Daniel Miller 2/24/2018 12:28 PM
Deleted: Figure 5

Daniel Miller 2/24/2018 12:28 PM
Deleted: Figure 5

Daniel Miller 2/26/2018 6:20 PM
Deleted: 4

Daniel Miller 2/27/2018 2:24 AM
Deleted: .

resulting in $r_e(2.13\mu m)<r_e(pol)<r_e(3.75\mu m)$. **(2)** There are numerous statistical outliers with small $r_e(pol)$~5-9 μm but broadly distributed $r_e(2.13\ \mu m)$ or $r_e(3.75\ \mu m)$. One way to understand these features is to constrain the data set to LES columns where both retrieval techniques yield reliable results. As discussed previously, both the bispectral and polarimetric retrievals are sensitive to biases for thin clouds ($\tau<3$) and the polarimetric retrieval is sensitive to biases for broad droplet size distributions ($v_e>0.15$). Based on these criteria ($\tau>3$ and $v_e\leq0.15$), the constrained joint histograms (Figure 6(c) and (d)) feature much tighter regression relationships ($R\approx0.99$) and reduced mean absolute biases are observed. These filters indicate that the poorly correlated population corresponds to situations in which both retrievals are expected to suffer from significant biases. The retrieval regression can be further improved if the bispectral retrieval is artificially provided with more complete information about the shape of the droplet size distribution. Providing the $v_e(pol)$ retrieval as an a priori assumption for the bispectral LUT can demonstrate the sensitivity of the bispectral r_e retrievals to the $v_e=0.1$ assumption. This serves as a test of how collocated bispectral and polarimetric retrievals might assist one another. To create these new retrieval results we created a bispectral retrieval LUT for different values of v_e and then selected a different LUT for each pixel depending on the $v_e(pol)$ retrieval. The new coupled $r_e(2.13\ \mu m)$ retrievals (Figure 6(e)) are largely unchanged from the $v_e=0.1$ results, although a slight increase in the two biases indicates that $v_e=0.1$ was both an appropriate and sufficient assumption for the $r_e(2.13\ \mu m)$ retrieval. In contrast, the $r_e(3.75\ \mu m)$ retrieval (Figure 6(f)) is shown to benefit from this additional a priori information. The coupled 3.75 μm result has an increased correlation, an order of magnitude smaller bias (0.008 μm), and an absolute bias that is half as large as the original comparison (0.24 μm). The differences between the two SWIR band retrievals can be explained in two ways. Firstly, the vertically weighted DSD of the 2.13 μm SWIR band might result in a broader DSD (i.e., a larger v_e) compared to the 3.75 μm SWIR band, due simply to deeper penetration into cloud. This could provide one explanation for why the $r_e(2.13\ \mu m)$ retrieval might improve with the $v_e=0.1$ assumption. Alternatively, the R(2.13 μm) reflectance might simply be less sensitive to the broader DSD shape than the R(3.75 μm) reflectance. Overall, these results demonstrate a feature well known to the cloud remote sensing community; the bispectral retrieval of r_e is not particularly sensitive to v_e (Nakajima and King, 1990a). Indeed, comparison of the coupled bispectral retrieval of r_e to the polarimetric retrieval of r_e confirms that the advantage of retrieving v_e changes the bispectral retrieval of r_e by less than a micron, so it is appropriate to neglect this level of detail of the DSD for bispectral retrieval purposes. In the context of measurement uncertainty, as discussed in section 4.2, this effect would be below retrieval uncertainty. Overall, this demonstrates that when the two retrievals are compared on equal footing they are very nearly equivalent, with only slight differences leading to $r_e(2.13\mu m)<r_e(3.75\mu m)<r_e(pol)$ as would be expected based on an increasing droplet size vertical profile and vertical weighting.

The origin of the broadly distributed high-biased bispectral retrievals in the small droplet size regime ($r_e(pol)$~5 μm) stems from the ATEX polluted case. A close examination of this case reveals that there are no bispectral retrievals below 5 μm, despite approximately 3.5% of the scene being characterized by $r_e(VW)<5\mu m$.[6] This feature is a consequence of

[6] Additionally, ~1% of the cloudy pixels in this scene exhibit values below 4 μm.

Daniel Miller 2/24/2018 12:28 PM
Deleted: Figure 5…(c) and (d)) feature mu… [9]

Daniel Miller 4/26/2018 10:53 PM
Deleted: , where such small droplets make up about 5% of the LES scene[5]. … close exami… [10]

the bispectral LUT state space[7], which spans a r_e range of 5-30 µm. In contrast, the polarimetric retrieval space spans 1-30 µm. The differences between these two LUT spaces is not so much a matter of decision-making, but is more reflective of complexities of the bispectral retrieval for small r_e. To demonstrate this point panels (a) and (b) of Figure 7 depict the cloud reflectances from the ATEX polluted case (colors) within the respective bispectral LUT. It is obvious that the black isolines for τ and r_e increasingly overlap with the standard LUT space as τ decreases. In this region of the state space, there are multiple solutions for a single reflectance pair; one solution is representative of a small r_e (<5 µm, extended LUT), while the other indicates a much larger r_e (≥5 µm, standard LUT). There is also a modest impact on τ, but due to the curvature of the LUT this impact is less severe. The overlapping region between the standard and extended LUT is referred to as the "multiple solution space" and the amount of LUT overlap is determined by both the observation geometry and the selected spectral bands. Depending on the optical thickness, the larger r_e retrieval may be significantly larger, because the extended LUT isolines cross numerous larger r_e isolines in the standard LUT. The associated bispectral retrieval bias, shown in Figure 7(c) and (d), highlights the conclusion that for optically thick clouds the bispectral r_e retrievals exhibits only moderate retrieval biases on the order of ±1 µm. However, for very thin clouds (near cloud edge) the retrieval bias can increase significantly. For some of these thinner clouds the retrievals also fall within the multiple solution space, so it is possible to attribute the very large biases to the presence of ambiguous retrieval results. Furthermore, the multiple solution space also provides an additional explanation for why the removal of optically thin (τ<3) observations significantly improved the bispectral retrieval comparisons.

In contrast to the intercomparison of r_e retrievals, the τ retrieval intercomparison in Figure 8 reveals very few differences between the bispectral and polarimetric techniques. This is not surprising, because the τ(pol) retrieval is simply an implementation of the bispectral technique with additional constraints on r_e and v_e (as discussed in section 2.2).

4.4 Sensitivity to Unresolved Spatial Inhomogeneity

Unresolved spatial inhomogeneity influences the bispectral and polarimetric cloud retrievals in very different ways. Even for 100% cloudy pixels these retrievals can exhibit sensitivity to sub-pixel inhomogeneity. This section focuses on the ATEX cases because they exhibit a broader distribution of H_σ, allowing us to highlight the impact of spatial inhomogeneity on retrievals. Spatial resolution and sub-pixel inhomogeneity index (H_σ) are inherently intertwined with one another. This is demonstrated in Figure 9, where the broadening and shifting of the distribution of H_σ for increasingly coarsened spatial resolutions is clearly demonstrated using data from both the ATEX clean and polluted cases. In light of this relationship between resolution and inhomogeneity, the inclusion of data from all spatial resolutions together broadens our sampling of different inhomogeneity regimes. To that end, Figure 10 combines all of the coarse spatial resolution data from the two ATEX cases into a single retrieval bias histogram. For the bispectral retrievals in Figure 10 (a,b) we compare to the

[7] Note that the MODIS LUT extends its range down to 4 µm, and in situations with multiple solutions the larger retrieval value is selected.

Daniel Miller 4/26/2018 10:52 PM
Deleted: covers

Daniel Miller 4/26/2018 10:52 PM
Deleted: covers

Daniel Miller 2/24/2018 12:28 PM
Deleted: Figure 6

Daniel Miller 3/4/2018 4:45 PM
Deleted: r_e(SWIR)–r_e(2WT)

Daniel Miller 2/24/2018 12:28 PM
Deleted: Figure 6

Daniel Miller 4/26/2018 10:55 PM
Deleted:

Daniel Miller 2/24/2018 12:28 PM
Deleted: Figure 7

Daniel Miller 2/13/2018 10:16 AM
Deleted: 3

Daniel Miller 2/14/2018 3:30 PM
Deleted: affects

Daniel Miller 2/14/2018 3:31 PM
Deleted: These

Daniel Miller 2/14/2018 3:31 PM
Deleted: different

Daniel Miller 2/14/2018 3:32 PM
Deleted: ies

Daniel Miller 2/14/2018 3:31 PM
Deleted: even for 100% cloudy pixels

Daniel Miller 2/14/2018 12:54 PM
Deleted: As coarsened s

Daniel Miller 2/14/2018 12:54 PM
Deleted: the

Daniel Miller 2/24/2018 8:25 PM
Deleted: correlated

Daniel Miller 2/14/2018 12:55 PM
Deleted: r, so our comparisons here address these two properties simultaneously. To that end,

polarimetric retrieval, resulting in histograms that clearly show the two retrievals diverging from one another with increasing sub-pixel inhomogeneity, tends to result in larger biases. In contrast, the polarimetric r_e(pol) retrieval in Figure 10 (c) does not appear to have a clear systematic bias. The v_e(pol) retrieval in Figure 10 (d) tells a more complicated story, the median value of the bias is clearly close to zero, but there is a tendency toward low biased retrievals with increasing inhomogeneity. It should be noted that the v_e(VW) itself increases with increasing H_σ, which is presumably a consequence of the anticorrelation between τ and v_e(VW). This might explain why for large values of H_σ, where the v_e(VW)>0.15 population is more common, there are more negative biases.

To further emphasize how unresolved inhomogeneity can influence these two retrieval techniques, we will highlight a particularly inhomogeneous pixel from the ATEX clean case at the coarsest resolution (800m). Focusing first on the bispectral retrieval using the 2.13 µm SWIR band, the LUT scatterplot in Figure 11(a) reveals that there is significant variability in the sub-pixel (i.e., 50 m) VNIR reflectances, indicated by a large value of the sub-pixel inhomogeneity index (H_σ=0.5637). In contrast to the variability of VNIR reflectances, the microphysical properties are largely homogeneous in this 800 m pixel, indicated by the narrow distribution of sub-pixel r_e(VW)$_{50\ m}$ (color of the points). The sub-pixel mean of $\langle r_e(VW)\rangle_{50\ m}$ =19.71 µm agrees well with the mean of both sub-pixel retrievals, $\langle r_e(2.13\ \mu m)\rangle_{50\ m}$=18.73 µm and $\langle r_e(pol)\rangle_{50\ m}$=18.92 µm. This combination of optical inhomogeneity and microphysical homogeneity leads to an average reflectance (indicated by the black star) for the 800 m pixel that falls significantly below the r_e=20 µm isoline (i.e., the closest isoline to the mean sub-pixel retrievals). Thus, the coarse resolution 800 m reflectance results in an 800 m bispectral retrieval with $r_e(2.13\ \mu m)_{800\ m}$=23.62 µm, which is biased high by ~4 µm. This effect is attributable to the well-documented PPH bias induced by the curvature of the bispectral LUT with respect to the optical thickness (Zhang and Platnick, 2011; Zhang et al., 2012; 2016). The PPH bias has a stronger influence on the 2.13 µm retrieval compared to the 3.75 µm retrieval (shown in Figure 11(b)) because the curvature of the LUT space is more pronounced.

The polarimetric retrieval has a fundamentally different relationship to the unresolved sub-pixel inhomogeneity. This can be demonstrated with the sub-pixel polarized reflectance histogram in Figure 11(b). The reflectances in this figure have been binned by scattering angle to create a distribution of polarized reflectances for the 50 m sub-pixels within the selected 800 m pixel footprint. Within the plot there are also two curves, shifted in amplitude away from the histogram for clarity, that display the mean 800 m multi-angular polarized reflectance and corresponding 800 m retrieved polarized phase function (with appropriate fitting coefficients). Note that, while this histogram gives a sense of the variability of the magnitude and scale of the polarized reflectances, what ultimately matters for the coarse resolution polarimetric retrieval is the relative shape of the 800 m averaged polarized reflectance curve. It is evident from this histogram and these curves that the mean angular position of the supernumerary bow does not shift, indicating that there is no significant difference between $r_e(pol)_{800\ m}$, $\langle r_e(pol)_{50\ m}\rangle$, and $\langle r_e(VW)_{50\ m}\rangle$. This agrees with previous studies on the impact of unresolved inhomogeneity on polarimetric r_e retrievals (Shang et al., 2015). In contrast, there is clear variability in the amplitude of sub-pixel polarized reflectances. This variability owes itself to both optical (τ), and microphysical inhomogeneity (i.e., v_e(VW)>0.15) within the coarse resolution pixel. For thin clouds (τ<3) the supernumerary bow amplitude is dependent on both τ and v_e (Alexandrov et

Daniel Miller 2/14/2018 3:39 PM
Deleted: panels (a) and (b) of Figure 8 compare r_e(pol) to the r_e(2.13 µm) and r_e(3.75 µm) respectively at increasingly coarsened spatial resolutions (as indicated by the size of the circles). In addition to the spatial resolution, these plots also indicate the magnitude the of sub-pixel ... [11]

Daniel Miller 2/24/2018 8:34 PM
Deleted: probe how

Daniel Miller 2/26/2018 12:38 PM
Deleted: influences

Daniel Miller 2/24/2018 8:34 PM
Deleted: examine

Daniel Miller 2/14/2018 3:40 PM
Deleted: a very coarse resolution

Daniel Miller 2/24/2018 12:28 PM
Deleted: Figure 9

Daniel Miller 2/24/2018 12:10 PM
Deleted: of this

Daniel Miller 2/24/2018 12:10 PM
Deleted: are largely homogeneous

Daniel Miller 2/13/2018 1:38 PM
Deleted: 2WT

Daniel Miller 2/13/2018 1:38 PM
Deleted: 2WT

Daniel Miller 4/26/2018 10:56 PM
Deleted: 23

Daniel Miller 2/25/2018 8:47 PM
Deleted: Figure

Daniel Miller 4/26/2018 10:57 PM
Deleted:

Daniel Miller 2/16/2018 1:04 PM
Deleted: , as shown in

Daniel Miller 2/24/2018 12:28 PM
Deleted: Figure 9

Daniel Miller 2/26/2018 12:58 PM
Deleted: demonstrate

Daniel Miller 2/26/2018 12:58 PM
Deleted: the

Daniel Miller 2/26/2018 12:58 PM
Deleted: 50 m sub-pixel

Daniel Miller 2/16/2018 1:07 PM
Deleted: the

Daniel Miller 2/13/2018 1:38 PM
Deleted: 2WT

Daniel Miller 2/13/2018 1:38 PM
Deleted: 2WT

al., 2012b). With v_e fixed the polarized reflectance converges towards an asymptotic maximum for optically thick clouds ($\tau \geq 3$), a consequence of increasing depolarization due to multiple scattering. Similarly, for a fixed τ, reflectances corresponding to $v_e(\mathrm{VW}) > 0.15$ also produce decreased polarization in the primary and supernumerary bow features, as discussed in section 2. Each of these effects reduces sensitivity to the cloudbow features; and thus unresolved variability in τ and v_e could influence coarse resolution retrievals. For example, Shang et al. (2015) found that unresolved spatial inhomogeneity of τ and v_e increased retrieval biases in v_e(pol), while they were not able to discern a trend in retrieval biases in their study. However, in our case study featured in Figure 11(b) we do not see a significant difference between coarse ($v_e(\mathrm{pol})_{800\ \mathrm{m}}$) and fine scale ($\langle v_e(\mathrm{pol})_{50\ \mathrm{m}} \rangle$) retrievals, but both retrievals are low-biased relative to the mean LES property ($\langle v_e(\mathrm{VW})_{50\ \mathrm{m}} \rangle$). This result was surprising, because both fine and coarse resolution retrievals were biased similarly. It appears as though coarse resolution retrievals arrive at the same answer as the fine scale retrievals through different processes. The average of fine scale retrievals (that are systematically biased low) and the retrieval based on the average of fine scale reflectances (which are reduced for reasons discussed above) results in a similar retrieval outcome. Unlike the bispectral retrieval, where retrievals differ from one another at different resolutions, the polarimetric retrieval seems to compare well to itself at both resolutions – even when it might be biased relative to the underlying microphysics of the physical scene. To examine this this further we performed polarimetric retrievals on subpopulations of the 50 m polarized reflectances within this 800 m pixel that omitted either the $v_e(\mathrm{VW}) > 0.15$ or $\tau < 3$ from the population. Removing these thin or broad droplet size distributions from the high resolution dataset had little to no impact on either the coarse resolution r_e(pol) or v_e(pol) retrieval. From these results and the histogram in Figure 10 (d) it appears that the impact of spatial resolution on v_e(pol) retrievals is largely a consequence of an unresolved anticorrelation between τ and v_e rather than a feature directly related to spatial resolution.

4.4 Sensitivity to Angular Resolution and Sampling

The polarimetric retrieval requires high-resolution multi-angular data to resolve the supernumerary bow features. To test how angular resolution influences polarimetric retrievals we examined coarse spatial resolution (800 m) r_e(pol) retrievals at different angular resolutions. Each angular resolution (i.e., changing angular step size) was also convoluted with shifting angular sampling (i.e., changing the initial angle). This convolution is necessary in order to account for all possible sets of scattering angle observations associated with each resolution. These coarse resolution retrievals were then compared to the original high angular resolution retrieval. The results of this experiment (Figure 12(a)) reveal that coarsening angular resolution does not systematically bias r_e(pol) retrievals, although angular resolutions exceeding 3° do result in a marked increase in retrieval variability (i.e., a constant mean bias, but increased absolute bias). In contrast, Figure 12(b) demonstrates that angular resolutions exceeding 3° lead to both high-biased v_e(pol) and increased retrieval variability. An explanation for the origin of the observed degradation in retrieval accuracy above 3° angular resolution is demonstrated in Figure 13(a). Two different polarized phase functions with r_e=15 µm and v_e=[0.03, 0.2] (solid and dashed-dotted, respectively) are sampled at

Daniel Miller 2/26/2018 7:22 PM
Deleted: a

Daniel Miller 2/26/2018 7:22 PM
Deleted: v_e and varying τ

Daniel Miller 2/13/2018 1:38 PM
Deleted: 2WT

Daniel Miller 3/4/2018 9:50 PM
Deleted: Figure

Daniel Miller 2/26/2018 2:00 PM
Deleted: we find that these features do not systematically bias the v_e(pol) retrieval in this case. In fact, rather surprisingly, we

Daniel Miller 3/4/2018 2:33 PM
Deleted: find that the most important bias for the coarse spatial resolution v_e(pol) retrieval is the lack of sensitivity on v_e(2WT)>0.15, a feature that was also present for the high spatial resolution retrievals. This finding is also supported for

Daniel Miller 3/4/2018 2:44 PM
Deleted:

Daniel Miller 3/4/2018 2:33 PM
Deleted: performed on

Daniel Miller 2/26/2018 8:54 PM
Deleted: samples

Daniel Miller 2/26/2018 8:54 PM
Deleted: of

Daniel Miller 2/13/2018 1:38 PM
Deleted: 2WT

Daniel Miller 3/4/2018 2:33 PM
Deleted: ; removing either of them had little

Daniel Miller 2/26/2018 4:31 PM
Deleted: .

Daniel Miller 2/26/2018 3:47 PM
Deleted: Possible explanations for this behavior will be discussed in section 5.

Daniel Miller 2/13/2018 10:16 AM
Deleted: 4

Daniel Miller 2/24/2018 12:28 PM
Deleted: Figure 10

Daniel Miller 2/24/2018 12:28 PM
Deleted: Figure 10

Daniel Miller 2/24/2018 12:28 PM
Deleted: Figure 11

an angular resolution of 3.5° (indicated by the gray vertical lines). This resolution is coarser than the spacing between the supernumerary bow features. As a consequence, this particular angular sampling intersects these curves at nearly the same amplitudes. This degeneracy yields a relatively low cost function during the best-fit optimization step of the polarimetric curve fitting retrieval algorithm, making it possible to obtain an inaccurate solution if this results in a cost-function minimum. The lack of observed differences between these two curves results in a lack of v_e information, which could be exacerbated by observational uncertainty. However, under different angular sampling conditions, e.g., shifting the initial angle by a few degrees to the right, the supernumerary bow peaks of the low v_e curve would be sampled and the similarity between the observations of these two curves would vanish. This example highlights an important feature of multi-angular polarimetry: observations at poor angular resolutions can suffer from increased biases depending on whether or not important angles are sampled. Generalizing this result requires determining the angular spacing of the supernumerary bow features for other r_e. Pursuing this, we find that decreasing cloud droplet size widens and dilates supernumerary bow features, making it easier to resolve supernumerary bow features at coarse angular resolution. The peak-to-peak distance of the supernumerary bow oscillations can be treated as the Nyquist frequency, or in this case Nyquist resolution. In signal analysis, a sampling resolution finer than the Nyquist frequency is required to appropriately resolve features of an oscillatory signal. The Nyquist angular resolution required for resolving the supernumerary bow oscillations changes with both r_e and λ according to the behavior illustrated in Figure 13(b). This analysis indicates that multi-angular observations in a shorter wavelength spectral band would require finer angular resolutions. The Nyquist angular resolution for λ=0.865 and r_e=15 µm is 3°, providing an explanation for the increased variability in r_e(pol) and v_e(pol) LES retrievals at angular resolutions coarser than the Nyquist limit.

Daniel Miller 2/24/2018 12:28 PM
Deleted: Figure 11

Daniel Miller 3/5/2018 10:43 AM
Deleted: uncertainty

5 Summary and Discussion

The analysis in this study, which features comparisons of fundamentally different passive cloud property retrieval techniques, is facilitated by comparisons to LES cloud fields used as input to the retrievals. At the native LES resolution (50 m) there are promising results for both the bispectral and polarimetric retrievals (with 1-D radiative transfer assumptions). For the bispectral retrieval, the LES comparison shows significant biases for retrievals of very thin clouds, as well as only small differences between the vertically weighted cloud properties in each of the two SWIR/MWIR bands (2.13 and 3.75 µm). Meanwhile, for the polarimetric retrieval, the comparison demonstrates that the r_e(pol) retrieval agrees well with the vertically weighted in situ properties of each LES scene. However, the v_e(pol) retrieval exhibits persistent low biases due to a lack of retrieval sensitivity to very broad droplet size distributions (i.e., v_e(VW)>0.15). The optical thickness retrievals from both methods are effectively the same, with the caveat that the polarimetric technique performs the r_e(pol) retrieval as an a priori constraint on the τ retrieval space. Regarding τ, both bispectral and polarimetric retrievals were found to have a small systematic high bias on the order of 2-5%.

Daniel Miller 3/4/2018 3:00 PM
Deleted: vastly

Daniel Miller 2/13/2018 1:38 PM
Deleted: 2WT

The uncertainty in observed total and polarized reflectances was found to introduce only weak systematic biases in bispectral or polarimetric r_e retrievals (0.1% or less). Similarly, the bispectral τ retrievals were also not systematically biased. In contrast, total reflectance uncertainty did produce a slight systematic bias of -2.43% in the polarimetric τ(pol) retrieval that can be linked to the convexity of the single-band LUT used to perform the retrieval. This sort of bias, could perhaps be accounted for by introducing a Taylor expansion correction similar to the one discussed in Zhang et al. (2016) in the context of unresolved inhomogeneity. Beyond these systematic biases, we found that the induced uncertainties in the bispectral retrievals were δr_e=5% or $\delta\tau$=7%. The influence of polarimetric retrieval is likely sensitive the polarimetric LUT grid spacing, but here we found uncertainties that were less than the bispectral retrieval of r_e, δr_e(pol)=1 to 4%, and δv_e(pol)=10 to 20%. In the context of the rest of our comparison studies, the lack of systematic biases and relatively small uncertainties allowed us to discuss retrieval behavior in the absence of uncertainty.

The retrieval intercomparison of polarimetric and bispectral retrievals in this study demonstrates that both techniques yield very similar results, especially when the most reliable populations of cloud properties are selected for each method (τ>3 and v_e around 0.1). While the physical principles and measurement requirements are vastly different, both retrieval techniques seem to be able to capture similar information about r_e and τ. These results agree with high-resolution airborne observations obtained during the PODEX and ORACLES field campaigns, where RSP and AMS microphysical retrievals are compared (Alexandrov et al., 2015; Knobelspiesse et al., 2017). These high spatial resolution field campaign observations indicate that the two retrieval techniques agree well to within the tolerances also found in the present study. The bispectral r_e retrievals are found to be moderately sensitive to v_e in the 3.75 µm band, and less so in the less absorptive and more deeply penetrating 2.13 µm band. Coupling the retrieved v_e(pol) to the bispectral r_e(3.75 µm) retrieval led to slight improvements in the r_e(pol) and r_e(VW) comparison. It should be noted that for MODIS cloud products the bias due to the v_e=0.1 assumption does not substantially impact the r_e retrieval compared to other sources of bias (i.e., cloud inhomogeneity or 3-D radiative effects). In addition, the MODIS Collection 6 cloud product includes uncertainty estimates associated with the v_e assumption. The intercomparison of the bispectral and polarimetric τ retrievals indicates that the two produce very similar results. This was to be expected, as the polarimetric technique also uses a bispectral LUT approach to derive τ. When the results from the two methods diverge, the observations tend to be related to the thin cloud regimes.

The presence of a multiple solution space in the bispectral LUTs, where small droplet sizes (r_e<5) have the same reflectance as larger droplets, was shown to induce numerous outliers resulting in a significant high bias in the bispectral retrievals for both r_e and (to a lesser extent) τ. This multiple solution space likewise impacts the MODIS operational products, since the bispectral LUTs used in the MODIS collection 6 cloud products include theoretical r_e solutions as low as 4 µm. However, for retrievals with multiple LUT solutions the MODIS product only reports the larger r_e value, leading to a systematic bias if the observed cloud really includes a population of small droplets. As a consequence, for thin clouds with small droplet sizes one can expect the comparison of polarimetric and bispectral retrievals to disagree. This strong high-bias for small r_e retrievals provides a plausible explanation for the large discrepancies observed in the small droplet size regime in the intercomparison of MODIS and POLDER retrievals (Bréon and Doutriaux-Boucher, 2005). Absent a solution to this

Daniel Miller 3/4/2018 3:16 PM
Deleted: -

Daniel Miller 2/13/2018 1:38 PM
Deleted: 2WT

issue, future intercomparisons or combined climatological datasets should be limited to retrievals of r_e(pol) exceeding 5-7 µm (depending on the respective bispectral LUT multiple solution space properties).

At the coarse spatial resolutions of most satellite instruments, cloud inhomogeneity can significantly impact retrievals. In the context of this study we find that the influence of unresolved spatial inhomogeneity is a dominant source of bias between the polarimetric and bispectral r_e retrievals. In this study we found that even for 100% cloudy pixels (at a coarse 800 m horizontal resolution) the influence of the PPH bias is significant, with the average r_e bias exceeding 1 µm in the most inhomogeneous LES scene (ATEX clean). Based on these results we still expect that the overall systematic bias observed in the MODIS and POLDER intercomparison of moderate droplet size regimes is in large part attributable to the influence of this PPH bias (Bréon and Doutriaux-Boucher, 2005). Recently, great effort has been made to account for the influence of the PPH bias on bispectral MODIS retrievals. The 2-D Taylor expansion technique implemented by Zhang et al. (2016) offers the possibility of quantifying (and potentially correcting for) the impact of PPH bias on bispectral retrievals. This approach requires high spatial resolution measurements in at least one spectral band to obtain the sub-pixel reflectance variability, which is used to determine corrections for the bias of r_e and τ. In addition to PPH bias, 3-D radiative effects are also influenced by spatial resolution. The focus on 1-D radiative transfer in this study leaves questions for future studies regarding the influence of these 3-D radiative effects. Future work will need to identify the relative differences between 3-D radiative effects on total and polarized reflectances and retrievals.

Sufficient angular resolution is one of the more important requirements of the polarimetric retrieval technique. We find that resolving the multi-angular polarized reflectance at a resolution coarser than the Nyquist angular resolution of the supernumerary bow results in greater uncertainty (r_e(pol) and v_e(pol)) and biased (v_e(pol)) polarimetric retrievals. The required angular resolution is dependent both on droplet size and wavelength. Future cloud polarimetric instrumentation should consider these angular resolution requirements. While we have not explicitly tested the so-called "super-pixel" approach implemented for POLDER retrievals, these coarse spatial and angular resolution studies lead to some anticipated biases induced by this technique. We would expect such an approach to further bias v_e(pol) retrievals low, due to the lack of sensitivity to unresolved high-v_e populations. In addition, this current study indicates that r_e(pol) retrieval variance might increase, but the mean bias might not increase significantly. However, if there is significant correlation between the unresolved r_e and v_e populations within an observation footprint, the mean r_e bias would be expected to suffer.

Ultimately, the utitlity of any optical property dataset depends on the science questions for which the dataset will be used. These questions may focus on the determination of domain-averaged water mass, radiative flux calculations, or microphysical process studies on a range of scales. The appropriate retrieval may differ for each of these science questions and as a consequence the comparison of the bispectral and polarimetric retrievals discussed here ought to be viewed through the lens of a particular application.

Daniel Miller 2/26/2018 2:57 PM
Deleted: may

Daniel Miller 2/26/2018 1:48 PM
Deleted: be

Acknowledgements

The hardware used in the computational studies is part of the UMBC High Performance Computing Facility (HPCF). The facility is supported by the U.S. National Science Foundation through the MRI program (grant nos. CNS-0821258 and CNS-1228778) and the SCREMS program (grant no. DMS-0821311), with additional substantial support from the University of Maryland, Baltimore County (UMBC). See www.umbc.edu/hpcf for more information on HPCF and the projects using its resources.

Appendix

We often treat the droplet size distribution observed by in-situ instruments (on the order of meters) as relatable to the inferred size distribution properties obtained by remote sensing retrievals (on the order of kilometers). This mathematical analysis addresses how resolution and scale influence the inferred cloud microphysical distribution. The modified gamma-distribution not only suits observations of in-situ cloud droplet size distributions, but it also exhibits several useful mathematical relationships:

$$\begin{aligned} \langle r^2 \rangle &= r_e^2 (v_e - 1)(2v_e - 1) \\ \langle r^3 \rangle &= r_e^3 (v_e - 1)(2v_e - 1) \\ \langle r^4 \rangle &= r_e^4 (v_e - 1)(2v_e - 1)(v_e + 1) \end{aligned} \quad . \tag{5}$$

From a retrieval perspective all droplet size distributions are treated as gamma-distributed. There is a potential disconnect here, from the perspective of scale analysis, when retrievals at a 50 m spatial resolution (our LES resolution) and retrievals at 1 km (MODIS retrieval resolution), or even 150 km (POLDER retrieval resolution) each are being treated as gamma-distributed. However, not all droplet microphysics information is created equal; the droplet size distributions at higher resolution (subscript, *i*) influence the low-resolution (subscript, *lr*) droplet size distributions. With high-resolution information the different moments of the coarser resolution droplet size distribution should be able to be constructed from the high-resolution microphysics. For a distribution made up of the summation of gamma size distributions the moments of the low-resolution distribution can be expressed by the following relationship, because summation and integration are each linear operators:

$$\begin{aligned} \langle r^n \rangle_{lr} &= \int_r r^n \left[\sum_i^k N_i \left(r, r_{e,i}, v_{e,i} \right) \right] \mathrm{d}r \\ \langle r^n \rangle_{lr} &= \sum_i^k \left[\int_r r^n N_i \left(r, r_{e,i}, v_{e,i} \right) \mathrm{d}r \right] = \sum_i^k \left[\langle r^n \rangle_i \right] \end{aligned} \quad . \tag{6}$$

With this mathematical rule in mind, the values of r_e and v_e for the low-resolution droplet size distribution can be obtained by substitution into eq. (2) and eq. (3):

$$r_e' \equiv \frac{\langle r^3 \rangle_{lr}}{\langle r^2 \rangle_{lr}} = \frac{\sum_i^k \langle r^3 \rangle_i}{\sum_i^k \langle r^2 \rangle_i} \quad , \tag{7}$$

$$v_e' \equiv \frac{\left\langle r^4 \right\rangle_{lr} \left\langle r^2 \right\rangle_{lr}}{\left(\left\langle r^3 \right\rangle_{lr} \right)^2} - 1 = \frac{\sum_i^k \left\langle r^4 \right\rangle_i \left\langle r^2 \right\rangle_i}{\left(\sum_i^k \left\langle r^3 \right\rangle_i \right)^{2x}} - 1 \,. \quad (8)$$

Henceforth, we will refer to the r_e' and v_e' relationships in eq. (7) and eq. (8) as microphysical "aggregation rules." It should be noted that these rules fundamentally treat the DSD as gamma-distributed at all scales.

The microphysical aggregation rules allow for the explanation of some features of the coarse polarimetric retrieval experiments displayed in Shang et al., (2015). Referring to the inhomogeneous polarimetric retrieval experiments in table 2 and figure 4 of their paper, we reproduced their results and calculated the corresponding r_e' and v_e' in our **Table 2**, which contains the same retrieval examples and corresponding r_e' and v_e' results for the cases examined in their study. There is a clear difference between the mean r_e or v_e and the polarimetric retrieval results. Using the microphysical aggregation rules defined above, we derived that the appropriate distribution properties, r_e' and v_e', are generally in closer agreement with the polarimetric retrievals of r_e(pol). These results offer a possible explanation as to why the polarimetric retrieval does not agree with the average of the sub-scale microphysics in Shang et al.'s study. A couple of things should be noted here: **1)** When there is little variability in the unresolved r_e (e.g., r_e=[15,20] μm) the mean, retrieval, and the estimated mixture are generally all in agreement (e.g., $\langle r_e \rangle$=17.5, r_e(pol)=18, and r_e'=18.2 μm). **2)** When large variability in the unresolved r_e (e.g., r_e=[5,20]) is present, both the retrieved and estimated mixture strongly favor the larger droplet effective radius (e.g., r_e(pol)=19 and r_e'=19.12 μm). **3)** Large variability in unresolved r_e sometimes results in large differences between v_e(pol) and v_e'. The last two points are likely a consequence of the resulting coarse resolution (multi-modal) distribution differing significantly from the gamma-distribution assumption stated previously.

Applying this analysis to the aggregation of LES scene microphysics will allow for the determination of how accurate a spatial mean aggregation reflects the true coarse resolution microphysical parameters. We first assumed that all of the highest resolution vertically weighted size-distributions can be assumed to be appropriately characterized by a gamma distribution with r_e=r_e(VW) and v_e=v_e(VW). We then aggregated these LES microphysical properties at the 50 m native resolution to increasingly coarser resolutions (100, 200, 400, and 800 m), using both the mean and the aggregation rules. We found that the differences between the two techniques are negligible (Δr_e~0.01 μm and Δv_e~0.001) and do not significantly vary with final resolution. Apparently, the importance of the aggregation rules in the LES are far less important than what we had found in the multiple-moment cases tested in Shang, et al. (2015). One clear difference between the these multiple moment cases and the LES was that the toy models are reductive bimodal distributions, exhibiting very large sub-scale microphysical inhomogeneity in r_e. This non-physical variability is something that is not commonly observed in the LES or in observational studies. To address this, we performed a theoretical examination of how important the aggregation rules are for calculating the bias between simple average aggregation and mathematical rule aggregation. In this experiment we

Daniel Miller 3/2/2018 3:02 PM
Deleted: v_e'

Daniel Miller 2/13/2018 1:38 PM
Deleted: 2WT

Daniel Miller 2/13/2018 1:38 PM
Deleted: 2WT

established various distributions of unresolved DSD's with varying r_e and v_e populations. These joint distributions of r_e and v_e were used to test how the variance (i.e., the unresolved variability) would influence the average and mathematical rule aggregated results. This test confirmed, that large differences between the simple average and mathematical aggregation rules requires spatial inhomogeneity of microphysics that much larger than those observed in the LES or typical observational studies. Based on these results we recommend that future studies focusing on the effect of unresolved microphysical inhomogeneity on polarized retrievals should consider more realistic inhomogeneity conditions on both r_e and v_e.

References

Ackerman, A. S., Kirkpatrick, M. P., Stevens, D. E. and Toon, O. B.: The impact of humidity above stratiform clouds on indirect aerosol climate forcing, Nature, 432(7020), 1014–1017, 2004.

Ackerman, A. S., vanZanten, M. C., Stevens, B., Savic-Jovcic, V., Bretherton, C. S., Chlond, A., Golaz, J.-C., Jiang, H., Khairoutdinov, M., Krueger, S. K., Lewellen, D. C., Lock, A., Moeng, C.-H., Nakamura, K., Petters, M. D., Snider, J. R., Weinbrecht, S. and Zulauf, M.: Large-Eddy Simulations of a Drizzling, Stratocumulus-Topped Marine Boundary Layer, Mon. Wea. Rev., 137(3), 1083–1110, doi:10.1175/2008MWR2582.1, 2009.

Alexandrov, M. D., Cairns, B. and Mishchenko, M. I.: Rainbow Fourier transform, Journal of Quantitative Spectroscopy and Radiative Transfer, 113(18), 2521–2535, doi:10.1016/j.jqsrt.2012.03.025, 2012a.

Alexandrov, M. D., Cairns, B., Emde, C., Ackerman, A. S. and van Diedenhoven, B.: Accuracy assessments of cloud droplet size retrievals from polarized reflectance measurements by the research scanning polarimeter, Remote Sensing of Environment, 125, 92–111, doi:10.1016/j.rse.2012.07.012, 2012b.

Alexandrov, M. D., Cairns, B., Wasilewski, A. P., Ackerman, A. S., McGill, M. J., Yorks, J. E., Hlavka, D. L., Platnick, S. E., Thomas Arnold, G., van Diedenhoven, B., Chowdhary, J., Ottaviani, M. and Knobelspiesse, K. D.: Liquid water cloud properties during the Polarimeter Definition Experiment (PODEX), Remote Sensing of Environment, 169, 20–36, doi:10.1016/j.rse.2015.07.029, 2015.

Bréon, F. M. and Doutriaux-Boucher, M.: A comparison of cloud droplet radii measured from space, IEEE Trans. Geosci. Remote Sensing, 43(8), 1796–1805, doi:10.1109/TGRS.2005.852838, 2005.

Bréon, F. M. and Goloub, P.: Cloud droplet effective radius from spaceborne polarization measurements, Geophys. Res. Lett., 25(11), 1879–1882, 1998.

Cairns, B., Russell, E. E. and Travis, L. D.: Research Scanning Polarimeter: calibration and ground-based measurements, SPIE's Conference on Polarization: Measurement, Analysis, and Remote Sensing II, 186–196, doi:10.1117/12.366329, 1999.

Cho, H. M., Zhang, Z., Meyer, K., Lebsock, M., Platnick, S., Ackerman, A. S., Di Girolamo, L., C Labonnote, L., Cornet, C., Riedi, J. and Holz, R. E.: Frequency and causes of failed MODIS cloud property retrievals for liquid phase clouds over global oceans, J. Geophys. Res., 120(9), 4132–4154, doi:10.1002/2015JD023161, 2015.

De Haan, J. F., Bosma, P. B. and Hovenier, J. W.: The adding method for multiple scattering calculations of polarized light, Astronomy and Astrophysics, 183, 371–391, 1987.

Deirmendjian, D.: Scattering and polarization properties of water clouds and hazes in the visible and infrared, Appl. Opt., 3(2), 187–196, 1964.

Deschamps, P. Y., Breon, F. M., Leroy, M., Podaire, A., Bricaud, A., Buriez, J. C. and Seze, G.: The POLDER mission: instrument characteristics and scientific objectives, IEEE Trans. Geosci. Remote Sensing, 32(3), 598–615, doi:10.1109/36.297978, 1994.

Diner, D. J., Xu, F., Garay, M. J., Martonchik, J. V., Rheingans, B. E., Geier, S., Davis, A., Hancock, B. R., Jovanovic, V. M., Bull, M. A., Capraro, K., Chipman, R. A. and McClain, S. C.: The Airborne Multiangle SpectroPolarimetric Imager (AirMSPI): a new tool for aerosol and cloud remote sensing, Atmos. Meas. Tech., 6(8), 2007–2025, doi:10.5194/amt-6-

2007-2013, 2013.

Fridlind, A. M. and Ackerman, A. S.: Estimating the Sensitivity of Radiative Impacts of Shallow, Broken Marine Clouds to Boundary Layer Aerosol Size Distribution Parameter Uncertainties for Evaluation of Satellite Retrieval Requirements, J. Atmos. Oceanic Technol., 28(4), 530–538, doi:10.1175/2010JTECHA1520.1, 2011.

Hansen, J. E.: Circular Polarization of Sunlight Reflected by Clouds, http://dx.doi.org/10.1175/1520-0469(1971)028<1515:CPOSRB>2.0.CO;2, doi:10.1175/1520-0469(1971)028<1515:CPOSRB>2.0.CO;2, 2010.

Hansen, J. E. and Travis, L. D.: Light scattering in planetary atmospheres, Space Sci Rev, 16(4), 527–610, 1974.

King, M. D., Menzel, W. P., Kaufman, Y. J., Tanré, D., Bo-Cai Gao, Platnick, S., Ackerman, S. A., Remer, L. A., Pincus, R. and Hubanks, P. A.: Cloud and aerosol properties, precipitable water, and profiles of temperature and water vapor from MODIS, IEEE Trans. Geosci. Remote Sensing, 41(2), 442–458, doi:10.1109/TGRS.2002.808226, 2003.

Knobelspiesse, K., Cairns, B., Mishchenko, M., Chowdhary, J., Tsigaridis, K., van Diedenhoven, B., Martin, W., Ottaviani, M. and Alexandrov, M.: Analysis of fine-mode aerosol retrieval capabilities by different passive remote sensing instrument designs, Opt. Express, 20(19), 21457–21484, doi:10.1364/OE.20.021457, 2012.

Knobelspiesse, K., Segal-Rosenhaimer, M., Redemann, J., Cairns, B. and Alexandrov, M. D.: Multi-angle, polarimetric cloud observations using a radiative transfer model trained neural network, College Park, MD. 2017.

Liu, Y. and Diner, D. J.: Multi-Angle Imager for Aerosols, Public Health Reports, 132(1), 14–17, doi:10.1177/0033354916679983, 2017.

Lohmann, U., Stier, P., Hoose, C., Ferrachat, S., Kloster, S., Roeckner, E. and Zhang, J.: Cloud microphysics and aerosol indirect effects in the global climate model ECHAM5-HAM, Atmos. Chem. Phys., 7(13), 3425–3446, doi:10.5194/acp-7-3425-2007, 2007.

Marbach, T., Phillips, P., Lacan, A. and Schlussel, P.: The 3MI Mission: Multi-Viewing -Channel -Polarisation Imager of the EUMETSAT Polar System - Second Generation (EPS-SG) dedicated to aerosol and cloud monitoring, in Sensors, Systems, and Next-Generation Satellites XVII, vol. 8889, p. 88890I, International Society for Optics and Photonics. 2013.

Marshak, A., Platnick, S., Várnai, T., Wen, G. and Cahalan, R. F.: Impact of three-dimensional radiative effects on satellite retrievals of cloud droplet sizes, J. Geophys. Res., 111(D9), D09207, doi:10.1029/2005JD006686, 2006.

Martin, G. M., Johnson, D. W. and Spice, A.: The measurement and parameterization of effective radius of droplets in warm stratocumulus clouds, J. Atmos. Sci., 51(13), 1823–1842, 1994.

Martins, J. V., Fernandez-Borda, R., McBride, B., Espinosa, R. and Remer, L.: Combination between in-situ and remote sensing of tropospheric aerosols, College Park, MD. 2017.

Miles, N. L., Verlinde, J. and Clothiaux, E. E.: Cloud Droplet Size Distributions in Low-Level Stratiform Clouds, J. Atmos. Sci., 57(2), 295–311, doi:10.1175/1520-0469(2000)057<0295:CDSDIL>2.0.CO;2, 2000.

Miller, D. J., Zhang, Z., Ackerman, A. S., Platnick, S. and Baum, B. A.: The impact of cloud vertical profile on liquid water path retrieval based on the bispectral method: A theoretical study based on large-eddy simulations of shallow marine boundary layer clouds, J. Geophys. Res., 121(8), 4122–4141, doi:10.1002/2015JD024322, 2016.

Mishchenko, M. I., Cairns, B., Travis, L. D., Kopp, G., Schueler, C. F., Fafaul, B. A., Hooker, R. J., Maring, H. B.,

Itchkawich, T., Hansen, J. E., Kopp, G., Schueler, C. F., Fafaul, B. A., Hooker, R. J., Maring, H. B. and Itchkawich, T.: Accurate Monitoring of Terrestrial Aerosols and Total Solar Irradiance: Introducing the Glory Mission, http://dx.doi.org/10.1175/BAMS-88-5-677, 88(5), 677–691, doi:10.1175/BAMS-88-5-677, 2007.

Nakajima, T. and King, M. D.: Determination of the Optical Thickness and Effective Particle Radius of Clouds from Reflected Solar Radiation Measurements. Part I: Theory, J. Atmos. Sci., 47(15), 1878–1893, doi:10.1175/1520-0469(1990)047<1878:dotota>2.0.co;2, 1990a.

Nakajima, T. and King, M. D.: Determination of the optical thickness and effective particle radius of clouds from reflected solar radiation measurements. Part I: Theory, J. Atmos. Sci., 47(15), 1878–1893, 1990b.

Planck, M.: The theory of heat radiation, 2nd ed., P. Blakiston's Son & Co., Philadelphia, PA. [online] Available from: http://gutenberg.org/ebooks/40030, 1914.

Platnick, S.: Vertical photon transport in cloud remote sensing problems, J. Geophys. Res., 105(D18), 22919–22935, 2000.

Platnick, S., King, M. D., Ackerman, S. A., Menzel, W. P., Baum, B. A., Riedi, J. C. and Frey, R. A.: The MODIS cloud products: algorithms and examples from terra, IEEE Trans. Geosci. Remote Sensing, 41(2), 459–473, doi:10.1109/TGRS.2002.808301, 2003.

Platnick, S., Meyer, K. G., King, M. D., Wind, G., Amarasinghe, N., Marchant, B., Arnold, G. T., Zhang, Z., Hubanks, P. A., Holz, R. E., Yang, P., Ridgway, W. L. and Riedi, J.: The MODIS Cloud Optical and Microphysical Products: Collection 6 Updates and Examples From Terra and Aqua, IEEE Trans. Geosci. Remote Sensing, 55(1), 502–525, doi:10.1109/TGRS.2016.2610522, 2017.

Pruppacher, H. R. and Klett, J. D.: Diffusion Growth and Evaporation of Water Drops and Ice Crystals, in Microphysics of Clouds and Precipitation, pp. 412–463, Springer Netherlands, Dordrecht. 1978.

Roebeling, R. A., Feijt, A. J. and Stammes, P.: Cloud property retrievals for climate monitoring: Implications of differences between Spinning Enhanced Visible and Infrared Imager (SEVIRI) on METEOSAT-8 and Advanced Very High Resolution Radiometer (AVHRR) on NOAA-17, J. Geophys. Res., 111(D20), D20210, doi:10.1029/2005JD006990, 2006.

Rosenfeld, D., Liu, G., Yu, X., Zhu, Y., Dai, J., Xu, X. and Yue, Z.: High-resolution (375 m) cloud microstructure as seen from the NPP/VIIRS satellite imager, Atmos. Chem. Phys., 14(5), 2479–2496, doi:10.5194/acp-14-2479-2014, 2014.

Shang, H., Chen, L., Breon, F. M., Letu, H., Li, S., Wang, Z. and Su, L.: A better understanding of POLDER's cloud droplet size retrieval: impact of cloud horizontal inhomogeneity and directional sampling, Atmos. Meas. Tech. Discuss., 8(7), 6559–6597, doi:10.5194/amtd-8-6559-2015, 2015.

Stevens, B., Ackerman, A. S. and Albrecht, B. A.: Simulations of trade wind cumuli under a strong inversion, J. Atmos. Sci., 58(14), 1870–1891, doi:10.1175/1520-0469(2001)058<1870:sotwcu>2.0.co;2, 2001.

Stevens, B., Lenschow, D. H., Vali, G., Gerber, H., Bandy, A., Blomquist, B., Brenguier, J. L., Bretherton, C. S., Burnet, F., Campos, T., Chai, S., Faloona, I., Friesen, D., Haimov, S., Laursen, K., Lilly, D. K., Loehrer, S. M., Malinowski, S. P., Morley, B., Petters, M. D., Rogers, D. C., Russell, L., Savic-Jovcic, V., Snider, J. R., Straub, D., Szumowski, M. J., Takagi, H., Thornton, D. C., Tschudi, M., Twohy, C., Wetzel, M. and van Zanten, M. C.: Dynamics and chemistry of marine stratocumulus–DYCOMS-II, Bull. Amer. Meteor. Soc., 84(5), 579–593, doi:10.1175/BAMS-84-5-579, 2003.

Stevens, B., Moeng, C.-H., Ackerman, A. S., Bretherton, C. S., Chlond, A., de Roode, S., Edwards, J., Golaz, J.-C., Jiang,

H., Khairoutdinov, M., Kirkpatrick, M. P., Lewellen, D. C., Lock, A., Müller, F., Stevens, D. E., Whelan, E. and Zhu, P.: Evaluation of Large-Eddy Simulations via Observations of Nocturnal Marine Stratocumulus, Mon. Wea. Rev., 133(6), 1443–, doi:10.1175/MWR2930.1, 2005.

Tampieri, F. and Tomasi, C.: Size distribution models of fog and cloud droplets in terms of the modified gamma function, Tellus, 28(4), 333–347, doi:10.1111/j.2153-3490.1976.tb00682.x, 1976.

Twomey, S.: The Influence of Pollution on the Shortwave Albedo of Clouds, J. Atmos. Sci., 34(7), 1149–1152, doi:10.1175/1520-0469(1977)034<1149:TIOPOT>2.0.CO;2, 1977.

Werner, F., Siebert, H., Pilewskie, P., Schmeissner, T., Shaw, R. A. and Wendisch, M.: New airborne retrieval approach for trade wind cumulus properties under overlying cirrus, J. Geophys. Res., 118(9), 3634–3649, doi:10.1002/jgrd.50334, 2013.

Wiscombe, W. J.: Mie scattering calculations: Advances in technique and fast, vector-speed computer codes, NCAR Tech, National Center for Atmospheric Research, Boulder, Colorado. 1979.

Zhang, Z. and Platnick, S.: An assessment of differences between cloud effective particle radius retrievals for marine water clouds from three MODIS spectral bands, J. Geophys. Res., 116(D20), D20215, doi:10.1029/2011JD016216, 2011.

Zhang, Z., Ackerman, A. S., Feingold, G., Platnick, S., Pincus, R. and Xue, H.: Effects of cloud horizontal inhomogeneity and drizzle on remote sensing of cloud droplet effective radius: Case studies based on large-eddy simulations, J. Geophys. Res., 117(D19), n/a–n/a, doi:10.1029/2012JD017655, 2012.

Zhang, Z., Dong, X., Xi, B., Song, H., Ma, P. L., Ghan, S. J., Platnick, S. and Minnis, P.: Intercomparisons of marine boundary layer cloud properties from the ARM CAP-MBL campaign and two MODIS cloud products, J. Geophys. Res., 122(4), 2351–2365, doi:10.1002/2016JD025763, 2017.

Zhang, Z., Platnick, S., Yang, P., Heidinger, A. K. and Comstock, J. M.: Effects of ice particle size vertical inhomogeneity on the passive remote sensing of ice clouds, J. Geophys. Res., 115(D17), doi:10.1029/2010JD013835, 2010.

Zhang, Z., Werner, F., Cho, H. M. and Wind, G.: A framework based on 2-D Taylor expansion for quantifying the impacts of subpixel reflectance variance and covariance on cloud optical thickness and effective …, Journal of …, doi:10.1063/1.4975502, 2016.

Zinner, T., Wind, G., Platnick, S. and Ackerman, A. S.: Testing remote sensing on artificial observations: impact of drizzle and 3-D cloud structure on effective radius retrievals, Atmos. Chem. Phys., 10(19), 9535–9549, doi:10.5194/acp-10-9535-2010, 2010.

Daniel Miller 2/26/2018 1:23 PM

Deleted: Ackerman, A. S., Kirkpatrick, M. P., Stevens, D. E. and Toon, O. B.: The impact of humidity above stratiform clouds on indirect aerosol climate forcing, Nature, 432(7020), 1014–1017, 2004. ... [12]

Table 1: Mean values (μ) and standard deviations (σ, in parenthesis) of various optical (τ and H_o) and microphysical properties (r_e(VW) and v_e(VW)) of the LES scenes examined in this study. Note that vertically weighted properties are listed for the polarimetric vertical weighting function and H_o for nadir viewing 0.865 µm reflectance. Cloudy pixels is defined using a threshold of τ_{LES}>0.1.

LES Case	CCN Concentration [#/cm^3]	Scene Cloud Fraction	τ [unitless]	r_e(VW) [μm]	v_e(VW) [unitless]	H_o(800 m) [unitless]
DYCOMS-II	60	0.998	17.95 (6.22)	15.52 (1.00)	0.071 (0.11)	0.13 (0.10)
ATEX Clean	40	0.941	7.90 (8.02)	16.93 (2.62)	0.16 (0.12)	0.42 (0.17)
ATEX Poll.	600	0.985	17.48 (14.71)	7.29 (0.91)	0.13 (0.068)	0.24 (0.13)

Daniel Miller 2/13/2018 1:38 PM
Deleted: 2WT

Daniel Miller 2/13/2018 1:38 PM
Deleted: 2WT

Daniel Miller 2/27/2018 2:24 AM
Deleted: .

Daniel Miller 2/13/2018 1:38 PM
Deleted: 2WT

Daniel Miller 2/13/2018 1:38 PM
Deleted: 2WT

Table 2: The influence of unresolved microphysical inhomogeneity on polarimetric retrievals is explored in Shang et al. (2015). There results are replicated here and compared to the arithmetic mean r_e ($\langle r_e \rangle$), and the mathematical aggregation results (r_e' and v_e') defined in eq. (7) and eq. (8).

Sub-scale Size Distribution Mixture		**Arithmetic Mean**	**Polarimetric Retrieval**		**Aggregation Rules**	
r_e	v_e	$\langle r_e \rangle$	r_e(pol)	v_e(pol)	r_e'	v_e'
[5, 10]	[0.01, 0.01]	7.5	8.0	0.10	9.00	0.060
[5, 15]	[0.01, 0.01]	10.0	14.5	0.01	14.00	0.056
[5, 20]	[0.01, 0.01]	12.5	19.0	0.01	19.12	0.044
[10, 15]	[0.01, 0.01]	12.5	13.0	0.05	13.46	0.040
[10, 20]	[0.01, 0.01]	15.0	16.5	0.10	18.00	0.060
[15, 20]	[0.01, 0.01]	17.5	18.0	0.01	18.20	0.028
[5, 10, 15]	[0.01, 0.01, 0.01]	10.0	12.0	0.10	12.85	0.069
[5, 10, 20]	[0.01, 0.01, 0.01]	11.7	14.0	0.10	17.38	0.087
[5, 15, 20]	[0.01, 0.01, 0.01]	13.3	17.5	0.02	17.69	0.049
[10, 15, 20]	[0.01, 0.01, 0.01]	15.0	16.0	0.10	17.07	0.055

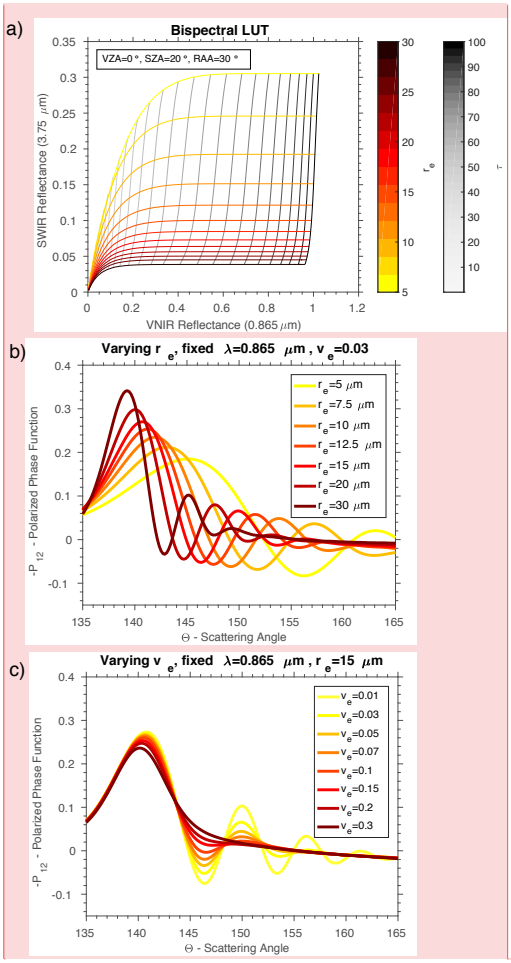

Figure 1: Demonstrations of the microphysical sensitivity of the bispectral and the polarimetric techniques. Panel (a) features the bispectral LUT exhibiting sensitivity to r_e (colored iso-lines), due to absorption in the SWIR/ reflectance. The VNIR reflectances provide sensitivity to optical thickness (gray iso-lines). Panels (b) and (c) demonstrate the sensitivity of polarimetric technique to r_e and v_e respectively. The supernumerary bow peaks of the polarized phase function ($-P_{12}$) shift and become narrower with increasing droplet size (r_e), whereas the peaks erode in magnitude for broadened droplet size distributions (v_e).

Daniel Miller 2/12/2018 11:29 AM

Comment [1]: Figure updated to correct error in original axes label of panel (a).

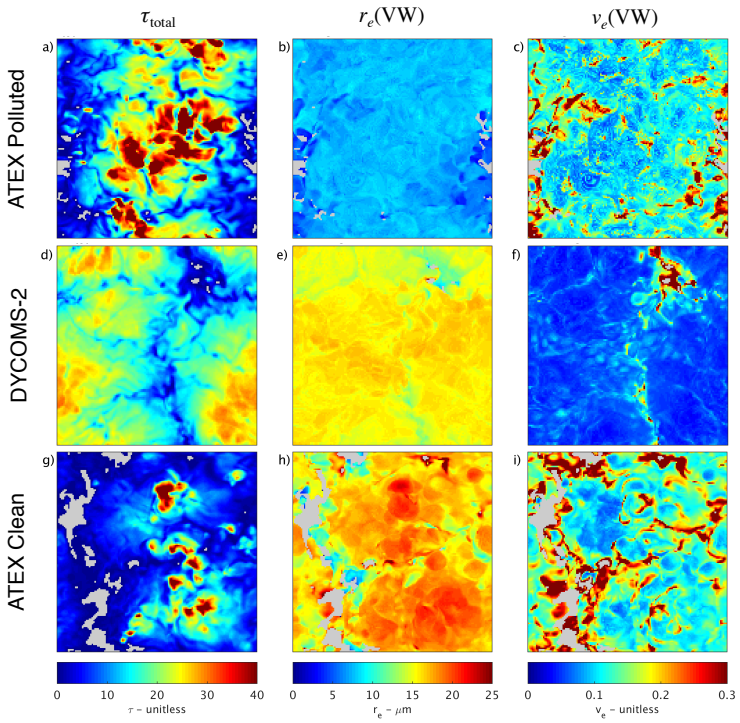

Figure 2: The optical and microphysical properties (τ, r_e, and v_e) of the LES cases examined in this study. The panels are arranged such that each LES case appears row-wise and the different properties are appear column-wise. Note that the vertically weighting functions used for the displayed re(VW) and ve(VW) correspond to single-scattering assumptions. Cloud-free masking in each of the images appears in gray. Refer to sections 2 and 3 for discussion and definition of each of these properties. Axes labels have been removed to enlarge each map, but the spatial dimensions of each scene are roughly 7 x 7 km (refer to section 3 for the specific resolutions of each LES case.)

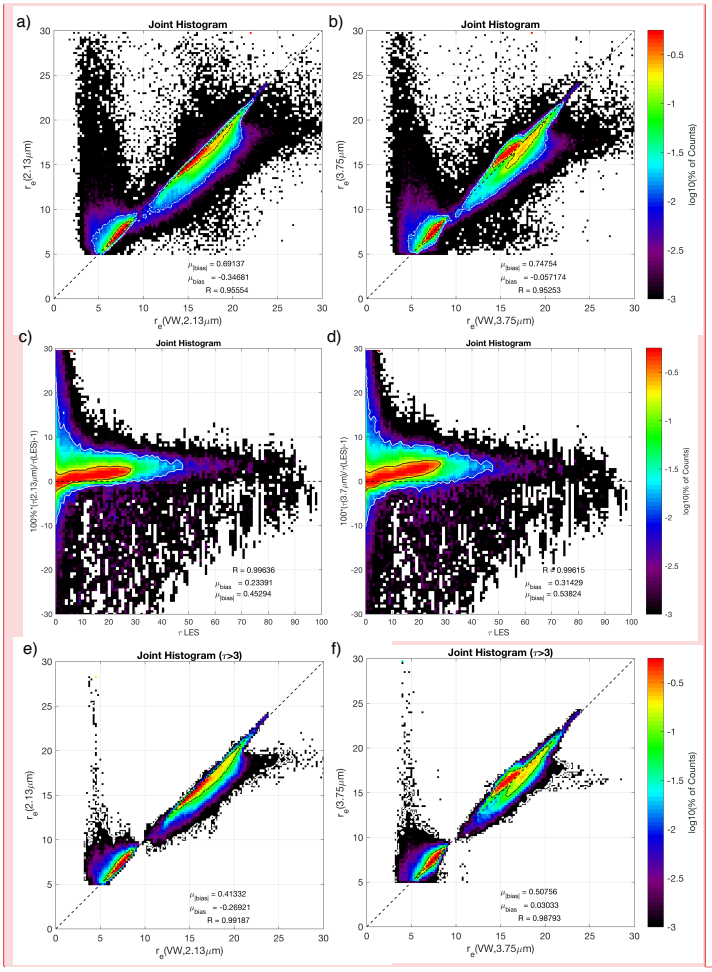

Figure 3: Joint histogram regressions of r_e and τ in all LES cases comparing the bispectral retrievals to the LES cloud microphysical properties. Panels (a) and (b) are regressions of the bispectral r_e(2.13 μm) and r_e(3.75 μm) retrievals against the physical analogue r_e(VW). Panels (c) and (d) are regressions of the bispectral τ(2.13 μm) and τ(3.75 μm) retrievals against the physical τ(LES). Panels (e) and (f) display the regression of the bispectral r_e(2.13 μm) and r_e(3.75 μm) retrievals for only optically thick pixels (τ>3). Note that in each panel the correlation is quantified with a linear correlation coefficient (R) and the black and white contours encompass 66% and 95% of the population, respectively.

Daniel Miller 4/26/2018 3:00 PM
Comment [2]: Figure updated again to newest vertical weighted properties

Daniel Miller 2/25/2018 4:25 PM
Comment [3]: Figure updated to include data from the new vertical weighting defintions.

Daniel Miller 2/13/2018 2:35 PM
Deleted: or

Daniel Miller 2/13/2018 1:38 PM
Deleted: 2WT

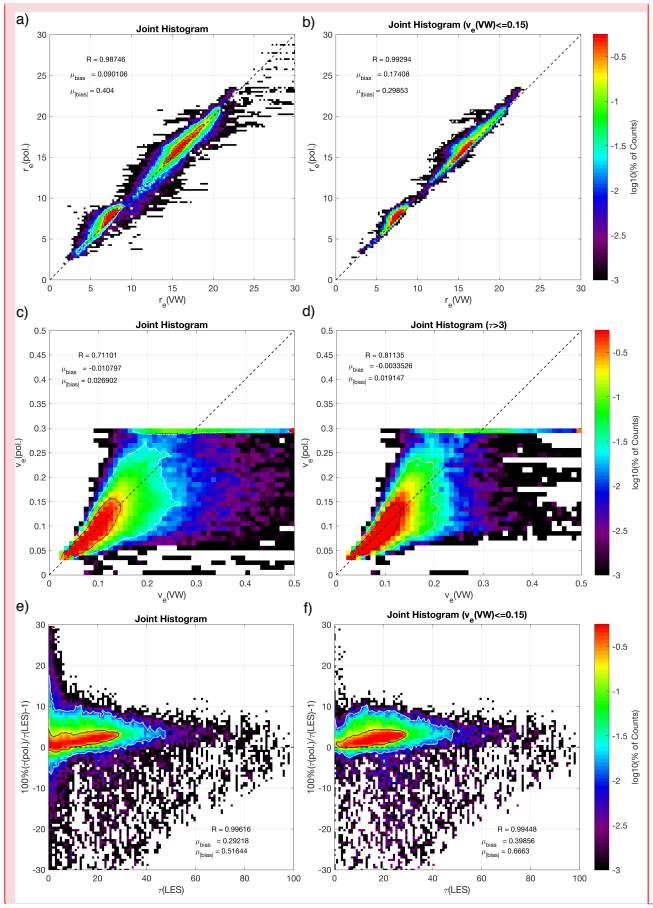

Figure 4: Joint histogram regressions of r_e, v_e, and τ in all LES cases comparing the polarimetric retrievals to the LES cloud microphysical properties. Panel (a) depicts the regression of the polarimetric r_e(pol) retrieval against the physical analogue r_e(VW), while panel (b) is sub-selection of the same regression for low v_e. Panel (c) depicts the regression of the polarimetric v_e(pol) retrieval against the physical analogue v_e(VW), while panel (d) is a sub-selection of the same regression for thick clouds (τ>3). Panel (e) depicts the regression of the polarimetric τ(pol) retrieval against the physical analogue τ(LES), while panel (f) is sub-selection of the same regression for low v_e. Note that in each panel the correlation is quantified with a linear correlation coefficient (R) and the black and white contours encompass 66% and 95% of the population, respectively.

Daniel Miller 4/26/2018 9:45 PM
Comment [4]: Updated for new VW properties…

Daniel Miller 3/2/2018 11:31 AM
Comment [5]: Figure updated to include data from the new vertical weighting defintions.

Daniel Miller 2/13/2018 1:38 PM
Deleted: 2WT

Daniel Miller 2/13/2018 1:38 PM
Deleted: 2WT

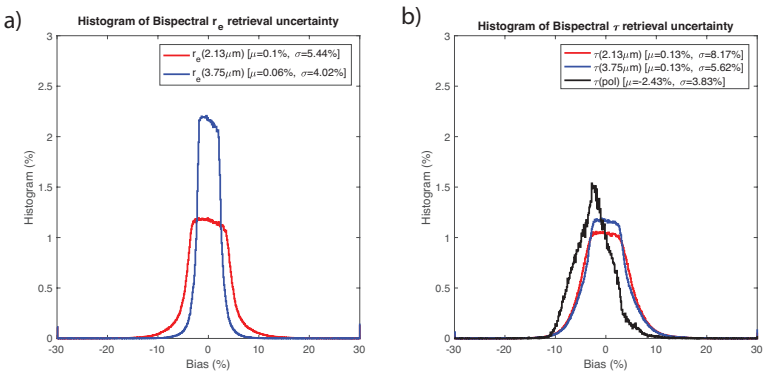

Figure 5: Histograms of the percent retrieval bias of retrievals based on perturbed reflectances stated relative to unperturbed retrievals. Panel (a) displays retrieval biases for the bispectral r_e retrieval. Panel (b) displays retrieval biases for the bispectral and polarimetric τ retrievals. Refer to the text for more information about the polarimetric r_e and v_e retrieval biases.

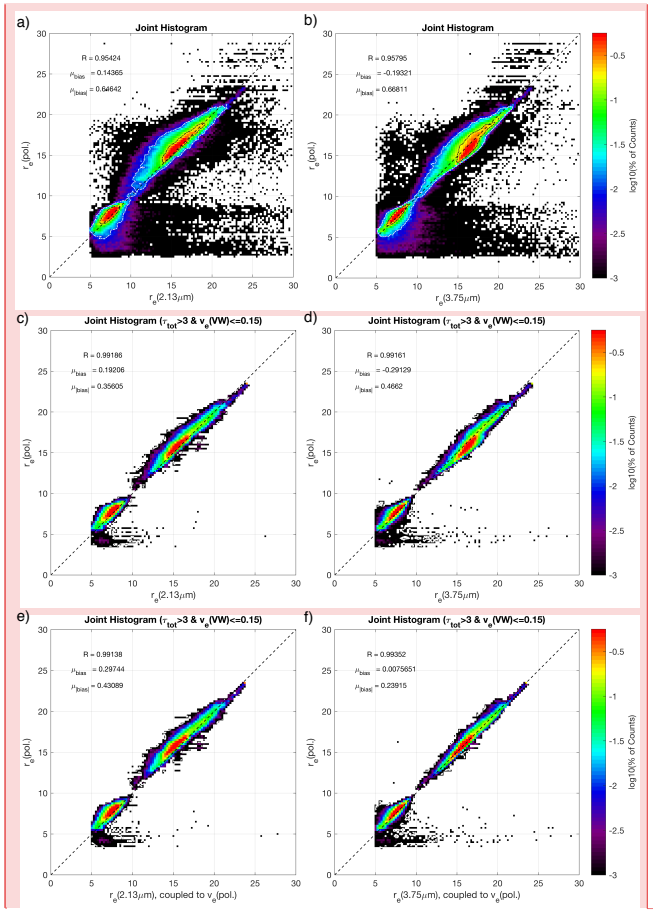

Figure 6: Joint histogram regressions of r_e retrievals for all LES cases comparing the bispectral and polarimetric techniques. Panels (a) and (b) display the unfiltered regressions of r_e(pol) at 0.865 μm wavelength against the r_e(2.13 μm) and r_e(3.75 μm) bispectral retrievals. After introducing filters to these regressions to remove thin clouds (τ<3) and broad droplet size distributions (v_e>0.15) panels (c) and (d) the retrieval intercomparison improves. Panels (e) and (f) each replicate the results from the previous selection criteria but additionally provide bispectral retrieval in this regression with v_e(pol) as an a priori for each retrieval. In each panel the quality of the correlation is quantified and a black iso-contour is drawn surrounding 75% data in the histogram. Note that in each panel the correlation is quantified with a linear correlation coefficient (R) and the black and white contours encompass 66% and 95% of the population, respectively.

Daniel Miller 4/26/2018 3:02 PM
Comment [6]: Figure updated for newest vertical weighting definition.

Daniel Miller 3/2/2018 12:13 PM
Comment [7]: Figure updated to include data from the new vertical weighting defintions.

Daniel Miller 2/23/2018 4:08 PM
Deleted: 5

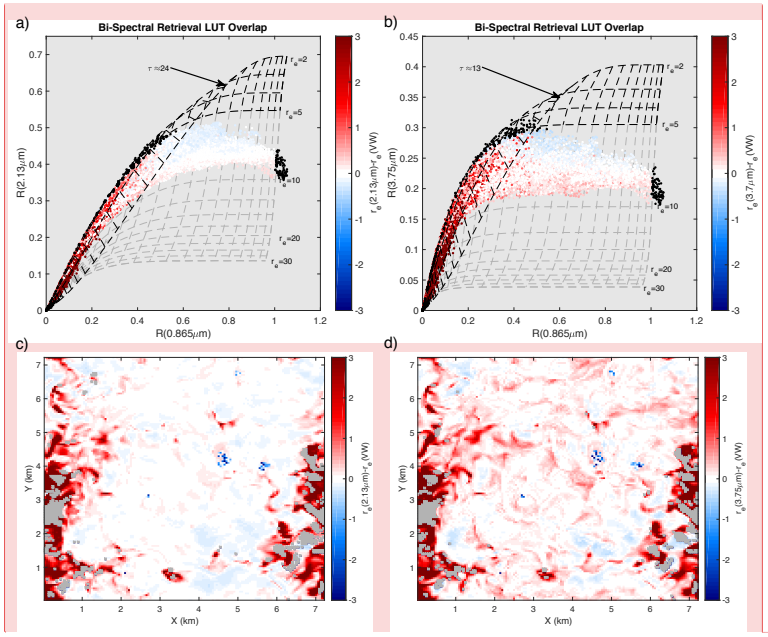

Figure 7: Panel (a) and (b) depict the standard bispectral LUT (light gray dashed lines) for both SWIR bands with the scattered reflectance points for the ATEX polluted LES case plotted overtop. The scatterplot is colored by the bias between the bispectral retrieval and the physical reference (r_e(bispectral)−r_e(VW)), which is also shown below as a spatial variability map. Note that some points are colored in black to indicate retrieval failure due to falling outside the LUT space. In addition to the standard LUT, an extended LUT including droplet sizes from 2-4μm is included (black dashed lines), revealing an overlapping region of the two LUT for smaller τ referred to as the "multiple solution space".

Daniel Miller 2/25/2018 6:07 PM
Comment [8]: Figure updated with new vertically weighted properties.

Daniel Miller 3/4/2018 4:47 PM
Deleted: (SWIR

Daniel Miller 2/13/2018 1:38 PM
Deleted: 2WT

Daniel Miller 2/13/2018 2:36 PM
Deleted: reflectance

Daniel Miller 2/13/2018 2:37 PM
Deleted: standard

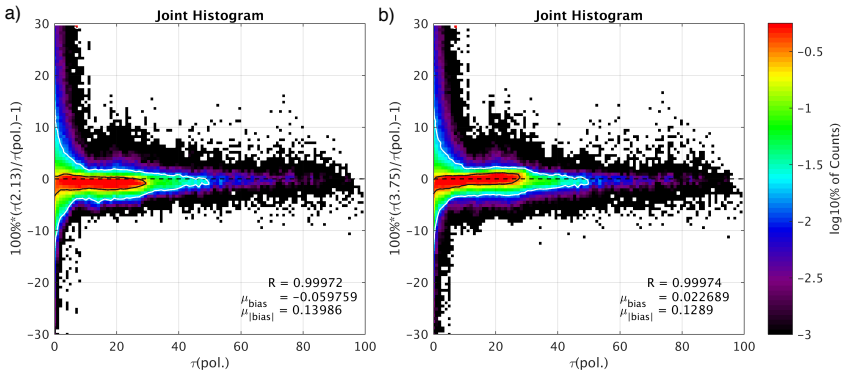

Figure 8: Joint histogram regressions of τ retrievals for all LES cases comparing the bispectral and polarimetric techniques. Panel (a) and (b) display the τ(2.13 µm) and τ(3.75 µm) retrievals respectively. In each panel the quality of the correlation is quantified and the black and white population density iso-contours are drawn surrounding 66% and 95% of the data respectively.

Daniel Miller 2/23/2018 4:08 PM
Deleted: 7

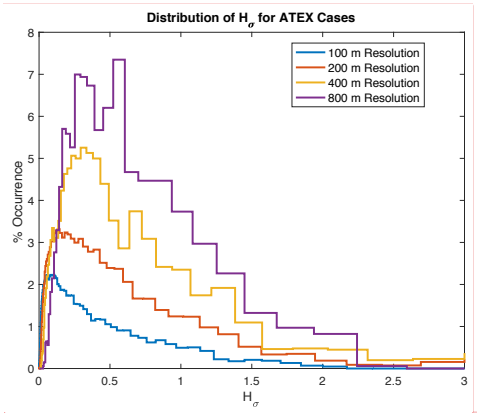

Figure 9: Probability distributions of H_σ for the combined ATEX polluted and clean datasets at all coarsened spatial resolution (100, 200, 300, 400, 800 m).

Daniel Miller 4/26/2018 6:00 PM
Comment [9]: Figure updated for line thickness and readability.

Daniel Miller 2/25/2018 9:45 AM
Deleted: 10

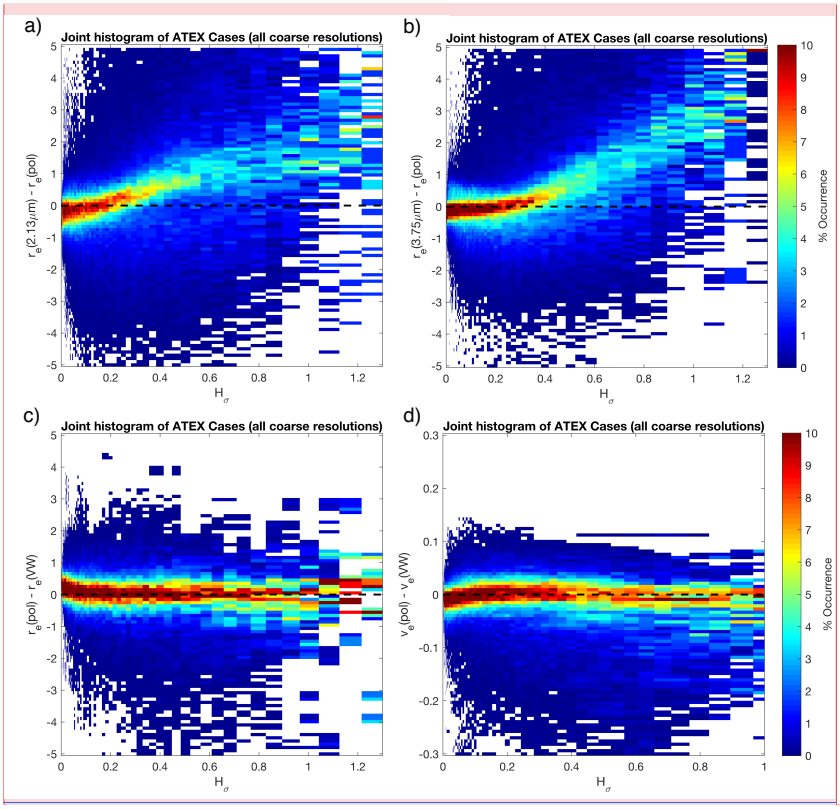

Figure 10: Joint histograms of retrieval biases (relative to each relevant vertically weighted LES property) with respect to H_σ for the combined ATEX clean and polluted datasets at all observation geometries and including all coarsened spatial resolutions (100, 200, 300, 400, 800 m). The color bar indicates percent occurrence. Panels (a) and (b) depict the difference between the two bispectral r_e retrievals and the polarimetric retrieval, while panels (c) and (d) depict biases for the polarimetric r_e and v_e retrieval against r_e(VW).

Daniel Miller 4/26/2018 5:57 PM
Comment [10]: Figure changed and updated.

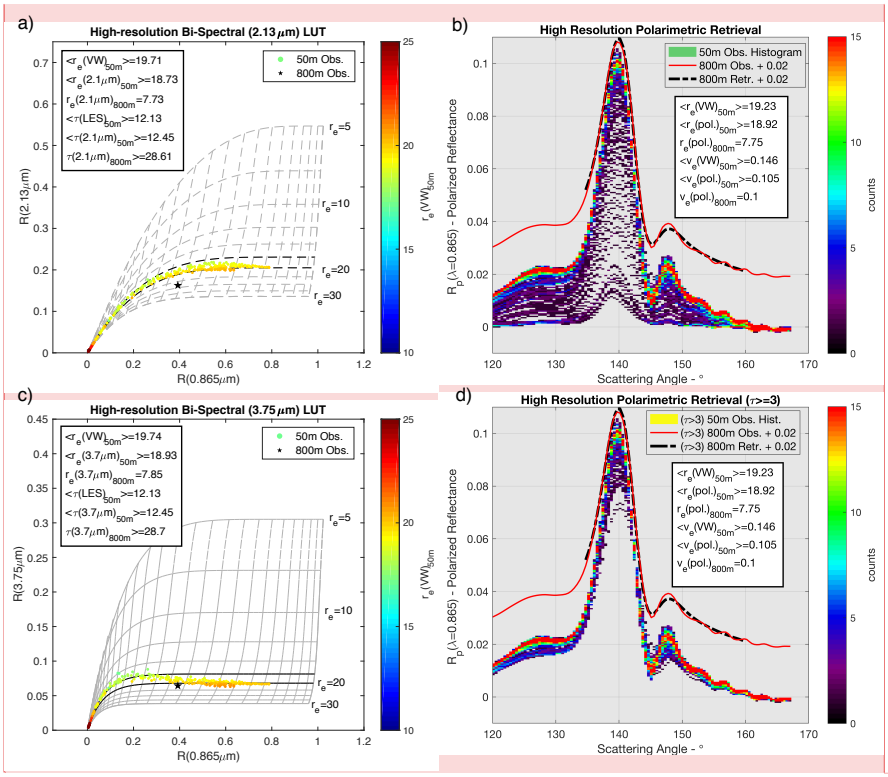

Figure 11: Panels (a) and (c) depict the bispectral LUT's and 50 m reflectances for the 2.13 and 3.75 μm bispectral retrievals respectively for a particularly inhomogeneous 800 m pixel. The scattered points correspond to 50 m reflectances with color corresponding to r_e(VW), while the black star corresponds to the 800 m reflectance pair (the average of the 50 m data). The polarimetric reflectance distribution histograms in panels (b) and (d) address how the high-resolution (50 m) reflectance distribution influences the polarimetric retrieval at coarse resolution (800m). The two curves (plotted with a 0.02 reflectance shift for clarity) are the 800 m observed reflectance (black dashed curve) and the 800 m retrieval (red solid curve). All of these figures include statistics on the high-resolution averages of physical properties and retrievals along with their coarse resolution counterparts for comparison.

Daniel Miller 4/26/2018 6:53 PM
Comment [11]: Figure updated with new vertically weighted retrieval information, font sizes increased, and background adjusted.

Daniel Miller 2/14/2018 11:45 AM
Deleted: 9

Daniel Miller 3/4/2018 4:47 PM
Deleted: SWIR

Daniel Miller 2/13/2018 1:38 PM
Deleted: 2WT

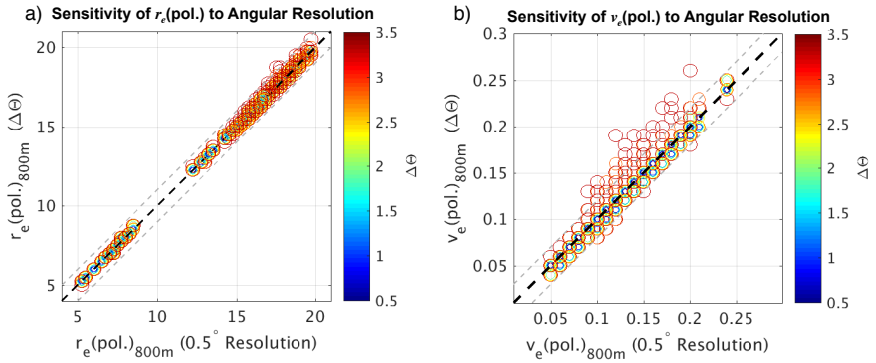

Figure 12: Angular resolution sensitivity experiments examining polarimetric retrievals of r_e (panel a) and v_e (panel b) for all LES scenes at the 800 m spatial resolution. The color and size of scattered points denote the angular resolution of each retrieval. The gray dashed lines denote the ±1 step in the LUT space of the polarimetric retrieval.

Daniel Miller 2/14/2018 11:45 AM
Deleted: 10

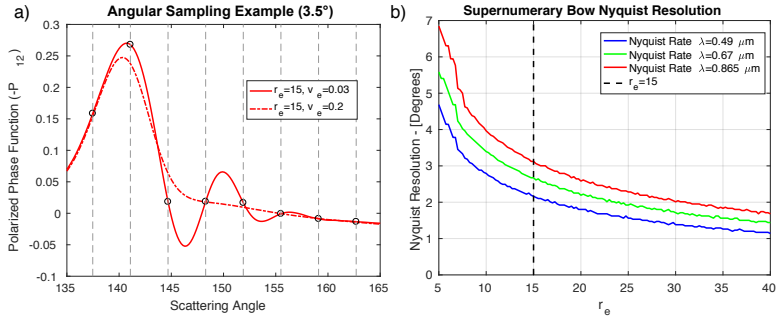

Figure 13: Panel (a) features the polarized phase functions r_e=15 (red) at v_e=0.03 (solid) and v_e=0.2 (dashed). Grey dashed lines and circles indicate a 3.4° observation sampling of the phase functions. The Nyquist resolution is obtained by measuring the peak-to-peak distance of the supernumerary bow oscillations and dividing that distance in half. The Nyquist resolution changes as a function of r_e and λ as shown in panel b, where the gray vertical line highlights the Nyquist resolutions required for the r_e=15 case.

Daniel Miller 2/14/2018 11:45 AM
Deleted: 11